

Uniaxial Alignment of Conjugated Polymer Films for High Performance Organic Field-Effect Transistors

Dongyoon Khim,^{†,+} Alessandro Luzio,^{‡,+} Giorgio Ernesto Bonacchini,^{‡,Δ} Giuseppina Pace,[‡] Mi-Jung Lee,[§] Yong-Young Noh,^{†,} Mario Caironi^{‡,*}*

⁺ equally contributing authors

[†]Department of Energy and Materials Engineering, Dongguk University, 26 Pil-dong, 3-ga, Jung-gu, Seoul 100-715, Republic of Korea
E-mail: yynoh@dongguk.edu

[‡]Center for Nano Science and Technology @PoliMi,
Istituto Italiano di Tecnologia,
Via Pascoli 70/3, 20133, Milano, Italy
E-mail: mario.caironi@iit.it

^ΔDipartimento di Fisica
Politecnico di Milano
P.zza L. da Vinci 32, 20133 Milan, Italy

[§]School of Advanced Materials Engineering, Kookmin University, 77 Jeongneung-ro, Seongbuk-gu, Seoul, 136-712, Republic of Korea

Keywords: aligned polymer films, polymer semiconductors, organic field-effect transistors, transport anisotropy, printed electronics

Abstract.

Polymer semiconductors have been experiencing a remarkable improvement in electronic and optoelectronic properties, which are largely related to the recent development of a vast library of high-performance donor-acceptor copolymers showing alternation of chemical moieties with different electronic affinities along their backbones. Such steady improvement is making conjugated polymers even more appealing for large-area and flexible electronic applications, from distributed and portable electronics to healthcare devices, where cost-effective manufacturing, lightweight, and ease of integration represent key benefits. Recently, a strong boost to charge carrier mobility in polymer-based field-effect transistors, consistently achieving the range from 1.0 to 10 cm²/Vs for both holes and electrons, has been given by uniaxial backbone alignment of polymers in thin films, inducing strong transport anisotropy and

favoring enhanced transport properties along the alignment direction. Herein, we provide an overview on this topic with a focus on the processing-structure-property relationships that enable the controlled and uniform alignment of polymer films over large areas with scalable processes. The key aspects are specific molecular structures, such as planarized backbones with a reduced degree of conformational disorder, solution formulation with controlled aggregation, and deposition techniques inducing suitable directional flow.

1. Introduction

Solution-processed conjugated polymers have received great attention owing not only to their unique optoelectronic, electrochemical, and electrical properties, which make them appealing from a scientific point of view, but also to their great potential for realizing large-area, lightweight, and flexible functional electronic devices using cost effective, scalable processes such as mass printing technologies.^[1, 2] Over the past two to three decades, various conjugated polymers have been synthesized, processed, and applied in a vast range of devices including organic light emitting diodes (OLEDs),^[3-6] organic photovoltaic cells (OPVs),^[7-9] and organic field-effect transistors (OFETs),^[10-14] and the performances of these state-of-the-art devices are comparable with or have overtaken their inorganic counterparts. For example, ~ 12 % power conversion efficiency has been reported in bulk heterojunction OPVs with a donor polymer;^[15] in OFETs, a field-effect mobility (μ_{FET}) exceeding 10 cm²/Vs has been demonstrated in devices based on donor-acceptor (D-A) conjugated polymers.^[16] Thanks to this recent rapid progress, we believe that marketable applications of conjugated polymers can be rapidly extended in the near future.

A strong boost to the impressive increase in μ_{FET} of polymer-based OFETs, difficult to predict only 10 years ago, has been brought about by the uniaxial alignment of highly planar conjugated polymers with largely extended highest occupied molecular orbitals (HOMO) or lowest unoccupied molecular orbitals (LUMO) along the backbone.^[17, 18] One interpretation is that

such a structural feature favors charge transport along the accumulated channel of a field-effect transistor (FET) in an anisotropic medium where carriers drift from the source to the drain electrode mainly through extended π -orbitals in the planar polymer backbone, thereby strongly reducing the number of slow and energetic demanding interchain hopping events. A limited degree of short-range order, possibly also present in very small aggregates not visible through common X-ray scattering techniques,^[19] is sufficient to enable favorable contact between conjugated segments of neighboring chains with good electronic overlap,^[19] thus rationalizing the observation of excellent transport properties in polymer films substantially lacking long-range order.^[20-23] This new paradigm for charge transport in OFETs can produce theoretically higher μ_{FET} at over $100 \text{ cm}^2/\text{Vs}$ compared to previous intermolecular hopping-based transport through edge-on-oriented interdigitated conjugated polymers.^[24]

There are various requirements to be satisfied at the same time in order to benefit from such improved transport, including chemical and structural ones, for which methods to achieve highly aligned and anisotropic polymer semiconducting films are key. In this review, we provide the recent progress in the development of the directional alignment of conjugated polymer films through the most successful and promising approaches for high performance OFETs. After briefly reviewing the basic concepts on the operation of OFETs and the impact of alignment on transport in Section 2, we describe the impact of stable preaggregation of chains in solution on the development of alignment protocols in Section 3. In Section 4, we review different approaches toward achieving aligned polymer films, especially focusing on strategies which lead to fast, single-step methods, therefore more suitable for high throughput future manufacturing processes, but also covering slower, multi-steps procedures with which alignment to an exceptional degree has been achieved at the laboratory scale. Lastly, we draw conclusions with some perspectives on the impact of the development of high-throughput processes delivering aligned polymer films with improved charge mobility.

2. Basics of FETs and charge transport

In this work, we cover the enhancement of the performances of polymer-based FETs through directional coating of semiconducting polymer films, and so we first introduce the basic aspects of such field-effect devices and their main figures of merit. Without aiming to be comprehensive, we also highlight aspects of charge transport in polymer films, which intuitively motivate the use of unidirectional alignment, according to current understanding.

2.1. FETs: main figures of merit

A transistor is as much a technologically relevant device as it is a basic building block of any digital and/or analog electronic circuit, and it is also a very useful testbed for the investigation of charge transport properties in active semiconductors. The FET is by far the most widely adopted transistor type in the framework of polymer electronics, and is composed of a thin semiconducting layer interfacing a gate-dielectric layer, source and drain electrodes. The most commonly employed device configurations are depicted in **Figure 1**: bottom-gate/bottom-contact architecture is easily accessible, for example on SiO₂/Si wafers with patterned electrodes; alternatively, staggered configurations where channel and gate electrodes are on opposite sides with respect to the semiconductor are adopted to enhance injection and have bottom-gate/top-contact and top-gate/bottom-contact geometries. Another less commonly adopted possibility is the top-gate/top-contact configuration, which was recently reported to yield ideal characteristics when suitable dopants are introduced at the contacts.^[25] Important structural parameters are the channel width (W) and channel length (L). For a more detailed description of the working principles of OFETs, we refer the reader to previous reviews,^[26-28] while herein we report on the main model assumptions and figures of merit only.

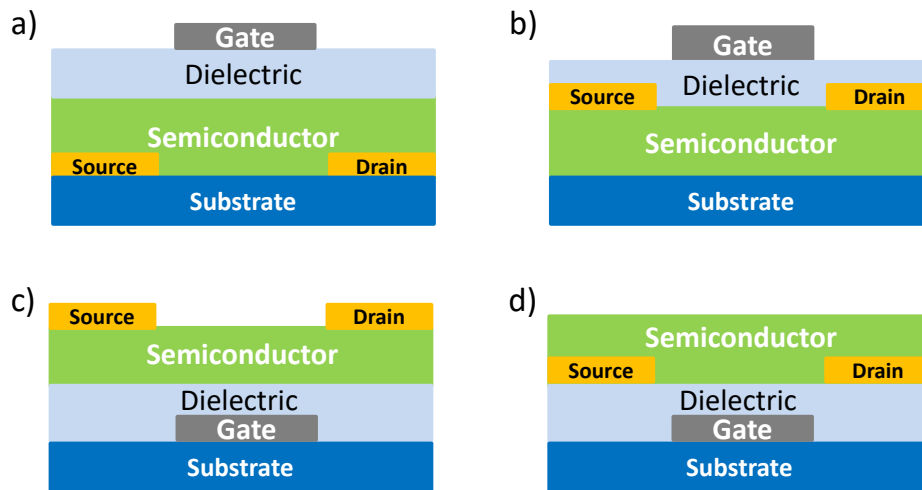


Figure 1: Device structure of the most commonly studied polymer FET configurations: a) top-gate/bottom-contact, b) top-gate/top-contact, c) bottom-gate/top-contact, and d) bottom-gate/bottom-contact.

The simplest analytical model so far employed to describe the device physics of polymer FETs has been borrowed from the gradual channel approximation theory used for inorganic metal-oxide-semiconductor FETs, MOSFETs.^[29] The fundamental assumption is that the vertical field, applied through the gate with respect to the source and drain electrodes dominates over the lateral field between drain and source electrodes. Through the gate dielectric capacitance, charges are electrostatically accumulated in a very thin active channel, formed within a few molecular layers of the semiconductor present at the gate dielectric interface.^[12] Charge density and distribution determines channel conductivity, which is probed by applying a voltage in between the source and drain electrodes. The channel is typically only a few nm thick and so may involve from one to only a few molecular layers.^{[30] [31] [32] [33]}

Fundamental figures of merit such as mobility and threshold voltage can be extracted from the fitting of the experimental electrical characteristics with the analytical expressions of the channel current defined for MOSFETs under different bias conditions. In the following we assume an n-type only device, i.e. a FET which works in electron accumulation regime; analogous equations hold, with different signs, for p-type devices, i.e. working in hole accumulation regime. Ambipolar devices can be seen as the parallel of two p- and n-type

devices, and equations are a combination of those for unipolar devices.^[27] For a unipolar n-type device with a grounded source electrode, when the drain-source voltage (V_{ds}) is very low compared to the gate-to-source (V_{gs}) voltage, i.e. when both V_{gs} and gate-to-drain voltage (V_{gd}) are well above the channel accumulation threshold voltage V_{th} , the FET is in the so-called linear regime in which the channel current is given by

$$I_{ds,lin} \cong \frac{W}{L} \mu_{lin} C_i (V_{gs} - V_{th}) V_{ds}. \quad (1)$$

where μ_{lin} is the field effect mobility in the linear regime and C_i the specific capacitance of the dielectric insulator. While in the context of silicon MOSFETs the threshold voltage V_{th} has a precise physical meaning,^[29] care must be taken in the case of polymer FETs where V_{th} in equation (1) is no more than a fitting parameter of experimental curves. Besides, alternative definitions as well as extraction methods have been proposed.^{[34] [12]}

The field effect mobility in the linear regime μ_{lin} can thus be extracted from the slope of $I_{ds,lin}$ versus V_{gs} at constant V_{ds} as follows:

$$\mu_{lin} = \frac{\partial I_{ds,lin}}{\partial V_{gs}} \cdot \frac{L}{WC_i V_{ds}}. \quad (2)$$

When increasing V_{ds} , V_{gd} is gradually reduced, eventually reaching $V_{gd} = V_{th}$; above this value, a non-accumulated region is present next to the drain electrode as the difference between the gate voltage and the local channel potential at the drain electrode is now below the threshold voltage, and the channel is defined as “pinched off”. The non-accumulated region is much more resistive than the accumulated one, thus any further increase in V_{ds} can be easily accommodated with an extremely small movement of the pinch-off point, inducing current saturation vs. V_{ds} .

Under saturation conditions, the current $I_{ds,sat}$ and mobility can be expressed as follows:

$$I_{ds,sat} = \frac{W}{2L} \mu_{sat} C_i (V_{gs} - V_{th})^2, \quad (3)$$

$$\mu_{sat} = \frac{2L}{WC_i} \cdot \left(\frac{\partial \sqrt{I_{ds,sat}}}{\partial V_{gs}} \right)^2. \quad (4)$$

Ideally, mobility Equations (2) and (4) should be valid over all of the voltage range in which the FET is fully accumulated, and in such cases, the extracted mobility has a clear physical meaning. However, that may not always be the case in polymer FETs where it is not rare to observe V_{gs} dependence of the slope found in the transfer characteristic curves. Previous works have highlighted the possible pitfalls present when reporting mobility based only on the maximum slope found along the transfer curve. While various works have already warned of the presence of kinks at low V_{gs} due to an effect of injection or of the use of the above equations in voltage ranges where they may not hold at all, ^{[16] [25, 35] [36]} care should also be taken at high gate voltages. ^[37] While at increasing gate voltages the voltage dependence may reflect the filling of a broad density of states (DOS), injection issues can also play a dominant role in such dependence. ^[38] In the following sections, we report on mobility values as claimed in the referenced works, which in any case would reflect, at least qualitatively, relevant structural and transport effects that are important to the scope of this review. However, we invite the reader to pay specific attention to the mobility extraction methods reported in each of them. To this end, a work of Gundlach and coworkers published in 2016 makes explicit reference to relevant cases of strongly overestimated mobility values ^{[39] [40] [41] [42] [43] [18] [17] [44]} and offers an effective guidance for their re-evaluation (**Figure 2**).^[45]

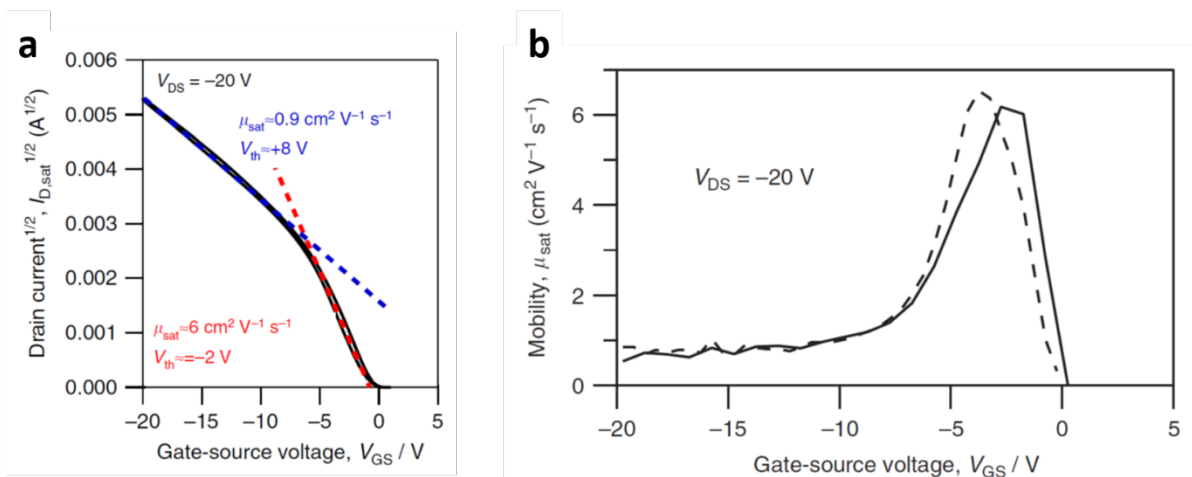


Figure 2. Plot of the transfer characteristic (a) and mobility (b), as defined in equation 4, in the saturation regime ($V_{DS} = -20$ V) for a bottom gate/bottom contact OFET, implementing a rubrene single crystal as the active layer, exhibiting non-ideal characteristics. Fit lines in red and blue illustrate the ambiguity associated with the OFET mobility extraction: strongly varying contact resistance at low V_{gs} results in a charge injection dominated transistor, leading to an overestimation of the channel mobility by an order of magnitude when extracted using the MOSFET model. Reprinted with permission from Ref ^[45]. Copyright 2016, Springer Nature.

Other sources of ambiguity and uncertainty in mobility extraction have been recognized in Joule self-heating effect during operation ^[46] and lateral field dependent phenomena.^[47] Efforts in defining criticalities and suitable device platforms for accurate mobility extraction are thus demanded, similarly to the valuable examples represented by the recent, highly recommended works by Liu et al. ^[38], Xu et al. ^[48], and the already cited one by Nikiforov et al. ^[46] The choice of a specific FET architecture is important since an ensemble of the properties and performance of a FET is not just a function of the intrinsic electronic properties of the selected organic semiconductor (as outlined in the following sections), it is also highly dependent on the dielectric and electrode materials as well as on the overall processing conditions, since different device layouts may pose different constraints on the choice of processing solvents and thermal budget.^[49] Heterogeneous interfaces between the electrodes and the semiconductor, and between the semiconductor and the dielectric, are in fact known to affect transistor performance strongly.^[49-51]

The transport in the thin accumulation channel is highly influenced by the nature of the semiconductor-dielectric interface through their relative dielectric constant and the dipolar disorder/order,^[52] and the roughness and physical extension of such interface, affected by the specific architecture and by the processing solvent used.^{[27] [53] [54]} Furthermore, the electrodes–semiconductor interface is critical as high contact resistance may reduce FET currents, thus strongly limiting the measured apparent mobility.^[55] Therefore, the possibility of benefiting from the chemical engineering of polymers to improve FET performance must always be followed by an overall device optimization.

2.2. Key aspects in the structure-transport relationship

The microstructure of an organic film together with the specific chemical properties of the conjugated molecules largely defines its solid-state opto-electronic properties. In this section, we briefly highlight some of the recent findings regarding the nexus between structure and transport properties along with suggested models to describe charge transport, which we believe to be critical for understanding the impact of unidirectional alignment. For more comprehensive and detailed reviews on the physics of charge transport in organics, we invite the reader to access the following excellent works.^{[22] [37] [56] [57] [58] [59]}

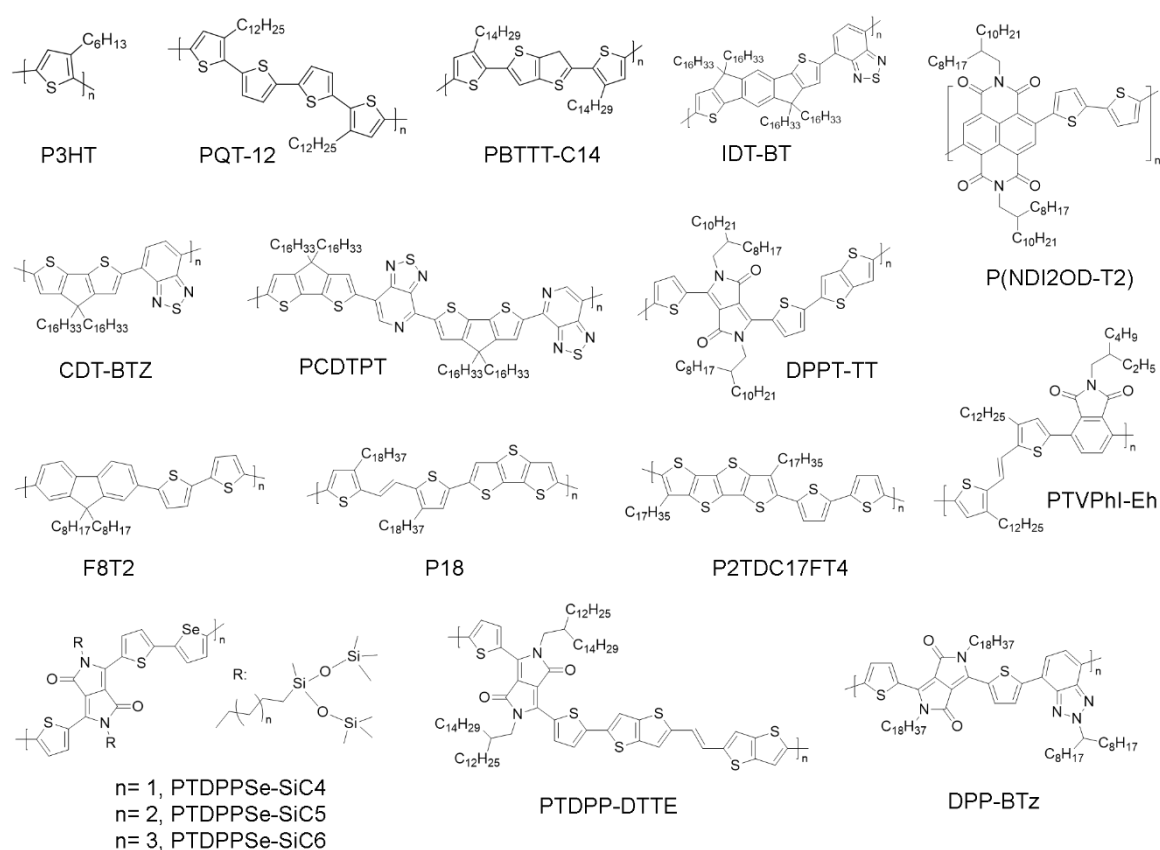


Figure 3. Molecular structures of conjugated polymers mentioned in this review.

The molecular structures of all the conjugated polymer mentioned from now on in this review are reported in **Figure 3**. The deposition of the active phase of a FET in the form of a solid thin

film from organic semiconductor solutions (either polymers or small molecules) is affected by kinetic factors that if not properly controlled, can often cause a high degree of structural and energetic disorder. In the particular case of small molecules, highly ordered crystalline materials can be deposited from the vapor phase under vacuum conditions, thereby enabling the formation of highly ordered semi-crystalline films. Small molecule single crystals can also be deposited and/or printed from solution under specific and highly controlled conditions.^[60-62] For such materials, high mobility values up to several tens of $\text{cm}^2 \text{V}^{-1}\text{s}^{-1}$ and a band-like transport have been well demonstrated.^[63, 64]

It is intrinsically more difficult to obtain a well ordered polymer film from solution, although there are cases where single crystals of conjugated polymers have been demonstrated.^[65, 66] Besides specific cases, with typical fast deposition methods such as spin coating, the general presence of structural defects is unavoidable and can broaden the DOS, thus introducing deep trap states. High mobility values over the $1 - 10 \text{ cm}^2 \text{V}^{-1}\text{s}^{-1}$ range and above are a relatively more recent observations for semiconducting polymers and are most of the time achieved at high voltages. In the large majority of cases, transport is thermally activated, while fingerprints of band-like transport have been observed so far for a limited subset of materials.^[16, 67-70] The achieved mobility values to date are in the range or even higher than the ones found in current thin-film amorphous silicon devices ($0.5 - 1.0 \text{ cm}^2 \text{V}^{-1}\text{s}^{-1}$), although still not at the level of highly ordered small molecule films and single-crystals, which have demonstrated mobilities up to few tens of $\text{cm}^2 \text{V}^{-1}\text{s}^{-1}$.^[63, 64, 71]

Since polymers are more prone to disorder, one question to ask is whether efforts should be focused mainly on synthesis, deposition and processing strategies leading to a continuous improvement in long-range crystallinity, trying to adopt the same paradigm working for small molecule systems. This strategy has led to milestones in the development of polymer electronics with the evolution of interdigitated polymers such as poly(3-hexylthiophene-2,5-diyl) (P3HT), poly[5,5-bis(3-alkyl-2-thienyl)-2,2 -bithiophene] (PQT), and poly(2,5-bis(3-

hexadecylthiophen-2-yl)thieno[3,2-b]thiophene) (pBTTT) mainly aimed at facilitating the charge transfer along the π -stacking direction.^[72-75] The first hint of an alternative approach came from the observation that pBTTT films, which are characterized by distinct crystallinity with optimized processing, show an energetic broadening along the π -stacking that is comparable to less structurally ordered systems.^[76] Correspondingly, a recent assessment of the Gaussian DOS for pBTTT at thermal equilibrium in a metal-insulator-semiconductor structure indicates a Gaussian standard deviation (σ) of 98 meV, which is larger than in other less crystalline semiconductors, such as the good electron transporting poly[N,N'-bis(2-octyldodecyl)-naphthalene-1,4,5,8-bis(dicarboximide)-2,6-diyl]-alt-5,5'-(2,2'-dithiophene) (P(NDI2OD-T2)), with $\sigma = 78$ meV.^[30]

With the advent of high mobility D-A copolymers with limited or almost absent long-range crystallinity, it became clear that a new understanding had to be developed.^[19, 77-79] Interestingly, it has been suggested that at a given degree of disorder, a weaker coupling between electronic states, at least until disorder is the source of localization, can favor charge transport.^[80] In fact, due to the small gap, the intragap states induced by energetic disorder are closer in energy to the transport levels, so that room temperature thermal energy might be effective in activating transport. Besides the previously cited P(NDI2OD-T2), which is in any case characterized by the presence of a substantial ordered phase, other D-A materials with an absence of long-range order, such as indacenodithiophene-co-benzothiadiazole (IDT-BT), obviously lack a clear framework for the rationalization of their high field-effect mobility ($1 - 3$ cm²/Vs).^[81] This indicates the possibility to enhance charge transport on the basis of an alternative paradigm along strategies which, from a general point of view, can be seen as a combination of synthetic efforts capable of making polymer films more resilient to intrinsic disorder.^[22]

The reduction of conformational freedom, as chain folding and torsion^[82] by increasing backbone rigidity, was recognized early on as an effective method to narrow the DOS.^[83] For example, in semi-crystalline polymers such as pBTTT, the higher rigidity imposed by the

thieno-thiophene unit compared to the parent P3HT limits the formation of long-lived trap states induced by chain distortion so that more delocalized states become thermally accessible.^[82, 84] A reduced degree of conformational freedom may also determine a lower reorganization energy, which is associated to the polaronic relaxation, i.e. the energy needed for the geometric reorganization of the conjugated segment hosting a charge, which should be as small as possible to favor charge transport.^[85] Chain planarity can also favor better packing of molecules, which reduces the π - π staking distance down to 3.6 - 3.7 Å and increases charge transfer integral, i.e. increased probability for the charge to be transferred to adjacent molecules or polymer segments.^[86] Yet, a wide torsional angle distribution has been reported for pBTTT when alkyl chain disorder is taken into account,^[19] while other D-A systems can maintain a narrow torsional angle distribution even in non-ordered phases. This occurs in the case of P(NDI2OD-T2) where steric hindrance imposes a large angle between the D and A units,^[87-92] and of the notable IDT-BT where the backbone remains rigid around a very small dihedral angle.^[19] Such a torsion-free backbone produces resilience to side-chain disorder, thus strongly narrowing the DOS and approaching a limit where all molecular sites along the backbone are thermally accessible at room temperature.

Molecular weight (weight-average molecular weight, M_w , and number average molecular weight, M_n) can strongly affect charge transport properties in D-A copolymer films, which was also previously found for homo-polymers such as P3HT.^{[93] [94]} As an example, an improved degree of crystallinity with M_w up to ~100 kDa (polydispersity index of ~3) was found in poly[2,6-(4,4-bis-alkyl-4H-cyclopenta-[2,1-b;3,4-b0]-dithiophene)-alt-4,7-(2,1,3-benzothiadiazole)] (CDT-BTZ) films, thereby achieving mobility higher than 3 cm²/Vs^[95]. A rationalization of the effect of increased M_w relates the improved transport to the enhanced probability of effectively bridging inter-domains (amorphous regions) in between small crystallites through the presence of long and planar tie chains. The work by Koch et al. clearly elucidates the effect of molecular weight on microstructure and transport in the paradigmatic

case of P3HT, processed both by melt and solution.^[96] The authors individuate a critical molecular weight M_c ($M_n \approx 25$ kg/mol in case of P3HT, a value which is expected to be higher for more rigid backbones like D-A copolymers), above which chains folding become possible together with polymer chains entanglements; as a consequence, a microstructural transition occurs, from small molecules-like chain extended crystals ($M_n < M_c$) to interlinked crystalline lamellae (through polymer chains shared from different crystallites, the so called tie-molecules) in an amorphous matrix ($M_n > M_c$). For $M_n < M_c$, lamellar thickness, crystalline content and lattice spacing improve with M_n (chain length and lamellar thickness mostly coincide) and increased mobility values are observed, as a consequence. For $M_n > M_c$ the chain length becomes relevantly bigger than the lamellar thickness and does not affect anymore the crystalline structure of the film; as a consequence, charge mobility becomes independent on M_n and maximized, also in virtue of an efficient lamellar interconnectivity through tie-molecules. Variations to this model may be indeed necessarily applied in case of fast film solidification (inhibiting crystallization) and if marginal solvents and liquid crystalline phases are employed, promoting both films interconnectivity and crystallization (as will be discussed in the following of this work).

In their work, Noriega et al.^[20] proposed a model where, when a sufficient degree of interdomains connectivity is achieved, i.e. above a certain molecular weight, the mobility depends only on structural imperfections within the lattice of crystallites, described by the paracrystallinity parameter.^[97] This parameter controls the width of an exponential intra-gap DOS below a mobility edge (ME), according to a transport model well known for disordered semiconductors in which carriers proceed from one localized state to the other by being promoted to transport levels.^[97-99]

Interestingly, from the point of view of the underlining transport mechanism, at least up to a moderate charge carrier concentration, the ME model cannot be distinguished from the hopping model on the basis of kinetic Monte Carlo simulations as both models can predict experimental

transfer characteristics, obviously with quantitatively different parameters.^[100] A hopping model depicts a scenario where transport occurs directly between localized states through tunneling events assisted by phonons. Both models are consistent with a thermally activated transport, which characterizes most of the reported conjugated polymers so far. In particular, already long ago Bässler et al.^[83, 101] described hopping in a Gaussian DOS, the width of which is correlated to the spatial and energetic disorder, and Vissenberg and Matters^[102] developed a very well-known model for FETs based on amorphous organic semiconductors under the assumption that extended states do not play a role in highly disordered films.

Recent reports on high-mobility polymers with carrier mobility well above $1 \text{ cm}^2/\text{Vs}$ cannot be fully described on the basis of a hopping model.^[37] Indeed, few examples have so far reported a negative temperature dependence of mobility in polymer transistors,^[16, 67-70] a so-called “band-like” regime occurring above a transition temperature, in most of the cases around room temperature, below which an activated transport, dominated by trap states, still holds. In all of the reports so far, the semiconductor has been a D-A copolymer based on either polycyclopentadithiophenebenzothiadiazole,^[68] diketopyrrolopyrrole (DPP),^[67, 70] or thiophene-thiazole.^[69]

Despite the fact that the inverted temperature dependence of mobility immediately recalls band transport, the exact origin of such a phenomenon in polymers is still being debated. According to the ME model, a decrease in mobility with increasing temperature should be observed above the transition temperature at which carriers can be promoted in extended transport states above the transport edge. In this representation, the conditions to observe band-like transport are linked to the density and energy difference between the localized states below the transport energy, which may fall below room temperature thermal energy under specific conditions of uniform energy landscape, low reorganization energy, and positive influence from a low disordered dielectric at the interface with the semiconductor.^[70] Interestingly, Hall effect mobility in some of these polymers is very similar to the field-effect mobility, indicating that

most of the charge can ideally couple with an external magnetic field, thus confirming the presence of states extended enough so that a wave vector can be defined and thus the possibility to observe the Lorentz force.^[57] Yet, the formation of extended band states apparently disagrees with typical optical markers indicating spatial localization in polymers, i.e. self-trapping polaronic effects^[103] and with a typically limited carrier mean free path estimated for organics.^[104] It has been suggested that the transport regime may be similar to that occurring in poor metals with a scattering length close to the inter-atomic distance.^[57] Such regime has found rationalization in the model of dynamic disorder proposed by Troisi et al.^[105] in which wavefunction localization is induced by thermal fluctuations of the electronic coupling in between molecules so that a reduction in thermal energy is effective in reducing disorder and increasing mobility.^[106] In the case of polymers, the nature of thermal fluctuations leading to negative temperature dependence requires further study; for example, to distinguish between in-chain orbitals overlap variation due to torsional motion along the backbone or modulation of inter-chain transfer integrals due to variation in the relative positions of the adjacent chains.^[67]

2.3. Impact of polymer unidirectional alignment on charge transport

Empirically, an increasing number of experimental reports have reported a strong improvement of charge transport in films where polymer chains have been preferentially aligned along a single direction in plane, with field-effect mobility maximized along the chain elongation direction and characterized by marked in-plane anisotropy.^[17, 42, 43, 107] The rationale for this effect of unidirectional alignment can be found on the basis of the current understanding of charge transport in polymer films, which we briefly overviewed in the previous section. The formation of efficient charge percolation pathways in polymer films strongly depends on chain elongation, entanglement, and relative alignment as a direct consequence of the anisotropic nature of such macromolecules. Their optical and electro-optical properties are dictated by the interaction of π molecular orbitals, which are necessarily spatially contiguous along the σ

bonded backbone and which can show a much wider scale of variation in between conjugated segments belonging to different chains.^[108] Indeed, the role of backbone rigidity in providing an efficient pathway for carriers has also been suggested for non-aligned films as a way to explain improved carrier transport in IDT-BT films with very poor long-range order.^[77] At the same time, it has been shown how short-range intermolecular aggregation is sufficient for efficient charge transport over channels several microns long for the good electron transporting copolymer P(NDI2OD-T2) diluted in an inert matrix.^[23] Within such a scenario, π -stacking does not need to be uniformly extended over macro-domains but instead can locally provide the necessary linking steps between different chain segments. This very qualitative description is in agreement with both the previously-mentioned model proposed by Noriega et al.^[20] and with quasi-1D (mono-dimensional) models, where coherent chain orientation through ordered and disordered phases sizes the predominantly intra-chain transport in between occasional π -stacked links (**Figure 4**).^[77] In both scenarios, chain alignment is clearly a strategy to improve transport, which is particularly favored in the case of rigid backbones, with impeded torsional angles, guaranteeing in-chain orbitals overlap and possibly more extended in-chain delocalization, even in the case of backbone bends necessary to accommodate side-chains disorder.^[19] A recent study by Di Pietro et al. proposes an alternative picture of the limiting step for charge transport in semi-crystalline polymers where the boundary between the ordered crystallites and the amorphous phase prevails over the disorder within the ordered phase.^[109] Coulomb interaction among carriers in the ordered phase enhances the probability to overcome such a barrier, and in this case, chains and aggregates alignment can be seen as an effective method to reduce inter-phase transport by limiting the number of barriers along the percolation path.

In this sense, directional alignment of elongated chains can provide a path to deploy the quasi-1D electronic structure of a semiconducting polymer in an organic thin film. Indeed, in-chain delocalization has been found to extend over several repeated units in highly unidirectionally

oriented PCDTPT (cyclopenta [2,1-b:3,4-b']dithiophene pyridyl[2,1,3]-thiadiazole) polymer with evidence of strong DOS anisotropy.^[110] Though π -stacking is needed to assist the transport over lengths much longer than single conjugated chains, chain alignment can drastically reduce the number of inter-chain hopping events a charge has to go through while drifting in a FET channel from one electrode to the other. Moreover, in-chain charge delocalization or less energetically demanding polaron hopping can allow a charge to sample many different π -stacking sites or aggregates, allowing it to select the most efficient ones with maximized charge transfer integrals and spatially tight stacking.^[111] The unidirectional alignment of chains through suitable deposition techniques can itself favor the formation of efficient inter-chain π -stacking sites by introducing a consistent molecular order with a coherent orientation of π -conjugated planes which can lead to further solid-state planarization.^[112] Since occasional local directionality of such extended chains in a non-macroscopically oriented film, possibly under the effect of non-uniform local forces and/or interactions with the substrate, may lead to consistent data scattering among devices, directional alignment over a large area can also bring about the additional advantage of reducing data dispersion, a crucial aspect for the implementation of complex circuits (see Section 4).^[21]

Based on the above information, it is intuitively clear that transport in the orthogonal direction with respect to the chain main orientation axis in an aligned film will result in a more energetically difficult process: in-chain pathways cannot be as efficiently exploited and π -stacking becomes the prevalent path for transport, thus an intrinsically more disturbance from and less resilience to disorder. Moreover, supra-molecular effects like those present in films with fibrils-like morphology can even introduce an inherently less dense molecular structure in the direction opposite to the preferential alignment, inherently creating dead ends for transport and drastically reducing film interconnectivity.^[21] ^[113] Therefore, efficient techniques to achieve polymer chain alignment have become extremely useful tools not only to enhance charge transport but also to access model systems to analyze the charge transport mechanism

in organic semiconductors toward the development of consistent quantitative models. As a remark, out of the present five reports on band-like transport in polymer FETs, three have achieved such regimes in uniaxially aligned films,^{[16] [67] [68]} further underlining the relevance of such an approach to observe ultimate transport capabilities of conjugated polymers.

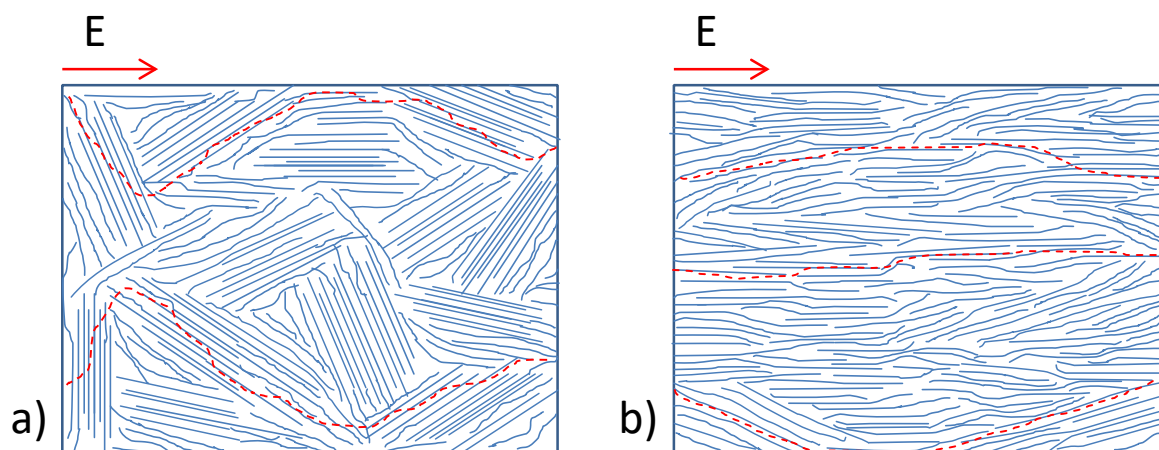


Figure 4. Indicative schemes of the different charge transport pathways (red dotted line) as a function of film morphology and electric field direction (E , red arrow). Semicrystalline films presenting (a) non-orientated domains and (b) prevalent polymer chains/domains orientation along the field direction.

3. The influence of conjugated polymer solution formulations on film microstructure

In this section, we want to emphasize how critical the choice of carrier solvent is within a semiconducting solution/ink formulation to gain control over the microstructural features and to enable efficient directional deposition strategies. Overall, we aim to outline the rationale behind the employment of marginal solvents to produce stable solutions whilst rich in molecular aggregates, as an intermediate step toward the fast coating of unidirectionally aligned liquid-crystalline-like thin polymer films.

3.1. Formulations based on highly solubilizing, slowly drying solvents

The importance of the carrier solvent employed in the formulation has been the subject of early investigations in solution processed polymers, especially in the case of the model polymer regioregular poly(3-hexylthiophene) (*rr*-P3HT). These studies have mainly outlined the

adoption of high boiling point, slow evaporating solvents as well as slow drying deposition techniques (i.e. drop casting rather than spin coating) as a strategy to enable slow film growth, thereby inducing a higher degree of crystallinity and better ordered morphology.^[13, 114] Importantly, in these works, good solubility of the polymeric semiconductor in the carrier solvent is regarded as a fundamental prerequisite to avoid strong precipitation during solvent evaporation that may result in disconnected non-uniform films, which is particularly true in the case of fast deposition processes like spin coating. High boiling point solvents with superior solubilization allow for the formation of solvent-rich polymeric thin films after spin coating deposition without precipitation, and within the wet film, molecules can self-organize on a time scale which exceeds (even by several minutes) the duration of the spinning process to form uniform films supporting the thermodynamically favored microstructure. Such microstructure in the case of *rr*-P3HT is highly crystalline and characterized by efficient inter-chain π -stacking mostly oriented parallel to the plane of current flow.^[114] Nevertheless, in 2005, Yang et al.^[115] enriched the description of this scenario by deviating from the binomial between the degree of crystallinity of *rr*-P3HT, dependent on the duration of solvent drying, and its transport properties. Independent of the drying duration, which was kept constant at around 30 minutes in a variety of solvents by covering the cast drops with a Petri dish, they found that different solvents resulted in variable lamellar orientation distributions with respect to the substrate and different degrees of interconnectivity of the crystalline nanofibrillar domains comprising the polymeric film, from multi-spherulitic to continuous network conformation.

Since 2005 and driven by the necessity of superior control over the final film microstructure through solution processing and post-processing, many *non-directional* deposition techniques have been developed mainly inspired by the beneficial effect of slow evaporating processes on morphology and charge transport; the most relevant ones are presented in **Figure 5**.

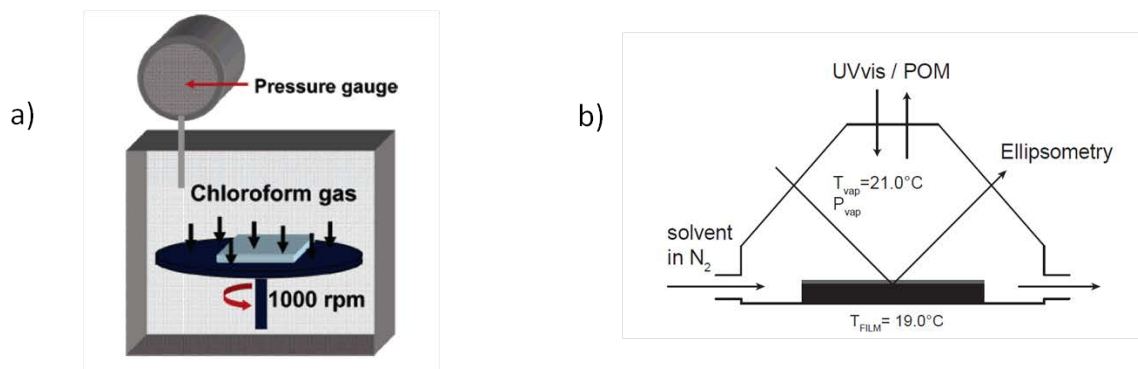


Figure 5. Sketches of the main isotropic deposition strategies based on slow solvent drying. a) Solvent vapor-assisted spin coating. Reproduced with permission from Ref. ^[116] Copyright 2006, American Chemical Society. b) Controlled vapor annealing. Reproduced with permission from Ref. ^[107] Copyright 2012, John Wiley & Sons, Inc.

Kilwon Cho's group realized a spin coating process inside a chamber with controlled temperature and solvent vapor pressure (chloroform: CF) during the deposition (**Figure 5a**), leading to the controlled monodimensional growth of ribbon-like *rr*-P3HT domains (width ~ 20 nm, height ~ 4 nm) whose length extended over micrometers.^[117] Apart from the first use for *rr*-P3HT-based FETs,^[116] this simple technique was then successfully applied to investigate the active role of polymer side-chains, on the one hand providing enough solubility for fine processing and on the other assisting self-assembling during film solidification, leading to a clear side-chain dependent fibrillar structure and transport.^[118] More recently, C. E. Park and co-workers adopted a high boiling point solvent additive strategy (5% chloronaphthalene (CN) into a CF solution) to induce higher crystallinity and superior transport properties of a group of DPP-based copolymers.^[119] In 2011, Ludwig's group largely revised and rationalized P3HT films formation and microstructure, and developed a smart strategy to finely tune the crystallization mode of P3HT films consisting of "swelling/deswelling".^[107] ^[120] The technique was based on the employment of a controlled solvent-vapor annealing process, using carbon disulfide vapor to transform solid semicrystalline films with an uncontrolled growth dynamic into wet films consisting of a concentrated solution of isolated and mobile P3HT molecules, where the effective concentration was tuned through the solvent vapor pressure (**Figure 5b**).

Recrystallization under different vapor pressure conditions allowed for good control of the nucleation density and, as a consequence, of the size of the spherulitic *rr*-P3HT domains.^[120] The domain dimensionality achieved with this technique, which is comparable to the micrometric channel length of a FET (many tens of micrometers), has allowed for the first direct measurement of transport anisotropy within a nanocrystalline morphology of quasi-parallel lamellae comprising π -stacked aggregates.^[107] While transport anisotropy has already been observed in liquid-crystalline or epitaxially-grown polymer films realized with dedicated techniques,^{[121] [122] [123]} this work represents the first demonstration of an anisotropic charge percolation within the self-seeded common spherulitic morphology of *rr*-P3HT polycrystalline film (**Figure 6**). Surprisingly, higher mobility was found in the direction perpendicular to the π -stacks (i.e. perpendicular to the radial growth of the spherulites, as evident in **Figure 5b**), deviating from the commonly accepted paradigm valid for small molecules indicating that transport properties are solely enhanced in the π -stacking direction in FET channels. This effect is better supported by the anisotropic grain boundaries (i.e. interconnectivity) model developed by Salleo and co-workers in which the nanocrystalline domains are bridged together across an amorphous interstitial zone through tie-molecules anisotropically distributed around each domain boundary.^[98] Thus, the lowest resistance to charge percolation generally occurs through aligned adjoining domains linked together through a high density of planar molecular segments, as presented in **Figure 6b**.

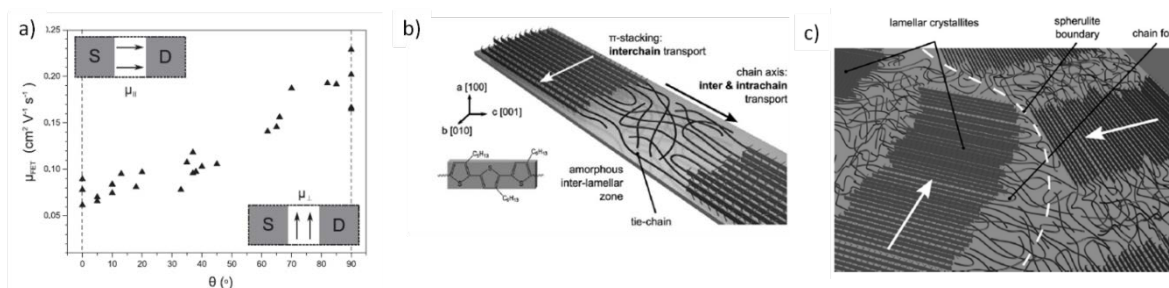


Figure 6. a) μ_{FET} within spherulites as a function of θ , the angle between the growth direction and the transistor channel conduction direction. The inset schematics show the spherulite growth direction in the transistor channels. b) Edge-on nanocrystalline lamellae comprising π -stacked aggregates (solid rectangles) with the π -stacking axis parallel to the radial growth

direction and the chain direction spanning the lamellar width separated by amorphous zones with occasional tie-molecules spanning adjacent lamellae. c) A diagram representing weakly interconnected spherulite boundaries. Reproduced with permission from Ref. ^[107] Copyright 2012, John Wiley & Sons, Inc.

3.2. Formulations based on marginal solvents

An alternative possibility to finely controlling film growth is offered by the use of marginal solvents (defined as solvents in which molecules tend to collapse so as to occupy a smaller volume and to reach minimum chain free energy) or poor solvents (defined as solvents in which attractive interactions between molecules dominate, mostly leading to phase separation), eventually used in a mixture with good solvents in which molecules exist in an expanded conformation,^[124] to guarantee ink stability and processability. One example is characterized by the use of apolar solvents for polythiophenes such as hexane, which are bad for aromatic backbones and good for alkyl side chains.^[125] In such formulations, polymer chains fold back on themselves into helical micelle-like structures favoring stacking interactions of the aromatic moiety and minimizing the unfavorable interaction between the poorly soluble backbone and hydrocarbon solvent. Depending on the concentration, 1D aggregation of helical conformed units can be induced already in solution, driven by the enhanced π - π interaction along the helical screw axes, leading to suspended particles with length up to several hundreds of nanometers.^[125] A recent molecular dynamics study has provided new insights on the conjugated polymer aggregation mechanism in solution, potentially useful as a guideline for a dedicated synthetic approach.^[126] In this work, Jackson et al. found that the solvation energy of a polymer is almost exclusively determined by the dispersive interaction sized by the number of π -electrons within the repeat unit rather than the electrostatic potential of the backbone, with the side chains mainly contributing through the steric interruption of π -system interaction. Thus, by using a solvent with low dispersive interaction, the polymer radius of gyration shrinks, leading to strong polymer aggregation.

Creating aggregates in solution prior to the deposition is an effective strategy to overcome the processing issues typically encountered with long drying deposition techniques. Under suitable conditions, polymer aggregates act as “precursors” for highly ordered microstructures in solid films, thus the fine tuning of solid film morphological features also becomes possible within the reduced time of a fast drying solvent. For example, in the case of *rr*-P3HT, Park et al. induced strong molecular aggregation, with aggregates dimension varying from 40 nm to 70 nm, as observed through dynamic light scattering, into a CF solution by adding a variable percentage of the poor-solvent acetonitrile.^[127] By keeping the concentration of the poor-solvent below a critical threshold, aggregate precipitation was avoided and highly ordered continuous films obtained even through fast and simple spin coating deposition. Field effect mobility and crystallinity comparable to those of films obtained passing through the slow evaporation of well-dissolved solutions or with vapor annealing post processing were then demonstrated. While the use of poor-solvent/good-solvent mixes was further adopted to induce solution aggregation and improve the transport of furan-containing DPP-based copolymers,^[128] other studies have demonstrated that it is possible to tune *rr*-P3HT aggregates content within a single marginal solvent by reducing the kinetic barriers to the thermodynamically favored aggregated conformation, either through very long aging,^[129] the application of low intensity ultrasound,^[130] or UV-irradiated solutions (**Figure 7**).^[131]

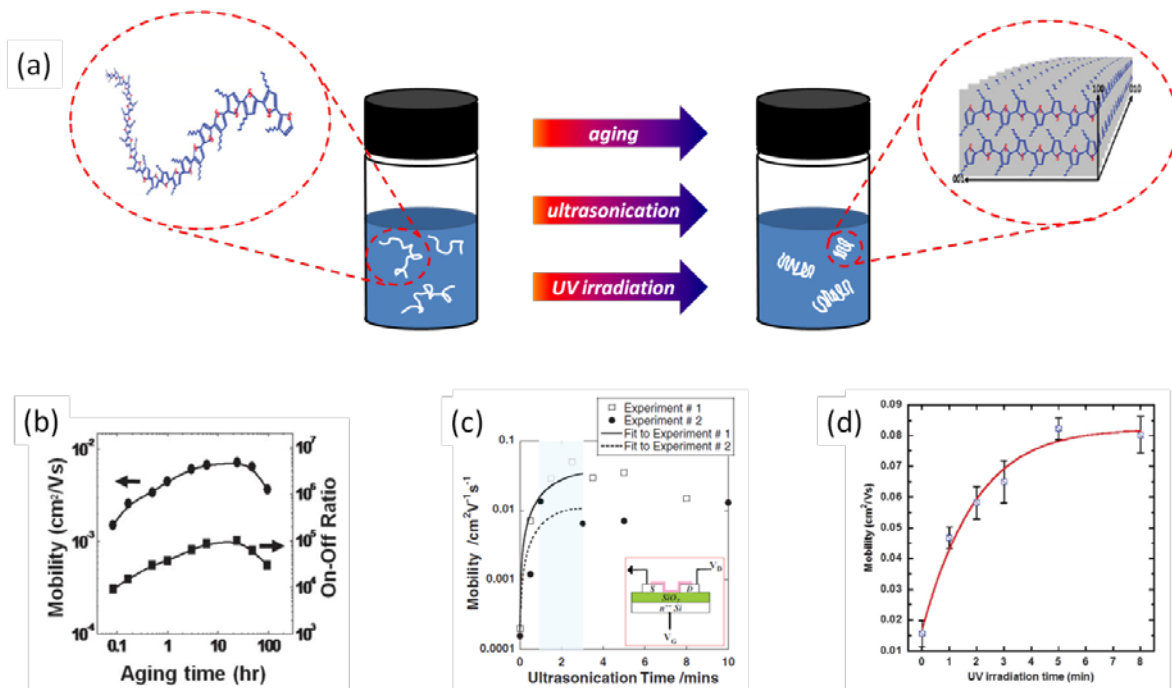


Figure 7. (a) The main strategies employed to enrich the aggregate content of a marginal solution of P3HT: solution aging, ultrasonication, and UV irradiation. (b) Field-effect mobility (left axis) and on-off ratio (right axis) obtained in the saturation regime of P3HT FETs as a function of aging time. (c) Evolution of field-effect mobility as a function of ultrasonication time (the inset shows the FET geometry used for testing). Mobility is calculated in the linear region of transistor operation using $V_{DS} = -3$ V. Solid and dashed lines are shown simply to provide a visual guideline to highlight the saturation of the field effect mobility. (d) Average field-effect mobility of P3HT films spin coated from CF based P3HT solutions irradiated by UV for specific times. Mobility is calculated in the saturation regime of operation with $V_{DS} = -80$ V. Reproduced with permission from Ref ^[130] ^[131]. Copyright 2011 and 2014, John Wiley & Sons, Inc.

Aging a methylene chloride solution of *rr*-P3HT was found to increase the average size and dimensionality of the microstructural domains obtained from spin coating, which passed in several hours from round shaped dots to well defined and increasingly interconnected rod-like structures with improved field-effect mobility (**Figure 8**).^[132] This strategy has also been employed to improve the transport properties of poly[(4,4-didodecyldithieno[3,2-b:2',3'-d]silole)-2,6-diyl-alt-(2,1,3-benzothiadiazole)-4,7-diyl], especially when scarcely solvating solvents like tetrahydrofuran and toluene are employed.^[133]

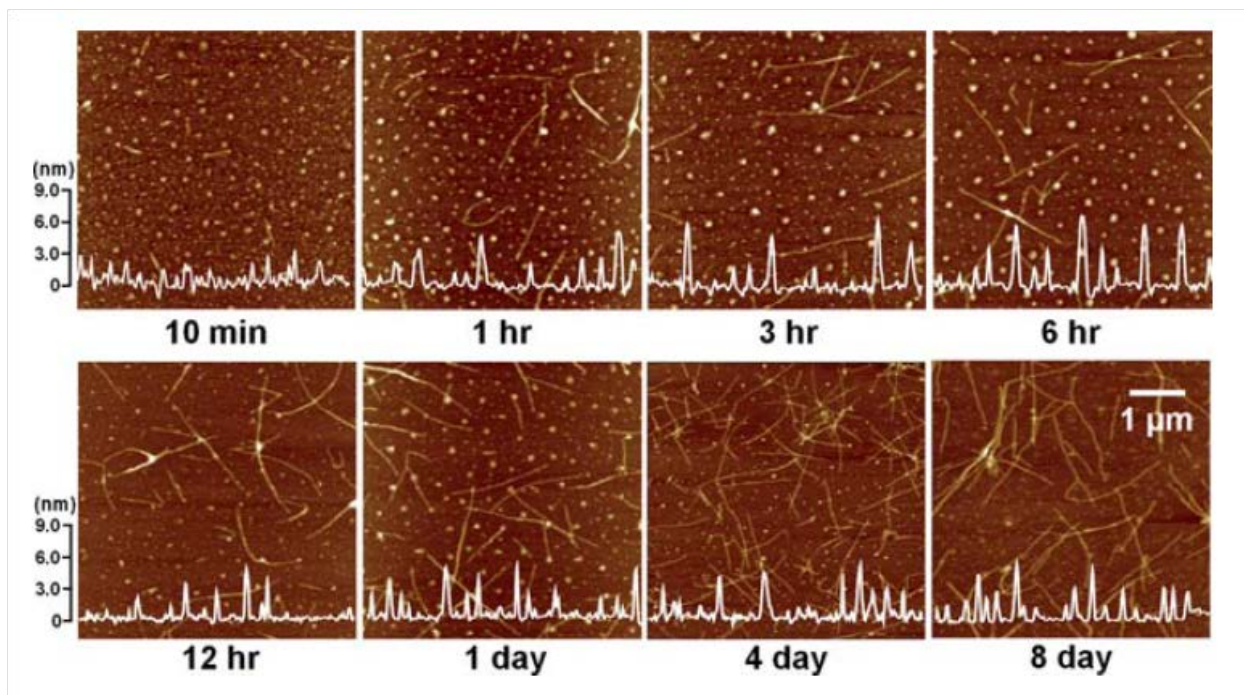


Figure 8. Tapping-mode atomic-force microscopy (AFM) height images of P3HT films prepared from 0.0005 wt% precursor solutions after various aging times. A clear transition with aging time from round shaped dots to increasingly interconnected rod-like structures can be observed. Reproduced with permission from Ref. ^[132] Copyright 2011, Royal Society of Chemistry.

According to the ultrasound strategy, it has been suggested that the flow fields created by ultrasonic irradiation results in a shear-induced conformational change of the individual polymer chains, thereby reducing inter-chain entanglement and finally promoting π - π stacking. An initial rapid increase in mobility of two orders of magnitude was observed for films deposited from solutions subjected to 1 min of sonication, followed by slow saturation with sonication time, in agreement with a scenario of percolation characterized by a threshold in the film crystallinity.^[130] The use of low intensity ultrasound on *rr*-P3HT formulations was investigated also by other groups with systematic studies as a function of molecular weights, solvents and concentrations.^{[134] [135]} Such studies confirmed the scenario suggested by Ayiar et al.^[130] and clearly show that macromolecules are highly entangled in solutions, which probably include coils, aggregates, as well as micro-crystallites. Polymer chains are gradually disentangled via ultrasonication, resulting in improved molecular and aggregates diffusivity,

formation of micro-crystallites already in solution, and formation of highly textured fibrillar films. Very interestingly, enhanced charge transport properties upon solution ultrasonication have been found in cases of high molecular weight molecules ($M_w = 68$ kDa), while low molecular weight ($M_w = 35$ kDa) resulted in reduced mobility. This is explained by accounting for the very limited number of entanglements and tie-molecules in low M_w solutions; disruption of the few entanglements of the polymer chains in solution while generally leading to improved thin-film crystallinity drastically reduces crystallite interconnectivity. By varying the molecular weight, polydispersity index (PDI), and degree of regioregularity of *rr*-P3HT directly spin cast from marginal solvents after proper sonication, Lee et al. were able to tune polymer chains assembled from 1D (fibrils) to two-dimensional (2D, nanoribbons) structures with mobility values exceeding 0.07 cm²/Vs without any post-processing, which is an interesting result considering the easiness and velocity of the deposition method employed.^[136]

Differently, the aggregation mechanism induced by UV irradiation encompasses an intermediate step of photoexcitation of the conjugated molecules, resulting in a change of chain conformation which stabilizes higher backbone planarity and enhanced π - π interaction.^{[137] [138]} Such UV-induced backbone rigidity reduces solubility and promotes molecular aggregation in solution.^[131] Chang et al. found that upon UV irradiation, both inter- and intra-molecular ordering of solutions and films are increased, resulting in increased crystallinity and transport properties as a consequence.^[131] Interestingly, they compared the effectiveness of UV irradiation with ultrasonication and finally concluded that UV irradiation results in an inferior degree of molecular ordering but much longer nanofibrils length (>1 μ m vs. < 300 nm), thus leading to higher macroscopic mobility, again highlighting the importance of interconnectivity within the several microns long FET channel.

Marginal solvents have also been employed in the post-treatment of polymer films. Dipping of preformed thin films into marginal solvents allows for further structuring of thin films without

dissolution and can also remove the lower molecular-weight polymeric fraction that may form isolated microstructures with a bad impact on transport properties.^{[139] [140]}

So far, we have highlighted how polymer film crystallinity can be controlled by tuning the content of aggregates in polymer solutions or by exposing solid films to marginal solvents. Within this scenario, the case of the model high electron mobility, polymer semiconductor P(NDI2OD-T2) is peculiar: as demonstrated in 2012 by Steyrlleuthner et al., despite clear signatures of a solvent-dependent aggregation mechanism, a rapid chain self-collapse (i.e. chains folding back on themselves) dominates films formation upon solvent drying independently on the solvent employed, thus inhibiting any diversification of crystalline content of P(NDI2OD-T2) solid films processed from different formulations.^[141] In other words, differently from P3HT, film-aggregate content tends to be independent of solution concentration. Moreover, an apparent insensitivity of P(NDI2OD-T2) transport properties to drastic thermally-induced micro-structural changes (i.e. edge-on vs. face-on, high crystalline vs. low crystalline films, and naphthalene-naphthalene stacking vs. naphthalene-thiophene stacking) has been mentioned in many reports, keeping open the question on the specific transport mechanism and bottleneck dominating the charge percolation.^{[142] [143] [144] [145]} Nevertheless, in 2013, Luzio et al. reported the possibility of fine tuning the transport properties of P(NDI2OD-T2) films by varying the processing solvent (**Figure 9a, b**).^[113] Independently of the boiling point of the solvent, a two orders of magnitude increase in field-effect mobility was registered by depositing the film from solvents such as toluene or mesitylene that induce a high degree of aggregation in solution with respect to films processed from solvents such as CN which do not form aggregates. This occurred in spite of identical content in aggregates within the deposited solid films owing to a liquid-crystal-like long-range orientational order induced through the employment of marginal solvents (as evidenced by the birefringence patterns reported in **Figure 9c** and d) within the short time of the spin coating process (30 s). Such orientational order is clearly associated with the orientation of fibrillar structures less than

10 nm wide observed in the topography of the film, within which the molecular backbones are oriented parallel to the fiber axis (**Figure 9e**).

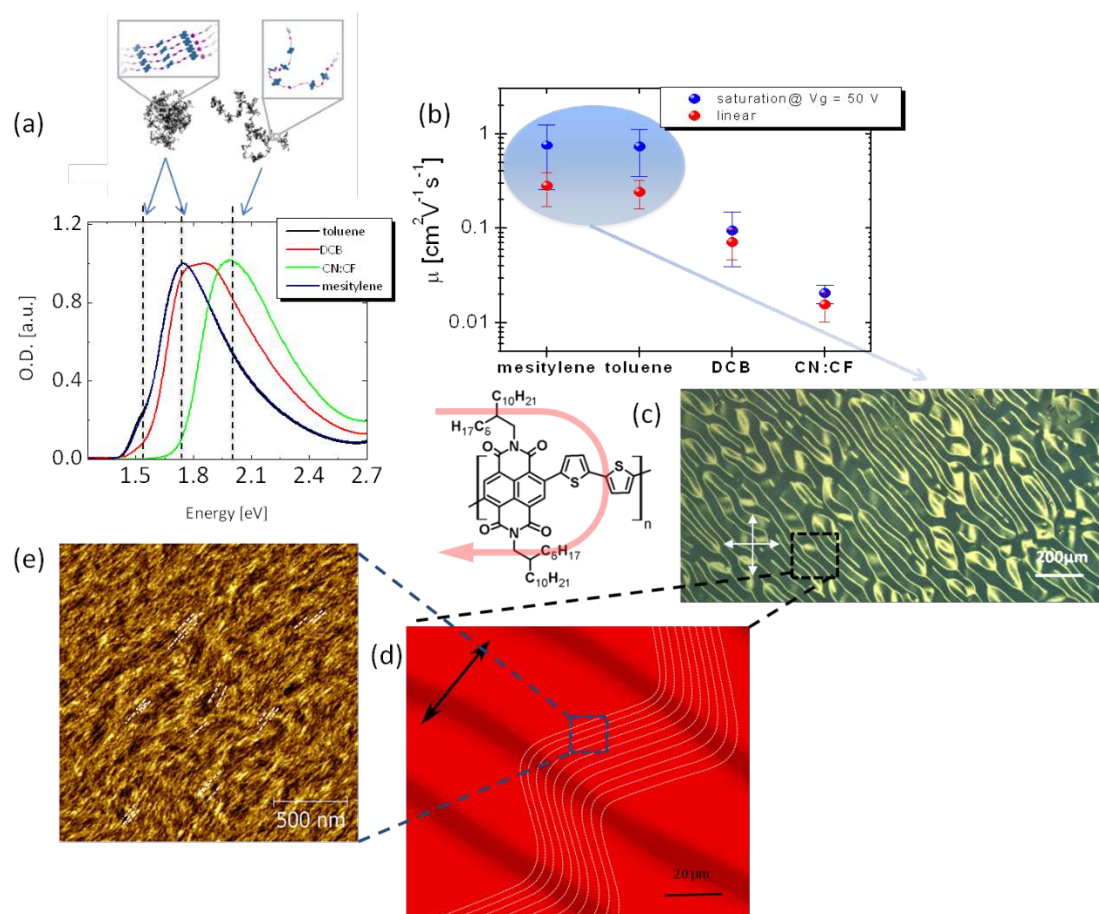


Figure 9. a) UV-Vis spectra of P(NDI2ODT2) dissolved in a mixture of CN:CF (80:20), dichlorobenzene (DCB), toluene and mesitylene; spectral signatures of aggregated species (low energy bands) and extended single molecules (high energy band) are highlighted (dashed lines). Marginal solvents like toluene and mesitylene have the highest aggregation content in solution, while DCB has a lower one and CN:CF has none. Adapted with permission from Ref ^[141]. Copyright 2012, American Chemical Society. b) Average linear and saturation mobility values of FETs based on P(NDI2OD-T2) films spun from different solvents; a neat increase in mobility going from good (CN:CF) to marginal (toluene and mesitylene) solvents can be observed. c) Birefringence pattern of P(NDI2OD-T2) films spun from marginal solvents; a clear liquid-crystal-like regular pattern can be observed along the whole covered area. d) Diagram of the molecular backbone alignment within the liquid-crystal-like pattern of the film, as extracted by polarized optical microscopy (POM). Areas with two distinct alignment directions can be observed, one orthogonal to the other, separated by an intermediate transition area. e) AFM image of a film spun from marginal solvents; a fibrillar morphology can be observed with strongly aligned, less than 10 nm wide fibrils, all of them parallel to the backbone direction of alignment (white dashed guidelines follow the fibrillar direction). Reprinted with permission from Ref ^[113]. Copyright 2013, Springer Nature.

Charge modulation spectroscopy (CMS) has been adopted to explore the energetic environment of the charges within the channel of working FETs, evidencing that the charge carrier is

similarly localized independently of the solvent employed (**Figure 10a**).^{[146] [147] [148] [149]} As previously underlined, since the aggregate content does not vary in different films, this suggests a situation in which short-range morphology is substantially independent of the solvent employed and transport is mainly sized by the degree of long-range directional alignment arising from the use of marginal solvents. This in agreement with a scenario of improved interconnectivity along the fibrillar direction. The high degree of orientational order within the channel induced by solution aggregates has been clearly depicted and quantified using charge modulation microscopy (CMM), where CMS is coupled with a confocal microscope.^{[21] [150]} CMM is a micro-spectroscopy tool where CMS is coupled with a confocal microscope, and it is able to map the orientation of the charged polymer segments which are involved in the transport of a working FET and their degree of orientational order (DO), defined as the ratio between the anisotropic signal, sensitive to the probe polarization, and the total signal. With this technique, just few micrometers wide regions of coherent molecular orientation were observed in films spun from DCB solutions, with an average DO of ~ 20% and local values of more than 50%. Conversely, many tens-of-micrometer areas of coherent orientation within charge segments were mapped in films spun from toluene (marginal solvent) displaying an extraordinarily high degree of order approaching 100% (**Figure 10b-e**).

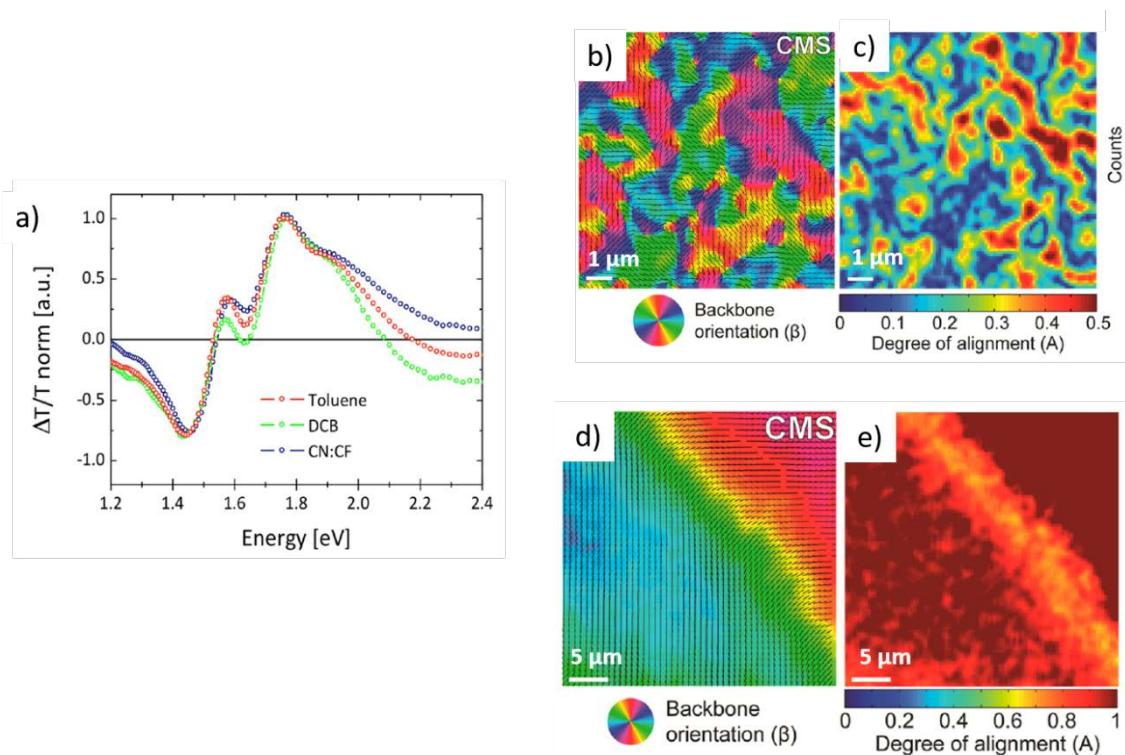


Figure 10. a) CMS spectra of films spun from toluene (red line), DCB (green line), and CN:CF (blue line) measured on semitransparent working FETs. The main peaks in both bleaching (positive signal) and absorption (negative signal) bands coincide independently on the solvent employed. Charge is thus hosted in a similar local packing conformation and is comparably localized. Reprinted with permission from Ref ^[113]. Copyright 2013, Springer Nature. Quantitative analysis of the local alignment of conjugated segments probed by charge via a CMM investigation: (b,d) angular map of the preferential charged segments orientation in the case of films spun from DCB (b) and toluene (d). (c,e) Local degree of orientational order (DO) of films processed from DCB (c) and toluene (e). Reprinted with permission from Ref ^[150]. Copyright © 2014, American Chemical Society.

In order to rationalize the observation of large directional domains in coated films from highly aggregated solutions, Bucella et al. investigated the early stages of growth of films deposited by different techniques such as spin coating and inkjet printing.^[22] In both cases, they found that at first a monomolecular layer that highly interacts with the surface is formed, with molecules filling up the wetted substrate surface prior to allowing the growth of a subsequent layer. Only after the completion of the first layer (as a function of concentration), the subsequent layers, which experience a low surface energy, start to deposit according to the typical fibrillar pattern (**Figure 11 a-g**). Specific to each deposition method, the independence of the growth mode from the drying dynamics and from the time scale suggests that the films usually grow

rapidly at the solution-substrate interface rather than at the drying front; this is especially exemplified in the case of an ink-jetted isolated drop of P(NDI2OD-T2) ink, which, despite the drop confinement and consequent complex drying,^[151] still results in the aforementioned layered growth (Figure 11 h-l).^[21]

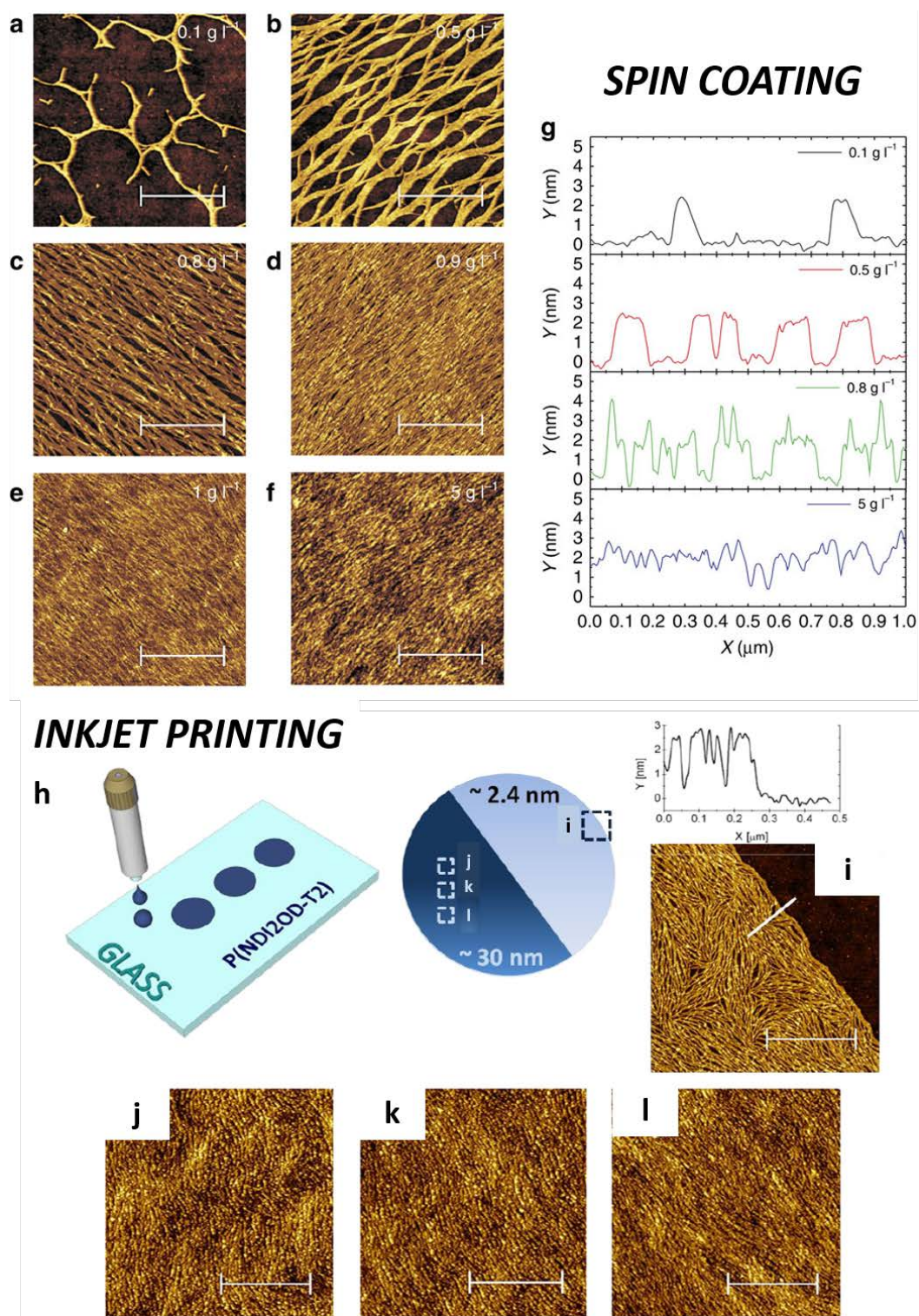


Figure 11. (a-g): AFM images of P(NDI2OD-T2) films spin coated from solutions with concentrations of (a) 0.1, (b) 0.5, (c) 0.8, (d) 0.9, (e) 1, and (f) 5 g/l. In (g), the section analysis of a–c and f is reported. (h) is a representation of the inkjet-printing process for the deposition of disk-shape films; a ~30 μm disk-shaped, ~2.4 nm-thick submonolayer is formed when inkjet printing a single 1 pl droplet of 5 g/l in mesitylene (see the profile), and (i) only at the disk edge do fibrils align along the contact line owing to pinning-induced confinement. In contrast, no preferential alignment is observed in the inner part of the disk, which is consistent with surface adhesion forces dominating the layer deposition rather than solvent evaporation. (j) to (l) AFM pictures taken from three different positions of a ~30 nm-thick disk-shape film obtained by multiple jetting in the same position. Similar to the spin coating results, thicker inkjet-printed films result in a fibrillar topography and in long-range alignment, in this case forming concentric rings. During the film formation, clear drop de-pinning occurs when the first layer(s) is (are) formed, and the contact-line freely flows toward the center during the drying. The ring-like alignment of supramolecular units is most likely connected to the circular shape of the drop edge along with the contact-line dynamics during the evaporation. Reprinted with permission from Ref ^[21]. Copyright 2015, Springer Nature.

The demonstration of the P(NDI2OD-T2) liquid-crystal-like macro-patterning allowed by solution preaggregation strongly suggests the transition through a lyotropic mesophase (i.e. a liquid-crystal behavior mediated by polymer dissolution) during film solidification under a specific force field. A direct observation of such lyotropic phase was reported by Pan et al. in 2015.^[113] They observed that solutions of aggregated P(NDI2OD-T2) were responsive to magnetic forces resulting in strong alignment through the application of a magnetic field during the deposition. According to this evidence, we can conclude that P(NDI2OD-T2) marginal solvent solutions already display liquid-crystalline characteristics before solidification at a stage where aggregates are sufficiently large and ordered and display large enough anisotropy of magnetic energy to be aligned by a magnetic field and initiate the formation of macroscopically orientated domains (**Figure 12a**).^[152] The handling of polymeric semiconductors with inherent liquid-crystalline characteristics is particularly appealing because it allows easier control of molecular assembling over macroscopic areas. Clear demonstrations of the beneficial influence of mesophase transitions in molecular assembling, and thus transport properties, are represented by well-established semiconducting polymers. A well-known case is pBTTT, which presents a thermotropic transition to a smectic mesophase at the relatively low temperature of 180 °C^[73] ^[153]. Poly-9,9' dioctyl-fluorene-co-bithiophene (F8T2) and poly(9,9-

dioctyl-fluorene-co-benzothiadiazole) (F8BT), two well-established nematic liquid-crystalline semiconducting polymers, have been efficiently aligned on large areas, in pioneering works.^[121, 154] To do so, the authors exploited the topographic features and the favorable crystal structure^[155] of nanostructured, anisotropic polymeric substrates, namely rubbed poly(p-phenylenevinylene)^[154] and rubbed polyimide^[121, 156], with a mechanism similar to epitaxial growth of conventional solid crystals.^[157] Within the mesophase, the semiconductor chains are oriented as a consequence of the interaction with the aligned chains of the substrate.^[158] Along the same line, other smectic and nematic liquid crystalline semiconductors have been successfully aligned on top of other alignment layers, i.e. on pre-aligned PTFE^[122] and photo-aligned films of polyimides (Azo-PIs),^[159] demonstrating the great potential of liquid crystalline semiconductors in the field of printed electronics. An important attempt to produce a general description of the chemical characteristics needed for a conjugated polymer to gain liquid-crystalline characteristics was carried out in 2013 by Kim and co-workers: they identified as key aspects a tendency to chain planarization upon solution free-volume reduction, a tetrahedral carbon linker with out-of-plane bonding, and bulky side chains to avoid interdigitation along the film thickness.^[112] Nevertheless, the demonstration of lyotropic mesophases enabled simply by solution preaggregation offers the chance of high structural control on large areas of many high mobility polymeric semiconductors already in use. Attempts in this direction were proposed by Lu et al. who measured *in situ* the optical anisotropy of a *rr*-P3HT in an *o*-DCB solution in a capillary and observed a strong birefringence in solution, thus demonstrating that *rr*-P3HT nanowires had already formed and not grown upon solidification, and that nematic alignment was induced by shear stress forces within the capillary.^[160] Interestingly, both the estimated degree of alignment and wires aspect ratio in solution corresponded to those observed after drying in the solid films. Similarly, Reichmanis and co-workers employed capillaries to study the time-dependent formation of P3HT nanostructures and their lyotropic liquid-crystalline behavior in a trichlorobenzene (TCB) solution (**Figure**

12b).^[161] They also developed a capillary system through which, in addition to shear stress for domains alignment, good hole (P3HT) and electron (P(NDI2OD-T2)) transporting conjugated polymers were subjected to sequential cooling followed by low-dose UV irradiation in order to control the nucleation and the growth of 1D nanoaggregates suspended in solution (**Figure 12c**). Furthermore, they observed a strong influence of the applied shear stress on the domains dimensionality and on their inner microstructural parameters (*i.e.* π -stacking distance); thus, strongly improved transport properties were demonstrated in films spin coated from such treated solutions with P3HT mobility reaching a value of $0.16 \text{ cm}^2/\text{Vs}$.^[162]

We have illustrated how lyotropic behavior can be induced in solutions of polymeric semiconductors, both through synthesis and solution formulation and processing. It is worth observing that lyotropic solutions are interesting because they pave the way to the development of smart low-temperature film-processing strategies, mainly based on the employment of external forces directly applied upon film solidification. On the one hand, such strategies, when compared to those based on highly solubilizing solvents, offer the advantage of a rapid and effective film micro-structuring, while on the other, as specifically reported in Sections 4.3 and 4.4, they can result in the one-step deposition of unidirectionally aligned films on large-area substrates with exceptional control of the inherent anisotropic transport properties of the polymeric film. For all these reasons, they represent a concrete chance of implementation in low time- and energy-consuming cost-effective continuous production lines.

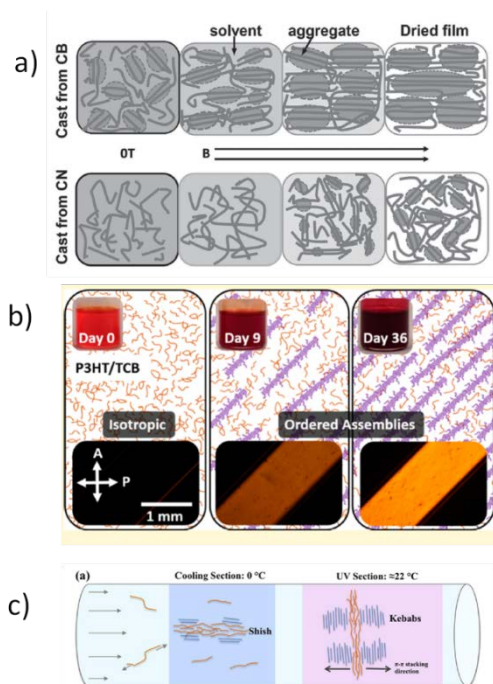


Figure 12. a) Schematic illustration of the magnetic alignment process in the formation of the P(NDI2OD-T2) film cast from chlorobenzene (CB) (top) and CN (bottom) under a high magnetic field. The thick lines denote the chains of P(NDI2OD-T2). Reproduced with permission from Ref. ^[152] Copyright 2015, John Wiley & Sons, Inc. b) Change in absorption as a function of capillary orientation with respect to a polarizer; POM images of a filled capillary on day 0, 9, and 36, showing increasingly linear dichroism. P3HT nanofibers (purple) oriented within the capillary are also presented. Reproduced with permission from Ref ^[161]. Copyright 2015, American Chemical Society. c) Schematic of the flow-cooling-UV system and proposed mechanisms of nucleation and growth. In the cooling section, solution instability and shear force cause the formation of shish nuclei. The π - π stacks align with the flow as they grow longer in the UV section. Reproduced with permission from Ref ^[162]. Copyright 2015, American Chemical Society.

4. Techniques for the unidirectional alignment of polymer films

In this section, we review some of the most effective techniques in achieving directional alignment of polymer films and their resulting electronic performances in FETs. Starting from a brief review of post-processing techniques on preformed films, we then report on methodologies based on the direct alignment of polymer chains subjected to flows and/or capillary actions during film formation. In the latter case, we first focus on highly effective approaches based on laboratory-scale demonstrations, and we make a distinction between techniques based on slow drying times and highly solubilizing solvents and on formulations inducing preaggregation in solution, which enable faster deposition methods. Finally, we report

on unidirectional coating and printing techniques, which are again demonstrated at the laboratory level but are compatible with highly scalable large-area processes.

4.1. Post-processing methods

The possibility of increasing polymer conductivity by alignment of polymer chains has been known for a long time, with very early experiments making use of mechanical stretching.^[163] As an example, conducting polymers films such as undoped and doped polypyrrole (PPy) were stretched by a hand-made apparatus of propylene carbonate by Osagawara et al. in 1986^[164] and later on by Nogami et al. in 1994.^[165] Such stretched films, which reached up to twice their original length, showed high electrical conductivity in the direction parallel to the stretching direction, up to 2000 S/cm in Nogami's work. Other pioneering works from 1992 and 1993 of Dyreklev et al. demonstrated the possibility to gain high alignment level and charge transport anisotropy in a FET by stretching Poly(3-octylthiophene) on a polyethylene support, with a maximum elongation of 4.5× and charge transport anisotropy of 4×. Interestingly, superior transport properties along the chains alignment directions rather than the π -stacking direction were observed.^[166, 167] More recently, on the basis of a delamination/lamination strategy proposed by Chabinye et al. in 2004,^[168] PDMS supports have been employed to first delaminate, stretch and finally laminate on OFET substrates polythiophenes semiconductor films, such as P3HT^[169] and pBTTT.^[153] In the case of P3HT, a maximum strain of 140% was applied, resulting in 9× higher mobility along the chains alignment direction compared to the π -stacking direction. In case of pBTTT, upon mesophase transition, an optical dichroic ration of ≈ 9 and a transport anisotropy factor higher than 10 were obtained with a 50% strain, leading to a mobility value of 1.7 cm²/Vs along the chain alignment direction, which is among the highest published for this material.

Besides mechanical stretching, rubbing has been one of the most exploited post-processing alignment techniques.^[170] Rubbing is traditionally performed by means of slow laboratory

procedures with the assistance of temperature, but is compatible with large-area processes and has been widely used for the alignment of polyimide substrates used in flat-panel liquid crystals displays (LCDs), as this allows the anisotropic epitaxial orientation of the liquid crystals.^[158, 170] The molecular orientation of the rubbed layer is affected by the cumulative effect of rubbing passes and depth, strength of rubbing, and substrate temperature. Heil and co-workers reported that mechanical rubbing perpendicular to the source and drain contacts increased the charge mobility of P3HT transistors of up to 800% ($1.4 \times 10^{-3} \text{ cm}^2/\text{Vs}$) with an additional annealing procedure.^[171] Furthermore, Yang et al. showed that the ordered domains of a rubbed P3HT film are mostly oriented with the c-axis directed along and b-axis perpendicular to the rubbing direction, showing significant anisotropy in their optical absorption and photocurrent.^[172] A high temperature during the rubbing process remarkably improves the alignment of conjugated films, an effect attributed to the increased plasticity of the polymer films.^{[173] [174]} In the case of pBTTT (**Figure 13**), a packing motif modification of crystalline domains from edge-on to face-on was verified after rubbing at high temperature. The high in-plane orientation of the films led to high mobility anisotropies, exceeding a factor of 70.^[173] Mechanical rubbing has also been applied to electron transporting semiconductors such as P(NDI2OD-T2) (**Figure 13**), for which highly oriented films with a high degree of in-plane chain alignment and improved charge transport along the alignment direction were achieved.^[174]

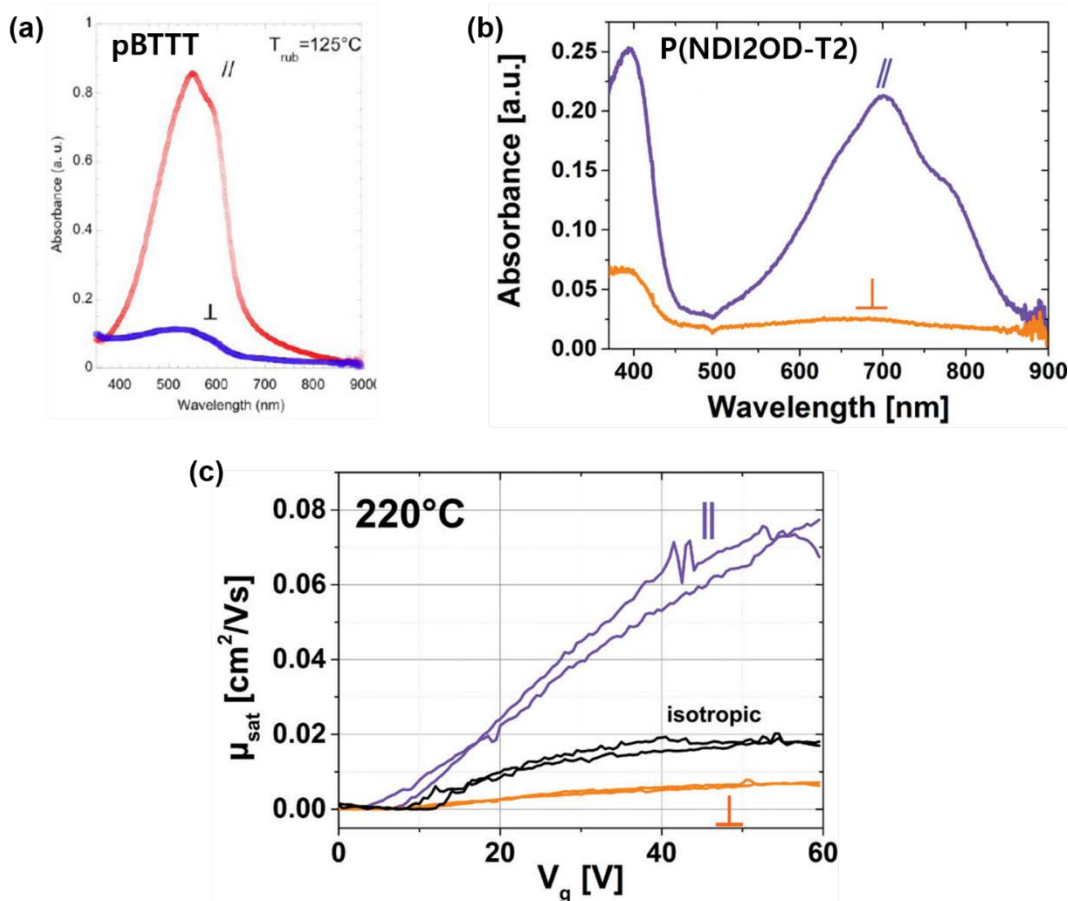


Figure 13. UV–visible polarized optical absorption of oriented (a) C12-pBTTT and (b) P(NDI2OD-T2) film after the rubbing process with parallel and perpendicular incident light polarization. (c) Mobility measurements of non-aligned and aligned samples of P(NDI2OD-T2) annealed at 220°C as a function of gate voltage. For the aligned samples, mobility was measured parallel ($\mu_{//}$) and perpendicular (μ_{\perp}) to the rubbing direction. Reproduced with permission from Ref. ^[173]. Copyright 2013, American Chemical Society and reproduced with permission from Ref. ^[174] Copyright 2014, John Wiley & Sons, Inc.

4.2. Techniques based on directional drying

A specific effort in exploiting engineered formulations to produce directional aligned polymer microstructures directly during film deposition has been carried out since 2006, when Brinkmann and Wittmann exploited a consolidated directional solidification method using crystallizable solvents (presented in **Figure 14**)^{[175] [155] [176]} to obtain mixed face-on and edge-on *rr*-P3HT lamellae up to 200 nm wide and well oriented along the drying direction.^[177] Briefly, a gradient of temperature along the substrate was employed to directionally cool down a mixture of *rr*-P3HT and 1,3,5-TCB. In the first step, cooling produced the directional crystallization of TCB along the gradient direction; as a consequence of the ongoing

crystallization, the concentration of *rr*-P3HT progressively increased until aggregation and crystallization of *rr*-P3HT occurred at the TCB crystals surfaces, which acted as both nucleating and orienting surfaces for the polymer. When Salleo and co-workers implemented such formed films into a FET architecture, they observed strong transport anisotropy with superior mobility along the lamellar axes (i.e. perpendicular to the π -stacking), overcoming mobility values of cast devices with much stronger edge-on character,^[123] an effect again rationalized through the more efficient control of the anisotropic grain boundary orientation.^[98]

Another notable example of unidirectional drying is dip coating, where a substrate is immersed in a solution and withdrawn at a controlled speed. The thin film is formed on the substrate upon gravitational draining and solvent evaporation in competition with viscous force, surface tension, and gravity.^[178] There are several reports on the fabrication of polymer FETs by dip coating, which allows good control over the semiconducting layer thickness. For dip-coated ultrathin P3HT films consisting of only 2 – 3 monolayers, Wang et al. reported mobility up to 0.20 cm²/Vs higher than that achieved by drop casting and spin coating.^[179] Improved structural order was observed in UV absorption spectra of the dip-coated film, showing a lower onset energy for absorption and a better-resolved vibronic structure. The morphology of pBTTT film was controlled by tuning the pulling speed of substrate from the solution reservoir,^[180] highlighting the role of the first monolayer in the microstructure evolution into the bulk film during the dip coating. At the lowest pulling speed of 2 μ m/s, a continuous long-range aligned polymer fibrous film with a high anisotropy ratio of ~20 was achieved. Furthermore, Li et al. demonstrated the controllable growth of aligned monolayers as multilayer microstripes of organic small molecules by varying pulling speed, where lower pulling speeds produced mixed multilayer and higher pulling speeds yielded monolayer microstripes over large areas.^[181] With a similar methodology, Wang et al. reported unidirectional nanofiber growth of P(NDI2OD-T2):^[182] at the lowest pulling speed of 2 μ m/s, long-range aligned films were obtained with the highest electron mobility of 0.06 cm²/Vs.

Unidirectional drying can also be achieved in confined structures. In 2011, Liu et al. induced the directional evaporation of carbon disulfide from a *rr*-P3HT solution by confining wet-cast films with a poly(dimethylsiloxane) (PDMS) top layer and constraining solvent evaporation from the edges of the wet film;^[183] this process resulted in *rr*-P3HT nanofibrils with the main axis well aligned along the drying direction.

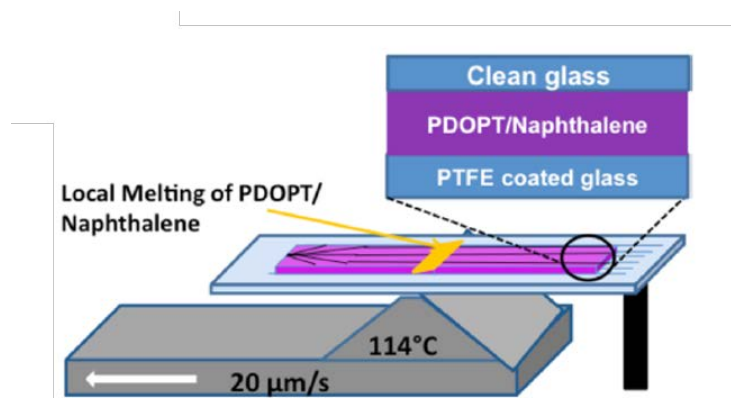


Figure 14. Techniques based on directional drying using a crystallizable solvent (naphthalene) successively playing the role of (i) a solvent for polymers in liquid form and (ii) once crystallized, the substrate for the epitaxial crystallization of the polymer. In brief, a polymer solution, in this example regioregular poly(3-(2,5-dioctylphenyl)thiophene) (PDOPT), is spread between two clean glass slides by capillary force. One glass substrate is coated with an oriented film of poly(tetrafluoroethylene) (PTFE) to guide the in-plane crystallization of naphthalene. The sample is moved to a homemade system allowing for the local zone melting of naphthalene at a setting temperature of 114°C and a translation speed of 20 $\mu\text{m s}^{-1}$. After directional crystallization of naphthalene, the polymer films are orange, indicating that they are non-crystalline, presumably because the polymer film is still swollen with naphthalene. The films are placed in a freezer at -6°C for 1 min to lower the high vapor pressure of naphthalene and induce crystallization of the polymer, indicated by a color change to violet-purple. The films remain crystalline at room temperature. Naphthalene is removed by sublimation under a primary vacuum, leaving a highly oriented film of polymer on the glass substrate. Reproduced with permission from Ref. ^[176] Copyright 2016, American Chemical Society.

Macroscopic alignment of semiconducting polymer films was then demonstrated by combining directional solvent evaporation and substrate templating effects. Highly ordered polymer films were demonstrated using the capillary action of nanogrooves fabricated on silicon substrates by scratching the surface with diamond-lapping films that acted on a solution confined between two substrates set face-to-face with two glass spacers in between to form a tunnel-like

configuration (**Figure 15**).^{[18] [43]} The process starts with the injection of the solution into the tunnel structures followed by slow drying (~5 hours) within a Petri dish. With respect to other approaches, the enclosed tunnel configuration enables a higher degree of control over solvent evaporation. After optimization of the capillary action of the functionalized spacers, long-range aligned regioregular poly[4-(4,4-dihexadecyl-4H-cyclopenta[1,2-b:5,4-b']dithiophen-2-yl)-alt-[1,2,5] thiadiazolo[3,4-c]pyridine] (PCDTPT) showed highly oriented crystalline films with a compact lamellar structure and improved transport properties, as a consequence (mobility values reported in Figure 15 need to be re-evaluated on the basis of reference^[45]).^[17]

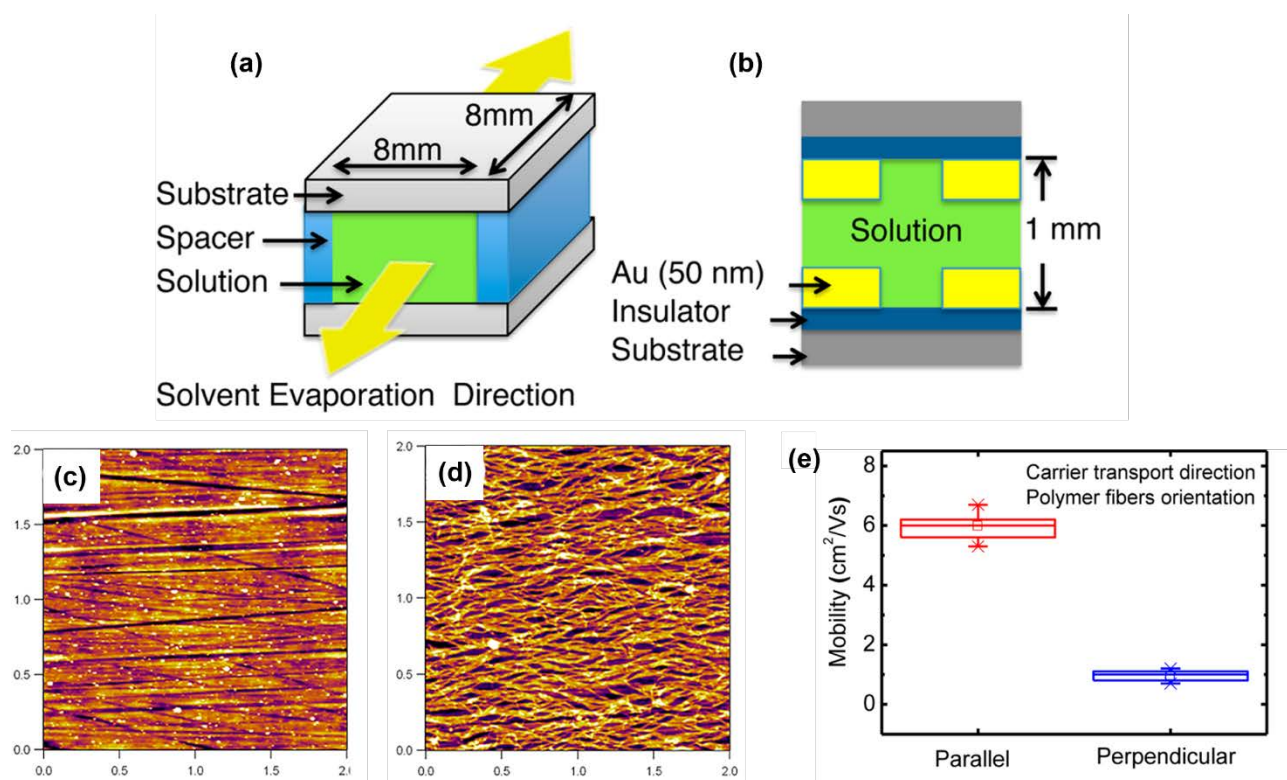


Figure 15. Diagrams of the tunnel-like configuration setup (a) and directional solvent drying (b). (c) AFM images of (d) the dielectric surface and (b) polymer fibers on a 250 nm structured surface. (e) Anisotropic mobility of the devices with carrier transport parallel or perpendicular to the polymer fiber orientation, to be re-evaluated on the basis of reference^[45]. Reproduced with permission from Ref^[43]. Copyright 2012, American Chemical Society.

More sophisticated substrate templating strategies can represent very powerful tools to support the controlled film directional growth in case that the evolution of the drying front is exploited as the main driving mechanism. Notably, Amassian and collaborators recently proposed an interesting and novel approach for easily programming and controlling the otherwise stochastic

nucleation process of small-molecule semiconductors, allowing the coherent and geometrically controlled evolution of the crystallization front.^[184] The aligned structures demonstrated in this work benefit from the thickness dependent nucleation behavior of small-molecules, while analogous control of their nucleation and crystallization has also been achieved by chemically tailoring the source/drain contacts interface, yielding crystalline films extending into the transistor channel, by Gundlach et. al.^[185] Both these approaches could in principle provide interesting synergies with directional drying techniques, both lab-scale and large area (like zone casting, see section 4.4.4.), although their application to polymers has yet to be demonstrated, to the best of our knowledge.

4.3. Off-center spin coating and other laboratory-scale film alignment strategies

A very simple and effective method that does not require waiting for long drying times and allows for the fast coating of highly ordered and oriented thin films is off-center spin coating.^[44] The method exploits the centrifugal forces of the common spin-coating process, which can be controlled and made uniform over the target substrate by placing the sample at a specified distance from the spin center (**Figure 16a**). We dedicate part of this section to describe its use as it is a very accessible methodology and has thus become a tool in widespread use, in order to study charge transport in highly aligned polymer samples.

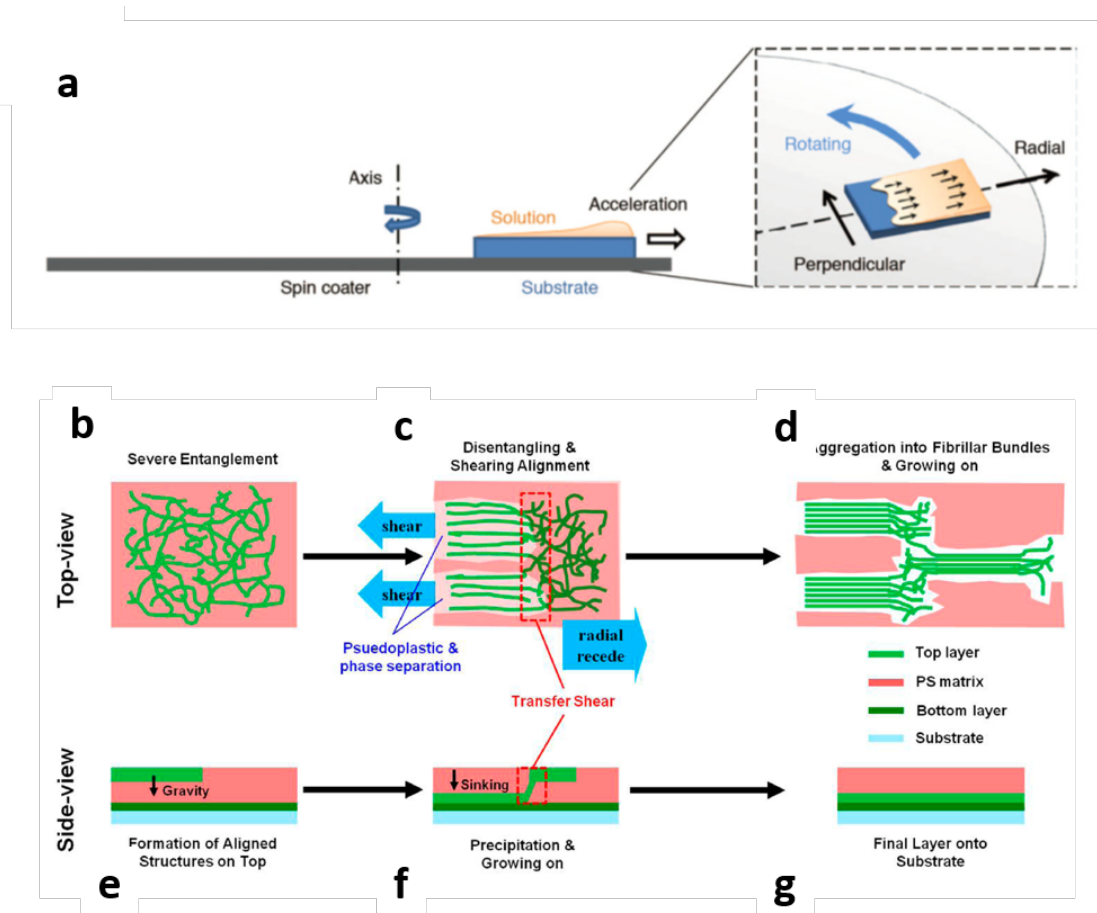


Figure 16. (a) Schematic of the off-center spin-coating process, where the substrates are located away from the axis of the spin coater. Reproduced with permission from Ref. ^[44]. Copyright 2014, Springer Nature. (b)-(g) Formation process of aligned fibrillary PDBT-TT bundles. Reproduced with permission from Ref. ^[186]. Copyright 2012, American Chemical Society.

Off-center spin coating was first convincingly reported by Bao and co-workers for the deposition of highly aligned films of a blend comprising a small molecule semiconductor, 2,7-dioctyl[1]benzothieno[3,2-b][1]benzothiophene (C8-BTBT) and a polymer insulator, polystyrene (PS).^[44] Despite the fact that no transport anisotropy was measured, a remarkably high mobility was demonstrated in such formed films (although extracted in the low V_{GS} range and to be critically revised according to Ref. ^[45]), thanks to the peculiar metastable molecular packing induced through the fast freezing of the highly ordered microstructure typical of this deposition method. Moreover, on the one side, the PS here contributed to increase the solution viscosity and thus to obtaining improved film continuity, and on the other to passivate traps at

the dielectric poly(4-vinylphenol) (PVP) semiconductor interfaces caused by the hydroxyl groups on the PVP chains.

The same technique was also later demonstrated to be effective for the directional deposition of semiconducting polymers and polymer blends. Wang et al. demonstrated well-aligned fibrillar bundles of a semiconducting DPP-based co-copolymer in a blend with PS.^[186] The authors reported that the pseudo-plastic nature of the blend in solution allowed for good shear force transfer to the polymer chains, resulting in chain disentanglement and fiber aggregation at the top liquid surface due to shear friction with air. Upon solvent evaporation, the dynamics of recession of the (three-phase) contact line matched with the solvent evaporation rate through the right choice of solvent and spin speed, and promoted the directional solidification of the fibrillar nanostructures, thus contributing to the final film alignment (**Figure 16 b-g**).

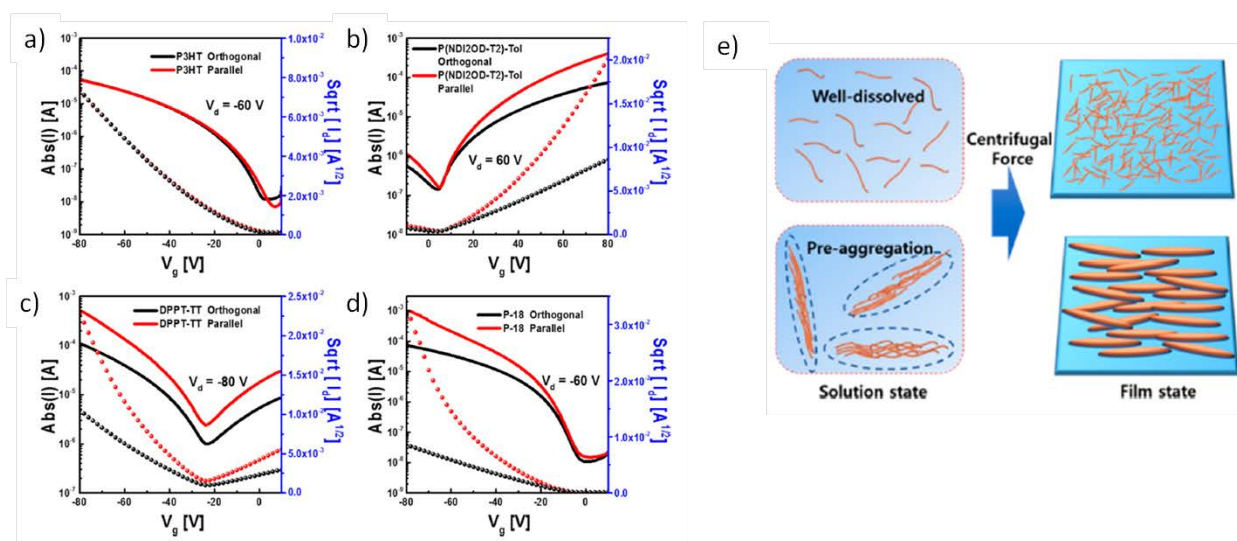


Figure 17. Transfer characteristics of anisotropic (a) P3HT, (b) P(NDI2OD-T2), (c) DPPT-TT, and (d) P-18 OFETs ($W/L = 1.0 \text{ mm}/20 \mu\text{m}$), highlighting superior transport properties in the direction parallel to backbone alignment. (e) Schematic illustration of well-dissolved and preaggregated polymer in solution and solid-state; aligned polymer films are obtained when a high degree of preaggregation is present in the solution, and deposition is performed by off-center spin coating. Reprinted with permission from Ref. ^[187] Copyright 2015, American Chemical Society.

The off-center spin-coating strategy is effective in achieving unidirectional alignment of pristine polymer films starting from preaggregated solutions, as described in Section 3.2, without necessarily requiring the addition of an insulator in a blend to induce pseudo-plastic

behavior to the wet film. Matsidik et al. first reported an improvement in field-effect mobility with off-center spin coating of different batches of P(NDI2OD-T2) with controlled molar mass and synthesized both by Stille and direct arylation polycondensation.^[188] When adopting commonly used centered spin coating with 1,2-DCB as the carrier solvent, mobility values in a wide range from 0.1 to 0.6 cm²/Vs have been obtained, while using the marginal solvent toluene and placing the substrate at a distance of 3.5 cm from the center during the spinning, much higher and more reproducible saturation mobility values (average $\mu_{\text{sat}} = 2.6$ cm²/Vs, maximum $\mu_{\text{sat}} = 2.9$ cm²/Vs) were achieved. The unidirectional alignment of polymer films was then generalized by Kim et al. who studied a wider set of polymer semiconductors, recognizing and rationalizing the role of the aggregates content as a fundamental prerequisite to obtain large transport anisotropy with spin centrifugal forces without requiring blending with inert matrices (**Figure 17 a-d**).^[187] Remarkably, in this work, hole mobility of 7.3 cm²/Vs with 37-fold transport anisotropy between the direction radial and tangential to the spinning was demonstrated, using the good hole transporter donor-donor copolymer poly[(E)-1,2-(3,3'-dioctadecyl-2,2'-dithienyl)ethylene-alt-dithieno-(3,2-b:2',3'-d)thiophene], a polymer characterized by a highly rigid and planar backbone that already strongly favors aggregation in solution.^[189] The independence of the aggregate-induced alignment from the solvent boiling point, previously demonstrated in case of standard spin coating by Luzio et al.^[21] and described in Section 3.2, was further confirmed by depositing P(NDI2OD-T2) via off-center spin coating both from CB (good solvent, higher boiling point) and toluene (marginal solvent, lower boiling point): much better transport properties and higher anisotropy were recorded in the case of the more volatile toluene. Using CMM, it was shown that the degree of molecular alignment was much higher when considered only in the top surface of the polymer film rather than in the whole bulk. Such an effect was attributed to the high adhesive force in direct contact with the substrate (high surface energy), thereby impeding coherent alignment of the whole bulk. The alignment process via off-center spin coating can be ascribed either to the radial flow fields

induced within the wet film, effectively aligning the aggregates present in the solution in virtue of their elongated shape (**Figure 17e**)^[190] or to the directional shear friction at the liquid air interface, as previously observed by Wang et al.^[186]

It is worth mentioning that when lyotropic phases (like solutions of polymer aggregates) are involved, effective film alignment can also be achieved with standard centered spin coating or simple solution casting, by exploiting the capillary forces acting on a pre-patterned nanogrooved substrate, as largely demonstrated in the cases of F8T2^[121] ^[159] and other high mobility polymeric semiconductors.^[112] ^[191] We end this section by reporting on a very smart laboratory-scale directional deposition technique, based on compressing a thin liquid film of a fairly diluted polymeric solution, dropped onto an ionic liquid surface.^[192] By adopting this strategy, Yamashita et al. demonstrated band-like transport characteristics of uniaxially-oriented CDT-BTZ-based FETs along the backbone direction.^[68]

4.4. Large-area compatible and scalable single-step unidirectional alignment methods

In this section, we describe laboratory experiments on unidirectional alignment of polymer semiconductors with techniques that are potentially highly scalable and compatible with large-area processing, namely solution shearing, blade coating, slot-die coating, zone casting, and wire-bar coating. The methods covered herein have demonstrated efficient alignment by producing transport anisotropy and a noticeable increase in charge mobility, and they can all be classified under the general class of meniscus-guided coating, in which the relative unidirectional motion of the solution meniscus with respect to the substrate produces shear stress on the fluid that promotes alignment. In general, the fundamental operational parameters of this class of deposition techniques are the coating speed, substrate, and solution temperature. Additionally, control over the alignment of polymer semiconductors must also take into account complex substrate-solution-air interactions, multi-phase heat, and mass transport in the proximity of the meniscus as well as solvent evaporation rate.^[190]

4.4.1. Solution shearing

In solution shearing, an organic semiconductor solution droplet is confined between the substrate and a top movable blade that can be positioned parallel or tilted with respect to the substrate. By moving the top blade at a fixed speed on a temperature-controlled substrate, solvent evaporation is restricted at the edges where the solution meniscus is exposed. This special drying kinetic has been reported to induce a strained lattice of modified π - π stacking distance, which may be instrumental in enhancing charge transport properties. Several examples of improved mobility with respect to other non-uniaxial deposition techniques have been achieved in the case of small molecule semiconductors, as first reported by Becerril et al. in 2008 (**Figure 18**).^[193] In this context, a particularly notable result was achieved by Diao et al. in 2013 with 6,13-Bis(triisopropylsilylethynyl) (TIPS)-pentacene by modifying the blade with specifically designed pillars to control the solution flow and by controlling nucleation through carefully designed surface energy patterning, thereby attaining large non-equilibrium TIPS-pentacene single crystals and a recorded mobility value for this material of $8.1 \pm 1.2 \text{ cm}^2\text{V}^{-1}\text{s}^{-1}$ (maximum $11 \text{ cm}^2\text{V}^{-1}\text{s}^{-1}$) (Figure 18).^[194]

The same technique applied to a polymer semiconductor was first reported in 2005 by Hiroshi Yabu and Masatsugu Shimomura (and later exploited by Makoto Karakawa et al.^[195] in an OFET structure) who achieved a certain degree of alignment and ordering in a *rr*-P3HT film, but induced only a modest increase in mobility by a factor of two with respect to spin-coated films (maximum mobility: $0.06 \text{ cm}^2\text{V}^{-1}\text{s}^{-1}$).^[196] The reasons behind such a moderate improvement have been provided in a recent work by Giri et al., in which they showed that molecular packing of P3HT is not significantly affected by different shearing conditions and thus is not of benefit to strained metastable crystalline structuring such as in the case of small molecule semiconductors.^[197] Indeed, the same work suggests that interdigitated thiophene-based polymers with relatively high crystallinity, such as poly(2,5-bis(thiophene-2-yl)-(3,7-

dihepta-decanyl tetrathienoacene) (P2TDC17FT4) and pBTTT, deposited by shear coating, are susceptible to increased disorder in the alkyl chain packing, which in turn limits transport properties due to the formation of strained lattices with higher lamellar distance compared to stable structures.

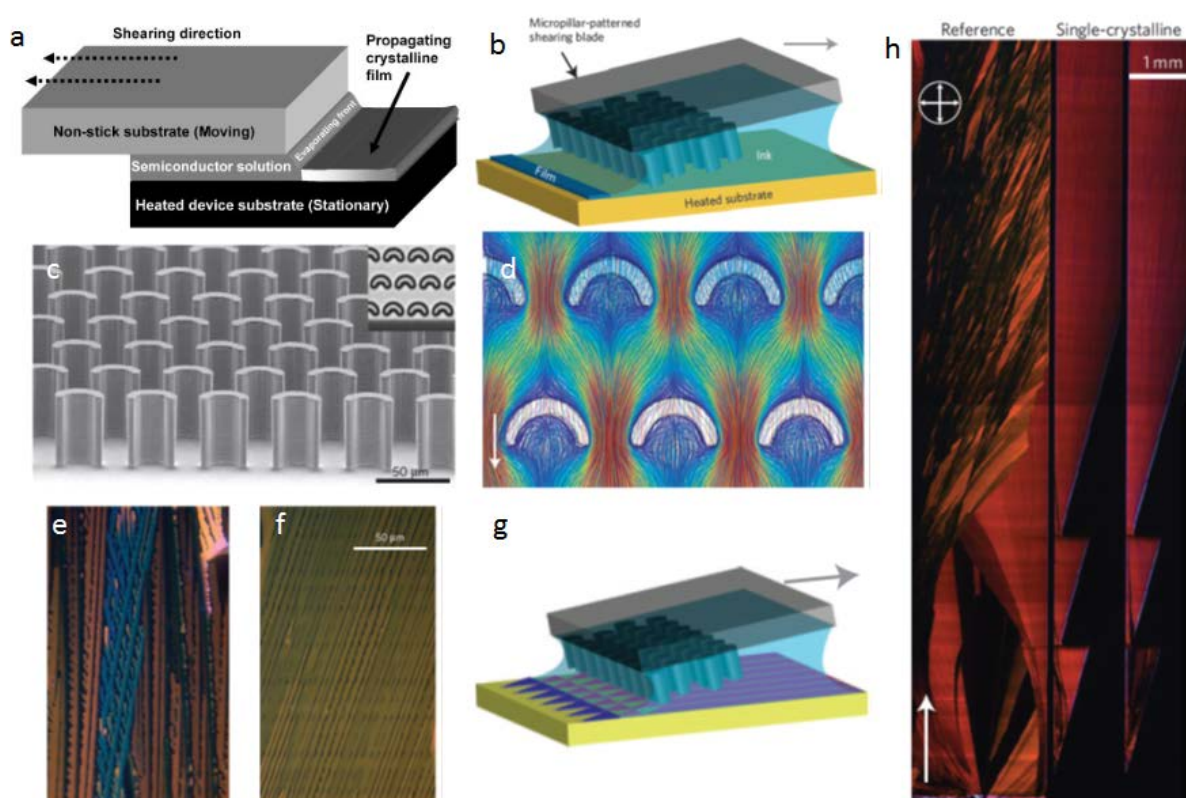


Figure 18. (a, b) Schematic of solution shearing using a standard rigid blade and a micropillar-patterned one (for clarity, the micropillars are not drawn to scale and the arrow indicates the shearing direction). (c) A scanning electron micrograph (SEM) of a micropillar-patterned blade (inset: top view of the micropillars under an optical microscope). (d) Streamline representation of simulated fluid flow around the micropillars (the arrow indicates the flow direction, and the streamlines are color coded to indicate the scale of velocity, ranging from 0 mm s^{-1} , deep blue, to 1.3 mm s^{-1} , dark red). (e, f) Cross-polarized optical micrograph of a TIPS-pentacene film coated from its mesitylene solution with (f) and without (e) micropillars. (g) Schematic of solution shearing with a micropillar-patterned blade on a surface energy-patterned substrate (the arrow indicates the shearing direction). (h) Cross-polarized optical micrograph of a TIPS-pentacene film coated from a solution in mesitylene on a micropillar-patterned blade: on a standard substrate (left) and a surface energy-patterned one (right). Reproduced with permission from Ref ^[193] and ^[194]. Copyright 2008, John Wiley & Sons, Inc and Copyright 2013, Springer Nature, respectively.

A remarkable demonstration of the aligning capability of shear coating, as well as preliminary evidence of the importance of preaggregation for the alignment process, was provided by Lee

et al. in two consecutive works on the investigation of the electronic transport properties of a family of diketopyrrolopyrrole-selenophene (PTDPPSe) copolymers featuring hybrid siloxane solubilizing groups (**Figure 19**).^[41,42] In particular, their first study mainly assessed the impact of siloxane terminated hexyl chains on the molecular packing of the ambipolar PTDPPSe copolymer with hybrid siloxane-solubilizing group SiC6 (PTDPPSe-SiC6), demonstrating how the π - π stacking distance was positively affected when long alkyl chains were substituted with hybrid siloxane moieties that minimized steric repulsion between the side chains. Nonetheless, the same report provides some evidence of improved molecular ordering and morphology in the case of shear-coated films, as indicated by the formation of larger interconnected nanofibrillar structures compared to the case of drop-cast films of PTDPPSe-SiC6. The extent to which side-chain engineering and the deposition technique concur in improving the performances of this D-A system was better exposed in their following work, in which the alkyl spacer length of the hybrid solubilizing side chain was systematically tuned to control the molecular structuring as well as to indirectly favor the formation of aggregates in the liquid phase. Indeed, when the alkyl spacer goes from 6 to 5 or 4 carbon atoms (PTDPPSe-SiC6 to PTDPPSe-SiC5 or PTDPPSe-SiC4, respectively), the authors witnessed the extensive formation of dense nanofibrillar structures with interconnected domains. The poor solubility of PTDPPSe-SiC4 did not allow filtration of the solution, which seems to imply the presence of a higher number of aggregates in the liquid phase acting as nucleation sites for the fibrils. For this reason, the fibrils of PTDPPSe-SiC4 films appeared smaller compared to those of the PTDPPSe-SiC5 film whose improved solubility allowed for a reduced presence of aggregates. AFM images clearly show that these fibrils were subject to good alignment when shear coating was chosen as the deposition technique, and this effect, along with the enhanced crystallinity of PTDPPSe-SiC5 films compared to PTDPPSe-SiC4 ones, is likely the reason behind the superior electrical performance achieved by the former. Hence, the average mobility measured for PTDPPSe-SiC5 was at least three times greater than spin-coated and drop-cast films for

both holes and electrons (despite a correction of mobility values reported in the work is needed, according to reference ^[45]).

The positive impact of controlled polymer preaggregation in solution on the performances of solution sheared films was later investigated by Lee et al.^[198] The researchers similarly demonstrated the formation of uniaxially aligned nanofibrillar film morphologies by controlling the size and mutual interaction of preaggregates in solution, although in this case the approach relied on an optimized mixture of good and marginal solvents rather than side-chain engineering. In agreement with the previously reported studies, the transport property enhancement was attributed to the elongated nanofibrils, although an improved molecular packing was also noticed in shear-coated films compared to spin coated ones.

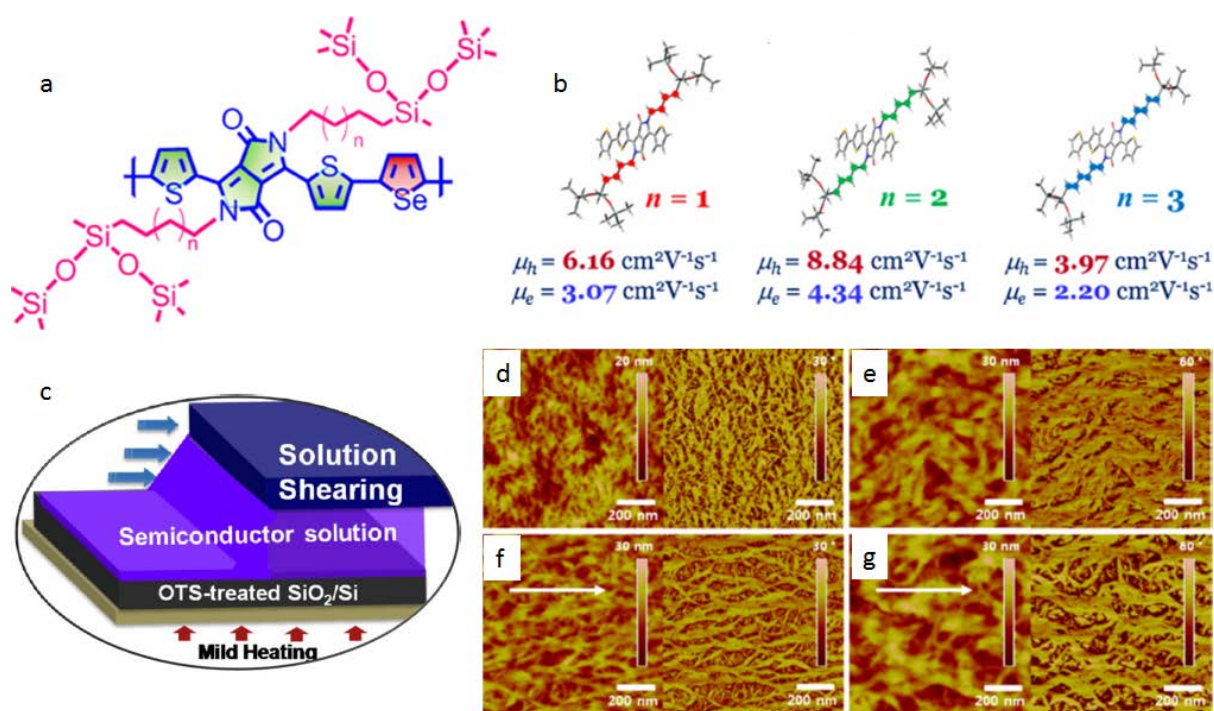


Figure 19. (a, b) Chemical structures of PTDPPSe-SiC4, PTDPPSe-SiC5, and PTDPPSe-SiC6, designed to allow systematic investigation of siloxane-terminated side chain-dependent molecular packing and FET performance. (c) Schematic illustration of the solution-shearing technique and substrate configuration: an OTS-treated SiO₂/Si wafer. (d-g) AFM height (left) and phase (right) images of solution-processed polymer films annealed at 220°C. Drop-cast films of (d) PTDPPSe-SiC4 and (e) PTDPPSe-SiC5. Solution-sheared film of (f) PTDPPSe-SiC4 and (g) PTDPPSe-SiC5 (the arrow indicates the shearing direction). Reproduced and adapted with permission from Ref. ^[41] ^[42] Copyright 2012 and 2013, American Chemical Society.

4.4.2. Solution shearing with soft or flexible blades

All the aforementioned studies relied on a standard solution-shearing technique that exploits a rigid blade, usually a glass or silicon substrate, but there are examples in the literature of slightly different approaches, such as the works of Shin et al.^[199] and Schott et al.^[67] in which the rigid element is substituted by a plastic material. In particular, the researchers in the former study employed a shearing blade composed of a PDMS mold in which a set of rectangular microgrooves acted as template for the polymer semiconductor film formation (**Figure 20**). The resulting films were organized into a few micrometer-wide micro-patterned prisms of a DPP-based copolymer flanked by thiophene (PTDPP-DTTE), characterized by higher hole mobility compared to films obtained either by spin coating or solution shearing with a rigid blade (spin coating: $2.7 \text{ cm}^2\text{V}^{-1}\text{s}^{-1}$, standard shear coating: $4.5 \text{ cm}^2\text{V}^{-1}\text{s}^{-1}$, and template-guided shear coating: $6.8 \text{ cm}^2\text{V}^{-1}\text{s}^{-1}$). The authors attributed the improvement in the transport properties to the larger contact area between the blade and the solution, which produced a greater degree of polymer alignment and increased the strain applied to the polymer chains, as suggested by the reduced π - π distance.

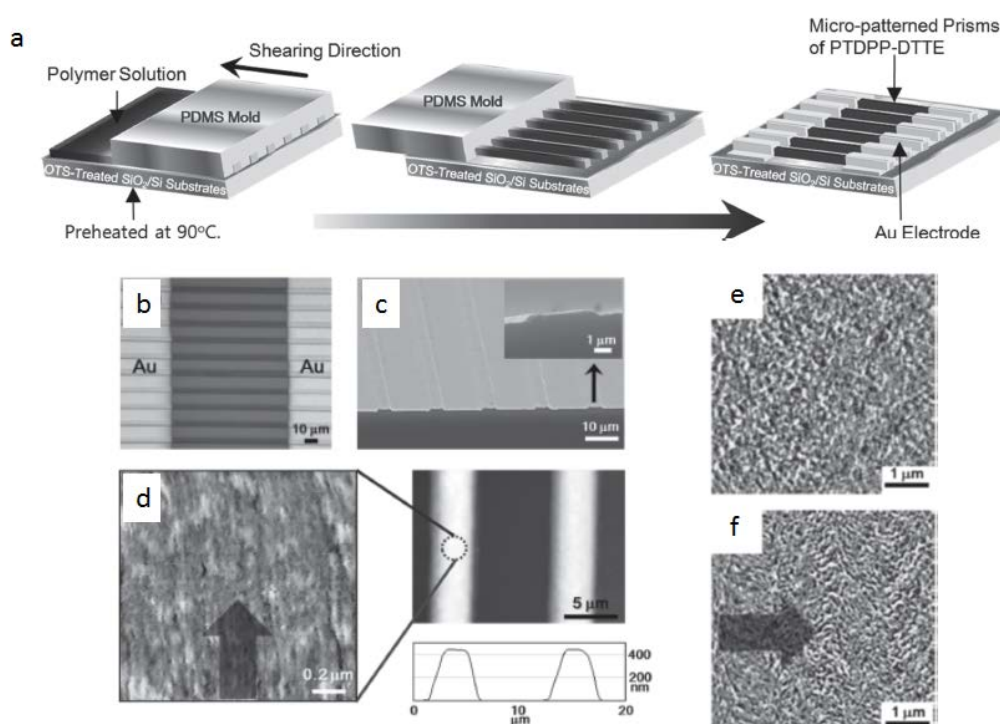


Figure 20. (a) Template-guided solution shearing method using a PDMS mold with uniaxially aligned microgrooves. (b) Optical microscopy image of micro-patterned prisms of PTDPP-

DTTE between a pair of Au electrodes. (c) A SEM of PTDPP-DTTE line patterns on a silicon wafer substrate (inset: magnified image of a single prism). (d) AFM image ($1.4\ \mu\text{m} \times 1.4\ \mu\text{m}$) of the upper surface of a prism, 2D image, and line profile (the arrow indicates the shearing direction). (e, f) AFM images of a spin-coated film (e) and solution-sheared film of PTDPP-DTTE polymer (f) (the arrow indicates the shearing direction). Reproduced with permission from Ref ^[199]. Copyright 2014, John Wiley & Sons, Inc.

In the second work, Schott et al. modified the standard shear coating technique by adopting a flexible, solvent-resistant perfluoropolyether blade on a similar D-A ambipolar material, a DPP-benzotriazole (DPP-BTz) copolymer (**Figure 21**).^[67] This approach proved to be extremely effective in obtaining highly aligned films, as confirmed by extensive optical, structural, and morphological characterization. Moreover, the study further underlines the relevance of polymer preaggregation in solution, as the use of this modified solution-shearing technique in conjunction with preaggregating solvent CB provided relevant insight into the experimentally evident correlation between film characteristics and charge transport anisotropy. Interestingly, the degree of alignment in the bulk appeared to be lower compared to the surface where the charges accumulated (OFETs in top-gate/bottom-contact configuration). This effect, possibly due to the deposition process, resulted in a lower ratio between the parallel and perpendicular mobilities compared to the expected value, which should have been in the order of the dichroic ratio of polarized absorption. Nonetheless, the mobilities extracted for aligned DPP-BTz films highlight remarkable anisotropy, reaching values of almost $7\ \text{cm}^2\text{V}^{-1}\text{s}^{-1}$ along the chain direction. It is noteworthy that these films also exhibited band-like charge transport along the chain direction above 270 K. As it can be thus deduced from these studies, shear coating is expected not only to enhance the mobilities of conjugated polymers but also, more importantly, to serve as a powerful and controlled deposition method for the study and understanding of the charge transport mechanism in high-mobility polymers.

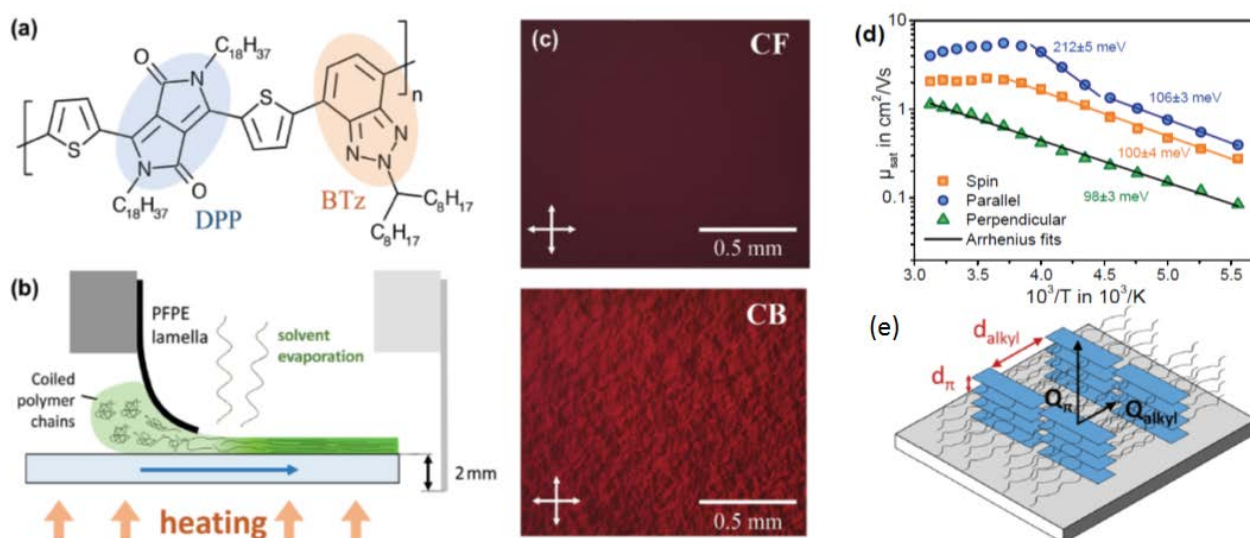


Figure 21. (a) Chemical structure of DPP-BTz. (b) Schematic of the shearing setup. The sample is fixed on top of a heated stage and can be moved beneath the lamella at speeds from $73 \mu\text{m s}^{-1}$ to 1.75 mm s^{-1} . (c) Optical microscopy images of DPP-BTz films spun from CF and CB. The samples are placed between two perpendicular polarizers (indicated by arrows on the images). Crystallites with polymer backbones parallel to one of the polarizers remain dark while those at 45° are brightest. (d) Temperature dependence of the mobility for spin-coated and aligned FETs, highlighting transport anisotropy. Arrhenius fits are labeled with the respective extracted activation energies. (e) Schematic of the face-on backbone orientation of DPP-BTz. Reproduced with permission from Ref ^[67]. Copyright 2015, John Wiley & Sons, Inc.

4.4.3. Blade coating

Blade coating, also known as knife coating, is a large-area processing method compatible with both rigid and flexible substrates. This technique involves the deposition of a controlled amount of ink on a given substrate in the proximity of a rigid blade, and the subsequent relative movement of the substrate with respect to the blade. Typically, in laboratory-scale processing, the blade is moved over a flat surface, while the blade is fixed over the moving substrate in large-scale roll-to-roll (R2R) processes. The main controlling parameters are the gap between the blade and substrate, the coating speed, and the substrate temperature; further coating parameters such as the surface energy of the substrate, and the surface tension of the fluid and its viscosity allow for suitable control of film microstructure formation. An evident difference in this technique with respect to solution shearing or slot-die is the fact that the entire solution droplet, effectively acting as solution reservoir, is exposed to the environment.^[190]

The potential of blade coating for large scale fabrication of multi-layered fully-printed organic devices has been demonstrated in a number of studies,^{[200] [201] [202]} but the ability of this meniscus-guided deposition method to efficiently align polymer semiconductors has recently been proved by Chu et al. with P3HT nanofibers obtained by preaggregation in solution.^[203] In accordance with what was previously described in Section 3.2, the formation of nanofibrillar aggregates of P3HT in a marginal solvent was obtained by a combination of a fixed-time UV-irradiation treatment and different solution-aging periods, and the resulting materials were later deposited by spin and blade coating (**Figure 22**).

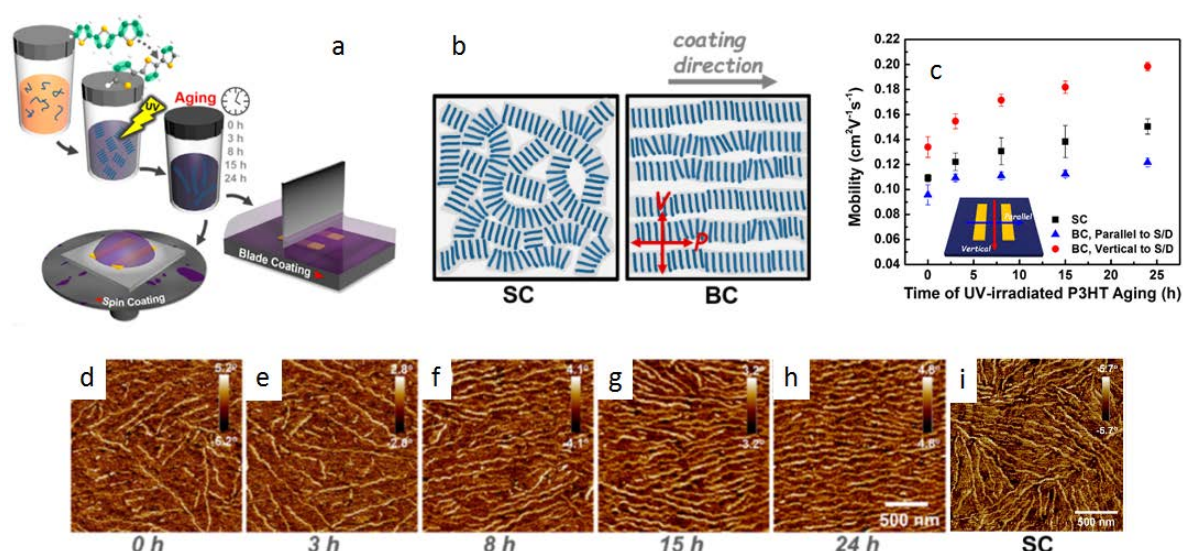


Figure 22. (a) Representation of the preaggregation inducing treatments (UV-irradiation and solution aging) and of the deposition techniques (spin and blade coating). (b) Schematic model for the molecular packing of P3HT backbones (dark blue) and fibrillar alignment (light blue) in spin-coated and blade-coated films. (c) Extracted mobilities for blade-coated films with the OFET channel orthogonal and parallel to the coating direction (spin coated in black for comparison). (d-i) Morphological characterization highlighting the presence of the aggregates and the anisotropy of the blade-coated films (d-e) compared to spin-coated ones (i) (24 h aging). For longer aging periods, the increased content of fibrillar form domains aligned in the direction of coating. Reproduced with permission from Ref ^[203]. Copyright 2016, American Chemical Society.

The OFETs fabricated in this fashion show hole mobility positively correlated with solution-aging time, and thus with the amount of preaggregate in solution, while their transport anisotropy is manifested with mobility values that are higher when the OFET channel length is orthogonal to the coating direction (the fibrillar-alignment direction). Indeed, X-ray diffraction

and polarized absorption data reveal that polymer backbones are oriented perpendicular to the fibrils, and efficient intramolecular transport is established thanks to the marked edge-on orientation obtained with blade coating compared to the spin-coated samples.

4.4.4. Slot-die coating

Besides the case of LCD displays, this process is a widely diffuse industrial coating technique whose proven up-scalability and compatibility with R2R processes has been demonstrated in the fields of organic photovoltaics and OLEDs,^{[204] [205]} and has also been exploited for the fabrication of electrochromic devices^[206] and OFETs.

In slot-die coating, ink is continuously pumped through a coating head placed in proximity of the substrate, as shown in **Figure 23**, and the formation of a meniscus thus occurs between the moving substrate and the head. The lateral extension of the slot-die head defines the maximum coating width, although it is possible to coat stripes of smaller size by adopting flow guides that limit the lateral spread of the meniscus. The presence of a pump allows precise regulation of the wet layer thickness as it is defined by the pumping speed along with the longitudinal width of the meniscus and the distance of the head from the substrate. As with all other coating techniques, other important parameters are coating speed, substrate temperature, and solution-substrate interaction.

Among the first reports on the use of slot-die coating to fabricate OFETs, the work of Chang et al. demonstrated the controlled growth of strained single crystals of TIPS-pentacene on a centimeter scale by exploiting a mixed solvent approach.^[207] The reported mobility for optimized devices exceeded $1 \text{ cm}^2\text{V}^{-1}\text{s}^{-1}$, which is about 100 times larger than spin-coated samples, and the thin-film anisotropy had a discernible impact on transport properties that varied by a factor of 4 depending on whether the transistor channel was parallel or perpendicular to the coating direction. The same authors investigated in 2015 the alignment of DPPT-TT using the same technique and obtained an improvement in the transport properties (average mobility

improved by a factor of 2-3) despite the modest anisotropy of the films (dichroic ratio: 1.2).^[208] In a later report by the same group, they implemented a preaggregating strategy by adding controlled amounts of an anti-solvent (MeOH) to a stable solution of a furan-substituted DPP in CF.^[209] Despite the evident presence of aggregates in solution with improved crystallinity (supported by UV-Vis absorption spectra and morphological characterization), the attempt provided a poor degree of alignment and an increase in mobility by a factor of 3, possibly because of the high molecular weight of the copolymer ($M_n = 24$ kg/mol, $M_w = 55$ kg/mol). Polymer alignment through slot-die coating has proved particularly effective when combined with an appropriate guiding channel for unidirectional solution flow where oriented nanogrooves were fabricated on a Si/SiO₂ substrate by diamond lapping.^[210] The deposition through slot-die coating in the presence of these shallow grooves (only a few nanometers deep) were instrumental in aligning the polymer PCDTPT (**Figure 23**) and in achieving enhanced long-range order and higher molecular packing density. Strong transport anisotropy was finally achieved, with mobility up to ~ 5.0 cm²V⁻¹s⁻¹ along the coating direction, compared to 1.9 cm²V⁻¹s⁻¹ in spin coated films.

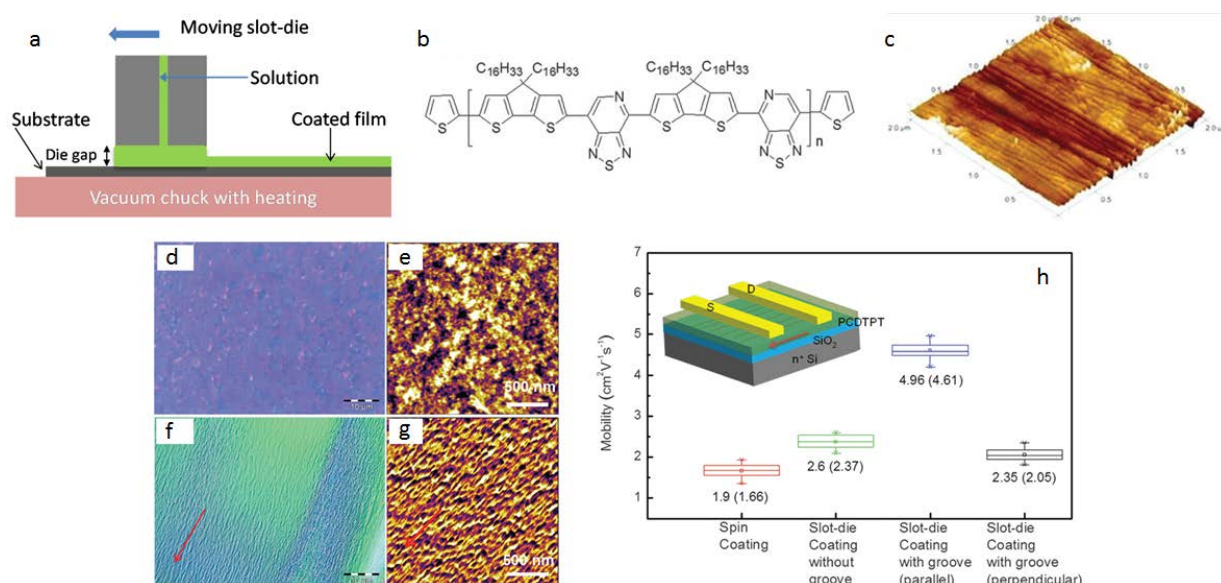


Figure 23. (a) Schematic illustration of slot-die coating. (b) Molecular structure of PCDTPT. (c) AFM image of nanogroove guides fabricated on SiO₂. (d-g) Cross-polarized microscopic images (left column) and AFM images (right column) of the bottom surface of PCDTPT film

deposited by spin coating (d, e) and nanogroove-guided slot-die coating (f, g) (the red arrow represents the direction of uniaxial nanogrooves and slot-die movement). (h) The mobility of FETs fabricated by spin coating, conventional slot-die coating, and nanogroove-guided slot-die coating in which the channel is parallel or perpendicular to the nanogrooves (inset: the red arrow represents the direction of slot-die movement in relation to the device architecture). Reproduced with permission from Ref ^[210]. Copyright 2015, Royal Society of Chemistry.

4.4.5. Zone casting

Zone casting consists of continuously supplying a solution of organic material through a flat linear-shaped nozzle on a moving substrate. In general, the ability of this technique to form ordered structures relies on the formation and linear translation of an appropriate concentration gradient of the solute. Hence, it is the spatial and temporal evolution of the drying front of the solution that drives the alignment rather than the shear stress imparted by the receding meniscus. For this reason, in order to effectively control the formation of ordered structures, most studies implement careful control over the solution dispensing rate, the temperature of the nozzle, and the movement and temperature of the substrate in order to prevent undesired nucleation in solution as well as to assist the drying of the solvent, thence matching its evaporation rate with the crystallization rate of the solute.^[211] A detailed review concerning the impact of solution drying kinetics and dynamics on organic semiconductor structure and morphology has recently appeared.^[212] For what concerns the zone casting technique, Tracz et al. suggest that to a first approximation and assuming a triangular meniscus, a stationary profile of the evaporation zone is then achieved when the following relationship is valid:

$$v_s = \frac{V_e}{\rho \sin \theta},$$

where v_s is the casting speed, V_e is the evaporation rate [kg / (m² s)], ρ denotes the solvent density, and θ indicates the contact angle. In this expression, temperature affects the evaporation rate and for this reason it is a key factor in setting the casting speed.^[211]

The first study on the use of zone casting was authored in 1983 by Burda et al.^[213] They reported the preparation of highly oriented conductive composites in which remarkable anisotropy of the electrical conductivity (10⁶) was attained from polycarbonate films doped with

tetrathiotetracene-tetracyanoquinodimethane (TTT-TCNQ) crystalline complexes. In the following 20 years, a diverse set of soluble organic materials relevant to OFET applications has been successfully processed with this technique to achieve uniaxial alignment, including small molecules (pentacene,^[214] TIPS-pentacene,^[215] and tetrathiafulvalene (TTF) derivatives^[216] ^[217]), liquid-crystalline discotic molecules,^[218] ^[219] ^[220] and polythiophene-based and high-performance organic polymers.^[108] ^[145] ^[221] ^[222] ^[223]

The first studies on exploiting low-molecular weight organic semiconductors made of small discotic molecules achieved notable in-plane long-range ordered structures with crystalline domains extending for centimeters and demonstrating marked morphological and optical anisotropy. Overall, these works provide an interesting set of indications for the fabrication of aligned films with several insights on the control of solvent slip-stick behavior, optimization of crystal nucleation, and film cracking prevention.^[214] ^[215] ^[217] However, only a small number of these studies performed a thorough characterization of the charge transport properties of the aligned films. In particular, experimental evidence provided by Miskiewicz et al. demonstrated anisotropy in hole mobility values reaching almost 2 orders of magnitude with small molecule tetrakis-(octadecylthio)-tetrathiafulvalene (TTF-4SC18),^[216] while Su et al. obtained aligned TIPS-pentacene films with maximum mobilities exceeding those of non-oriented layers by a factor of 10.^[215] In both of these studies the improvement in the transport properties was ascribed to both the high crystallinity of the zone-cast material along with the favorable alignment of the crystalline features of the films.

The earliest report of zone casting applied to a high-molecular weight compound, namely the block copolymer polyacrylonitrile-b-poly(n-butyl acrylate) (PBA-b-PAN), was instrumental in obtaining large-scale (3 x 5 cm) alignment of nanoscale domains composed of elongated rigid PAN separated by less ordered PBA ones, with an orientation perpendicular to the casting direction (**Figure 24**). The authors remarked that this particular alignment of the block copolymer was governed by its disposition along the solvent evaporation front, which is

contrary to other flow-induced orientation techniques that generally support alignment in the parallel direction.^[224]

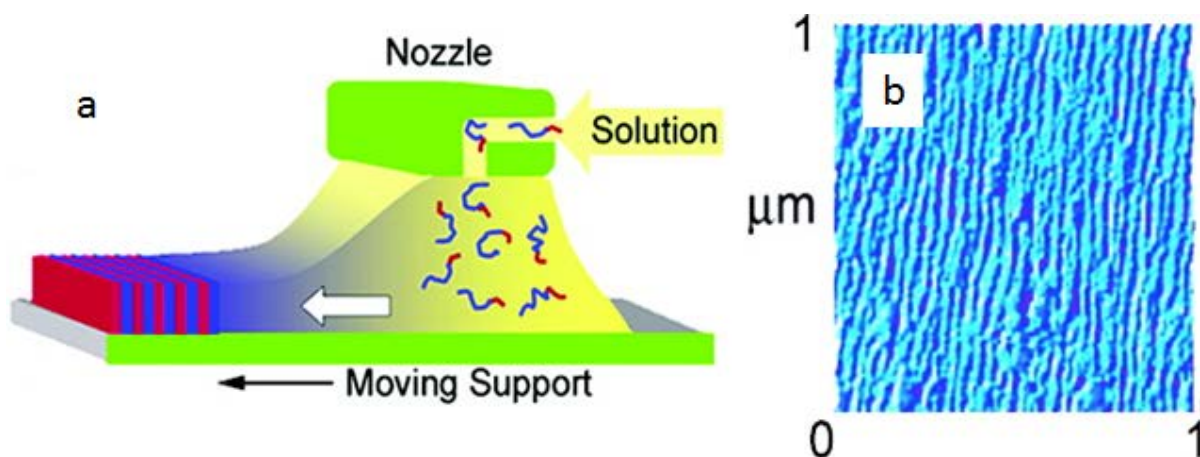


Figure 24. (a) Long-range order in thin films of PBA-b-PAN prepared by zone casting. (b) AFM phase images of the ordered structure. Reprinted with permission from Ref. ^[224]. Copyright 2005, American Chemical Society.

Aligned deposition of conjugated semiconducting polymers by zone casting was investigated extensively by Lee et al. using pBTTT.^[108, 222, 225] By probing the microstructure and domain structure evolution of pBTTT with surface and bulk-sensitive techniques, Schuettfort et al. observed that during the directional casting, polymer chain backbones were efficiently oriented along the casting direction at the top surface of the film.^[223] Such surface alignment then acted as a template for the further directional disposition of chains throughout the active layer, which occurred when the material was exposed to temperatures exceeding 275 °C, inducing the second phase transition of pBTTT that led to the formation of nanoribbons. These appeared as smectic-like conformation of crystallites (grain size of 20-30 nm) with a width comparable with the length of the polymer backbone (60-80 nm), and they extended in the direction of the π - π stacking of the polymer perpendicular to the casting direction. The mentioned templating effect was confirmed by measurements performed with scanning transmission X-ray microscopy (STXM) and polarized UV-Vis absorption, which were able to indicate the molecular and nanoribbon orientation in the bulk. Furthermore, near-edge X-ray absorption fine structure

spectroscopy (NEXAFS) along with AFM provided information on the superficial microstructure and morphology (**Figure 25**). Indeed, while the NEXAFS dichroic ratios (D_{surf}) for as-zone-cast films and films of aligned NR were similar (0.72 and 0.73, respectively), the corresponding optical values of the very same parameter (D_{bulk}) differed by a factor greater than four for the two separate systems (0.17 and 0.74, respectively). Moreover, the D_{bulk} value for aligned NR was compatible with D_{surf} , thus suggesting a templating effect.

A certain degree of transport anisotropy emerged from the oriented films both as-zone-cast and in the nanoribbon phase with the highest mobilities reported in the latter case along the casting direction, which is the backbone orientation. This result indicates that intrachain transport provides a more efficient path for conduction, despite being limited in the disordered boundary regions in between ribbons, where long misaligned chains probably act as tie molecules. In a later study, Lee et al. demonstrated with CMS that the possibly misaligned conformation of these tie chains led to rather short conjugation length and weaker interchain interaction.^[108] However, a careful analysis of the crystalline structure along the π - π stacking direction, which supports perpendicular interchain transport, pointed toward the presence of many grain boundaries of a diverse nature within the nanoribbons with a complex limiting effect on their charge transport capability, thus complicating the quantitative interpretation of their transport anisotropy.^[222]

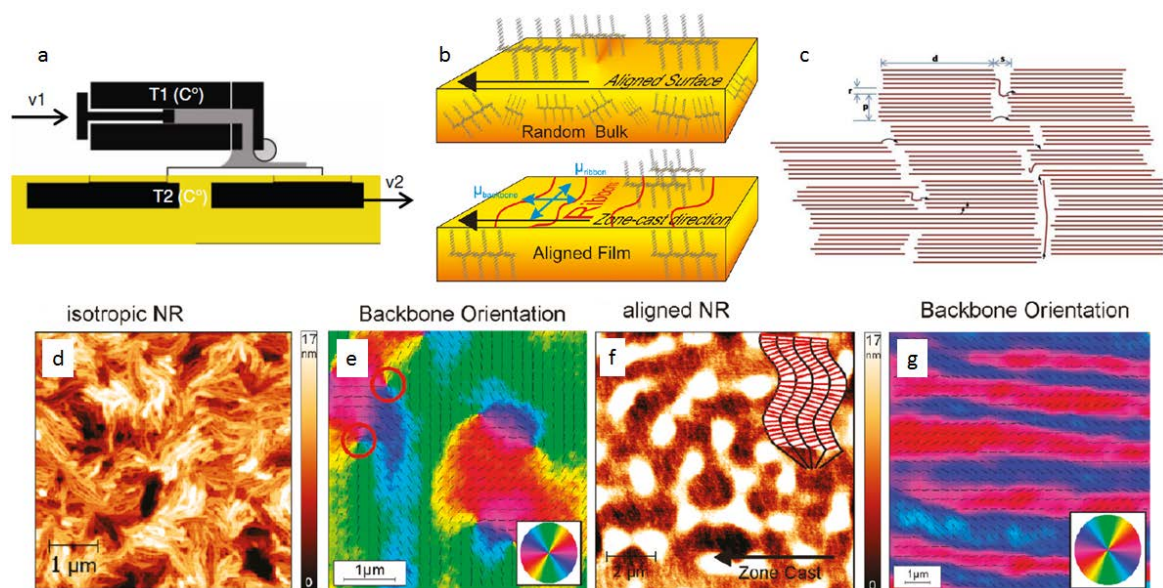


Figure 25. (a) Diagram of the setup for zone casting with controlled dispensing rate (v_1), substrate velocity (v_2), nozzle (T_1), and substrate temperature (T_2). Reproduced with permission from Ref ^[222]. Copyright 2011, John Wiley & Sons, Inc. (b) Illustration of as-zone-cast samples predominantly aligned at the surface with randomly oriented crystallites and amorphous chains in the bulk and the nanoribbon samples aligned throughout the bulk. (c) Model of charge transport along the casting direction. Charges flow preferably along the polymer backbones (in red), and charge transport is limited at the boundaries between the nanoribbons. (d-g) Comparison of AFM topography images (d, f) and bulk backbone-orientation maps calculated from polarized STXM (e, g) of disordered and aligned nanoribbon phases. When zone cast films are exploited, the templating effect translates nanoribbon alignment throughout the entire bulk. Reproduced with permission from Ref ^[223]. Copyright 2012, American Chemical Society.

Gao et al. demonstrated the efficient uniaxial alignment of P3HT with the polymer backbone oriented perpendicular to the zone casting direction, but in this case, it was achieved by inducing the presence of aggregates, either in a poor solvent or in a solvent-antisolvent mixture, acting as nuclei for the growth of oriented micrometer-sized nanofibrils.^[221] The study explored the impact of different solvent-antisolvent combinations and of different molecular weights of the polymer on the nanofibers length in the film, as well as the role of substrate temperature in achieving the proper evaporation rate to match the crystallization rate of the polymer. In a previous study, Lee et al. instead exploited a preaggregation strategy that relied on an ultrasound treatment in a poor solvent (xylene) and on the addition of insulating polymer PS to hinder semiconducting polymer precipitation, with the objective of favoring the formation of ordered aggregates and thus avoiding the formation of chain entanglements that are detrimental

to polymer self-assembly.^[226] Both approaches led to the growth of aligned micrometer-sized nanofibers, as demonstrated by morphological and optical probes, but no result was given on the resulting transport properties.

Zone casting has also been employed on high-performance D-A polymer P(NDI2OD-T2)^[145] to unambiguously assess the molecular orientation of the polymer on its surface. Previous reports have indeed provided strong evidence of face-on orientation in the bulk of the material,^[142] also supported by good out-of-plane mobilities.^[227] However, surface-sensitive techniques such as NEXAFS have provided data that could either point toward a more edge-on orientation of the polymer lamellae or suggest the presence of an amorphous in-plane arrangement at the interface.^[144] By inducing a well aligned surface through zone casting, with polymer backbones oriented in the direction of casting, Schuettfort and collaborators validated the indication of preferential edge-on orientation on the polymer surface.^[208] Such packing motif was observed on P(NDI2OD-T2) films fabricated with different deposition techniques (spin coating, gravure, and inkjet printing) and on different substrates, thus justifying the consistent mobility values obtained with top-gated OFETs under all these diverse conditions.^[228]

4.4.6. Wire-bar coating

Wire-bar coating, also known as rod coating, is a very simple doctoring method compatible with R2R continuous manufacturing processes over flexible substrates, thereby enabling the production of cost-effective large-area electronics.^[229] A stainless steel bar (Meyer bar) wound with a wire of a given diameter is placed either in contact with or in close proximity to the substrate according to coating conditions, and a quantity of ink in excess of what is required for the coating is placed in front of it. The bar is then moved over the ink, which doctors off the excess and leaves behind an amount of fluid which depends on the gaps produced by the wire.^[230] The fluid ridges formed behind the coating bar have to coalesce and level off in order

to produce a flat uniform film (**Figure 26**). Surface tension and viscosity play an important role at this stage, as both the Reynold number and the capillary number should be low to dampen oscillations caused by viscous forces and to ensure that leveling occurs before drying, respectively.^[231] The thickness of the wet layer is approximately 10 % of the wire diameter, although other parameters also influence the wet thickness, such as ink rheology and coating speed, while the dry layer thickness depends on the solid content of the coated formulation.^[230] ^[232] During evaporation, viscosity helps by hampering secondary flows which may lead to non-uniform film caused by for example local ruptures, while flows which can often occur in other printing processes, leading to coffee stain in inkjet for example, can be largely suppressed already with gradual solvent evaporation.

Bar coating has been adopted as a high throughput coating method to deposit a wide range of electronic materials comprising carbon-based conductors, such as transparent conducting carbon nanotubes^[231] and reduced graphene oxide,^[233] as well as graphene layer arrays,^[234] nanocomposite-based energy harvesters,^[235] and polymer and polymer/carbon nanotubes composite conductors for thermoelectric applications.^[236] ^[237] Moreover, ultrathin sol-gel-processed metal-oxide gate dielectric layers have been deposited by wire-bar coating to fabricate low-voltage metal-oxide-based FETs.^[238] A large-area oxide film (e. g. on 4" silicon wafer) was demonstrated by consuming less than 30 μl of a sol-gel oxide precursor solution, and excellent dielectric properties were exhibited with very low leakage current density ($< 10^{-8} \text{ A cm}^{-2}$ at 2 MV cm^{-1}) and high areal capacitance ($> 400 \text{ nF cm}^{-2}$).

Ouyang et al. reported one of the first examples where bar coating was adopted to deposit a polymer semiconductor, to realize a polymer light-emitting diode.^[239] However, the first application of this technique for the deposition of the active phase of a polymer FET was instead proposed by Murphy et al., who bar coated a blend of P3HT and insulating high-density polyethylene in ambient air at a temperature of $115 \text{ }^\circ\text{C}$ and a speed in the $1\text{-}10 \text{ cm s}^{-1}$ range, achieving uniform and controlled morphologies over a few cm^2 areas and good field-effect

mobility of $0.05 \text{ cm}^2/\text{Vs}$.^[240] More recently, Khim et al. demonstrated the strong potential of bar coating for high-throughput processing of high-performance organic electronics on plastic.^[229] Large polymer FET arrays with > 1000 devices and integrated circuits were fabricated by bar coating at a coating speed of 1.0 cm s^{-1} both a highly ordered conjugated polymer and a very smooth dielectric layer, by consecutive bar-coating steps either on a 4-inch glass or 4-inch plastic substrate. The best bar-coated top-gate/bottom contact FETs with PTVPhI-Eh or DPPT-TT showed high charge carrier mobility for holes, achieving 0.46 and $2.8 \text{ cm}^2/\text{Vs}$, respectively. This method provided a good yield (exceeding 99 %) and device-to-device uniformity with a small standard deviation of 5-6%. The possibility to control the polymer thickness down to a monolayer was later demonstrated, achieving at the same time highly transparent (up to 90% visibility) films with high charge carrier mobility ($\sim 1.1 \text{ cm}^2/\text{Vs}$ with DPPT-TT and $\sim 0.14 \text{ cm}^2/\text{Vs}$ with P(NDI2OD-T2)-based FETs) thanks to uniformly interconnected films.^{[21] [241]}

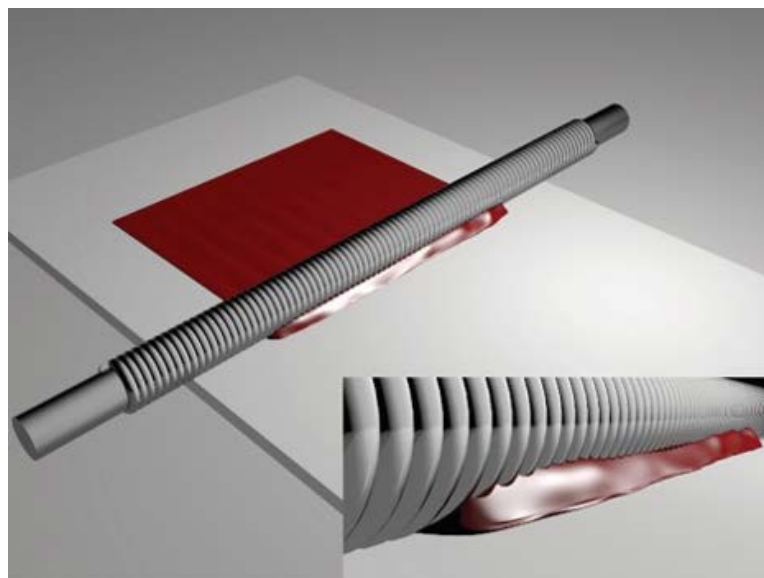


Figure 26. Schematic illustration of the bar-coating process: (i) Deposition of the ink just ahead of the coating bar, (ii) wet coating of the polymer ink onto the substrate by the horizontal movement of the coating bar along a fixed substrate, and (iii) gradual drying of the wet film from the edge to the center. (inset: interface between the solution and wire-wound bar). Reproduced with permission from Ref ^[241] Copyright 2016, John Wiley & Sons, Inc.

The possibility to adopt a fast deposition technique such as bar coating to align polymer backbones in a film over large areas, without requiring any substrate pre-patterning or any slow post-processing step, was recently demonstrated with solutions formulated with a high degree of aggregation, such as those presented in Section 3.2. Bucella et al. showed that only when suitable aggregating solvents such as mesitylene and toluene are adopted it is possible to induce chain alignment in P(NDI2OD-T2) film under the shear stress applied through the bar to the polymer formulation (**Figure 27**).^[21] In addition, molecular weight played a key role as M_w values that were too low (5 kDa, PDI = 1.8) did not lead to aggregates in solution, and optimal conditions were found for intermediate M_w values from 20 to 30 kDa (PDI 2.4-3.2). Interestingly, the coating speed used was as high as 10 cm s^{-1} , which was superior to any other effective polymer alignment methodology previously proposed, and highly discernible supra-molecular nanofibrillar structures, typical of P(NDI2OD-T2) processed from aggregating solvents, were well aligned over large substrates.

It is interesting to note that such fast coating cannot produce bulk films as ordered and aligned as achievable with other slower processes such as high-temperature rubbing.^{[174] [242]} Nevertheless, very thin films are sufficient for FET applications, and most importantly, the charge accumulates only in a very confined volume at the semiconductor-dielectric interface, which for P(NDI2OD-T2) is only 2-3 nm thick.^[30] Moreover, thanks to CMM performed in situ on working devices, it has been discovered that within such a restricted volume, the charge tends to select the most effective percolation pathways formed by the most aligned chain segments. Therefore, it is not surprising that while the optical dichroic ratio (as measured on a large mm^2 area) is quite limited (<1.8), anisotropy higher than 10 was found between the field-effect mobilities measured in FET devices parallel and perpendicular to the coating direction. On the one side, X-ray structural measurements suggest a high degree of structural alignment at the surface of the film, while on the other, the degree of order of polymer-conjugated segments probed by charge (i.e. the ratio between the segments giving rise to a charge sensitive

dichroic signal with respect to the total charge sensitive signal) is 98%. This corresponds to a dichroic ratio of 99, as compared to a dichroic ratio of only 3.5 on a similar area (degree of order of 56 %) recorded with a simple scanning optical density device. The latter evidence indicates the presence of much aligned functional morphology, i.e. structure of the subset of the only polymer chains participating in charge transport.

Aligned P(NDI2OD-T2) films have shown mobilities exceeding $6 \text{ cm}^2/\text{Vs}$, reaching one of the highest values for electron mobility in conjugated polymers FETs. Furthermore, bar-coated P(NDI2OD-T2) OFETs can already operate at frequencies up to 3.3 MHz in device structures non-optimized for fast dynamic operation thanks to the large improvement in transconductance achieved by alignment. To develop suitable patterning processes for the bar-coating method, several approaches have been proposed, among which a very promising one is based on the self-aligned patterning of coated film by selectively pre-defined hydrophobic self-assembled monolayers (SAMs).^{[238] [243]} Anhydrophobic SAMs can be easily pre-patterned by UV irradiation with a photomask so that the coated polymer solution can thus be selectively deposited on areas where the SAMs have been removed.

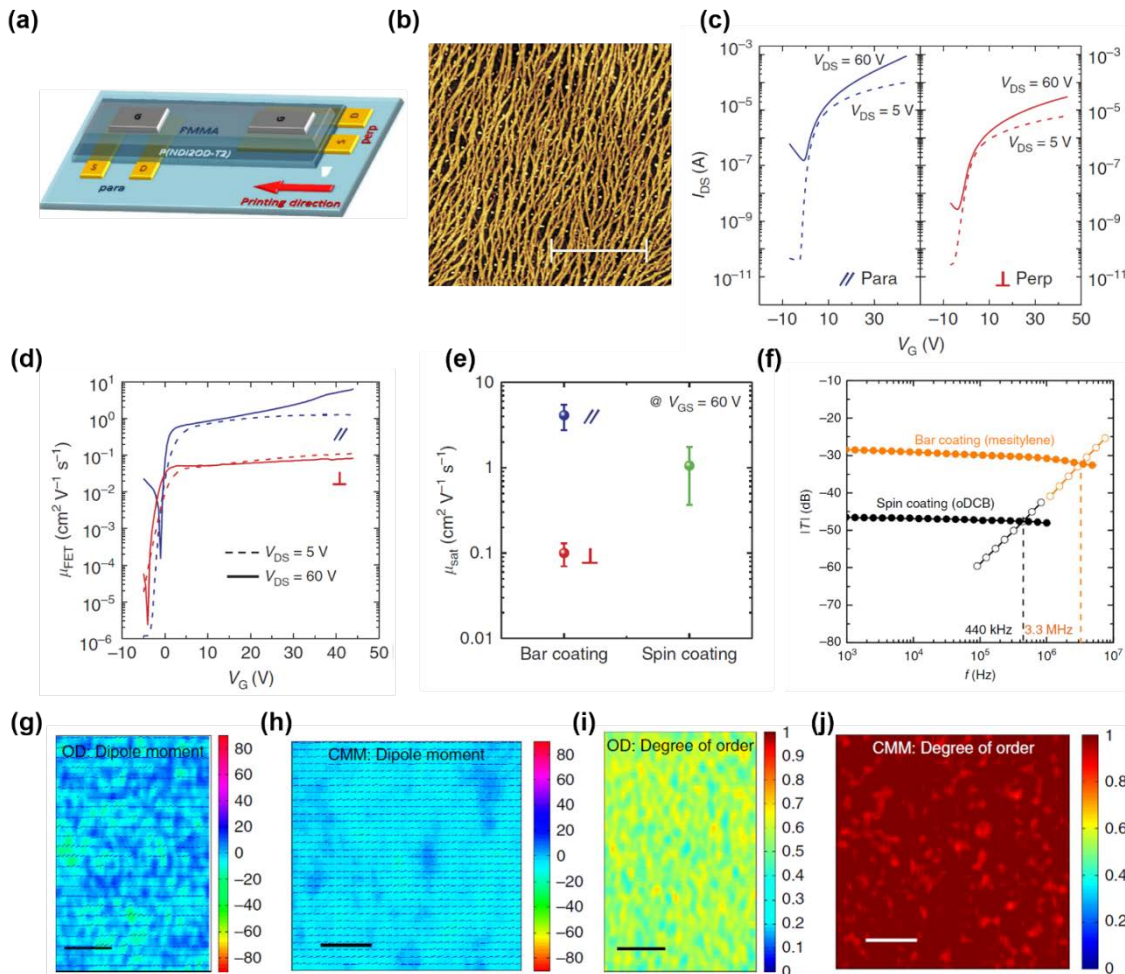


Figure 27. (a) Diagram of printing direction either parallel or perpendicular to the source to drain electric field. (b) AFM image of a sub-monolayer deposited from a bar-coating solution of P(NDI2OD-T2) in mesitylene. (c) Transfer characteristics in linear (dashed) and saturation (solid) regimes of 10 nm-thick film-based FETs with the fibrillar axis oriented parallel (blue) or perpendicular (red) to the probing direction. (d) Typical effective linear and saturation mobility as a function of gate voltage in the perpendicular and parallel directions; anisotropy is evident both with a high and a low lateral applied voltage. (e) Average saturation mobilities (circles) with their standard deviation (bars) for 56 FETs coated on an 8×8 cm² area in both the parallel and perpendicular directions compared to the distribution obtained from 8 spin-coated FETs. (f) Frequency characterization of devices made by standard spin coating of a solution of P(NDI2OD-T2) in DCB (black symbols) and bar coating with a solution of the same polymer in mesitylene (orange symbols). (g) 13×24 mm² polarized optical density map (a) and 18×18 μ m² CMM map (h) with the indication of the polymers backbone orientation (black dashed lines) and the relative DO maps (i,j) of a bar-coated film. Scale bars, 4 μ m. The mean dichroic ratio values are calculated relative to these scanned areas. Reprinted with permission from Ref^[21]. Copyright 2015, Springer Nature.

5. Conclusions

Uniaxial alignment of conjugated polymer backbones in solution-processed thin films is a powerful method to control and optimize charge carrier mobility and reduce device-to-device variability in polymer FETs. Optical and transport anisotropy are a consequence, and

perpendicular alignment of the polymer backbones with respect to source and drain electrodes in FETs maximizes charge carrier mobility through active intramolecular charge transport. Characterized by a planar backbone with a reduced degree of conformational freedom, D-A copolymers favor in-chain carrier transport along a path that is robust with respect to alkyl chain disorder. Their alignment provides suitable interconnectivity in between points of efficient π - π interaction, which largely lower energetic barriers for transport, in some cases inducing a transition from purely temperature-activated hopping transport to a band-like regime where there is vanishing or even inverted mobility activation energy close to room temperature.

Alignment of polymer films has been demonstrated with many different approaches: from well-known post-deposition methodologies, such as mechanical stretching and rubbing, to other techniques such as dip-coating and unidirectional drying in confined structures and/or under the capillary action induced by pre-patterned grooves, which are very effective at the laboratory scale for producing highly aligned films for charge-transport studies. Besides such examples, all based on slow directional drying, a very accessible and simple technique is off-center spin coating, which allows alignment under the effect of radial forces exerted on the sample, located typically a few cm from the spinning center. In this case, most of the solvent in the formulation is very quickly removed and alignment is imparted by shear stress in the presence of a suitable content of polymer aggregate in the solution. A key point is to devise suitable alignment schemes that can be adopted in scaled manufacturing processes, where enhanced throughput and high electronic performance favors the uptake of polymer electronics in cost-effective applications.

Large-area-compatible techniques inducing shear stresses such as shear coating, wire-bar coating, slot-die coating on patterned substrates, and zone casting have been demonstrated to produce anisotropic highly aligned films with high charge carrier mobilities in the alignment direction, in a single step deposition. While such processes are typically operated at low coating speeds of 0.4 mm s^{-1} , much higher speeds are possible in principle.^[244] As suggested by the off-

center spin-coating approach, formulation of polymer solutions plays a very important role in making the force fields produced by the specific deposition technique effective in aligning polymer backbones. For example, highly solubilizing solvents with high boiling points can induce a higher degree of microstructural order as they allow time for molecular arrangement in the thin film. However, on the one side, such timing is much slower than typical coating speeds, and on the other, molecularly dissolved polymers are less prone to be aligned. Instead, it has been largely reported that the presence of proper aggregates in the formulation induced by a specific solvent create the conditions for effective alignment. Large-area bar coating combined with solutions characterized by a large degree of preaggregation has been shown to enable alignment of films at coating velocities of up to several meters per minute, leading to mobility up to $\sim 6 \text{ cm}^2/\text{Vs}$ with reduced standard deviation, and with transport anisotropy ratios an order of magnitude higher than with other techniques.^[21]

Yet, the exact nature of aggregates and film formation has to be elucidated, and the stability of preaggregation further assessed. It is also plausible that other formulation strategies may be devised to control the viscosity and directionality of the solution under flow stress. Indeed, rheology properties and stability of semiconducting inks for fast-coating processes are relevant aspects to be addressed in the future. Moreover, it would also be desirable to achieve polymer alignment with techniques capable of high-resolution lateral patterning to reduce leakages and devices cross-talk, typically not easily achieved with large-area coating techniques. Along with these aspects, which would further strengthen the possibility to transfer high-mobility aligned polymer films approaches to actual applications, fundamental aspects of transport properties and their optimization have to be clarified to foster further progress.

If done successfully in the future, a combination of key observations on transport, advanced polymer synthesis, control of stable formulations, and reliable processes should enable fast coating of uniaxially aligned polymer films with mobility exceeding $10 \text{ cm}^2/\text{Vs}$. This is the level required for example, in backplanes for ultra-high resolution OLED displays, where

mobility needs to reach $80 \text{ cm}^2/\text{Vs}$ to address electronics for fast imagers, and in high-performance printed integrated circuits. With such improved mobility, provided that contact resistance effects are carefully controlled, it is not difficult to envision future polymer FETs with operating frequencies beyond 100 MHz, thus increasing computational capacity, bandwidth, and expanding the possible use of polymer electronics well beyond slow sensing applications.

Acknowledgements

This work was supported in part by the European Research Council (ERC) under the European Union's Horizon 2020 research and innovation program "HEROIC", Grant Agreement No. 638059. This work was also supported by the Center for Advanced Soft-Electronics (2013M3A6A5073183) funded by NRF and the Ministry of Science & ICT of Republic of Korea.

References

- [1] H. E. Katz, *Chem. Mater.* **2004**, *16*, 4748.
- [2] G. Malliaras, *Organic Semiconductors and Devices*, John Wiley & Sons, Hoboken **2003**.
- [3] J. H. Burroughes, D. D. C. Bradley, A. R. Brown, R. N. Marks, K. Mackay, R. H. Friend, P. L. Burns, A. B. Holmes, *Nature* **1990**, *347*, 539.
- [4] B. W. D'Andrade, S. R. Forrest, *Adv. Mater.* **2004**, *16*, 1585.
- [5] H. Uoyama, K. Goushi, K. Shizu, H. Nomura, C. Adachi, *Nature* **2012**, *492*, 234.
- [6] D. Han, Y. Khan, J. Ting, S. M. King, N. Yaacobi-Gross, M. J. Humphries, C. J. Newsome, A. C. Arias, *Adv. Mater.* **2017**, *29*, 1606206.
- [7] G. Yu, J. Gao, J. C. Hummelen, F. Wudl, A. J. Heeger, *Science* **1995**, *270*, 1789.
- [8] G. Li, V. Shrotriya, J. Huang, Y. Yao, T. Moriarty, K. Emery, Y. Yang, *Nat. Mater.* **2005**, *4*, 864.
- [9] F. C. Krebs, *Sol. Energy Mater. Sol. Cells* **2009**, *93*, 394.
- [10] H. Sirringhaus, P. Brown, R. Friend, M. M. Nielsen, K. Bechgaard, B. Langeveld-Voss, A. Spiering, R. A. Janssen, E. Meijer, P. Herwig, *Nature* **1999**, *401*, 685.
- [11] H. Sirringhaus, T. Kawase, R. Friend, T. Shimoda, M. Inbasekaran, W. Wu, E. Woo, *Science* **2000**, *290*, 2123.
- [12] G. Horowitz, *Adv. Mater.* **1998**, *10*, 365.
- [13] Z. Bao, A. Dodabalapur, A. J. Lovinger, *Appl. Phys. Lett.* **1996**, *69*, 4108.
- [14] J. H. Cho, J. Lee, Y. Xia, B. Kim, Y. He, M. J. Renn, T. P. Lodge, C. D. Frisbie, *Nat. Mater.* **2008**, *7*, 900.
- [15] H. Bin, L. Gao, Z.-G. Zhang, Y. Yang, Y. Zhang, C. Zhang, S. Chen, L. Xue, C. Yang, M. Xiao, *Nat. Commun.* **2016**, *7*, 13651.
- [16] Y. Yamashita, F. Hinkel, T. Marszalek, W. Zajaczkowski, W. Pisula, M. Baumgarten, H. Matsui, K. Müllen, J. Takeya, *Chem. Mater.* **2016**, *28*, 420.
- [17] H. R. Tseng, H. Phan, C. Luo, M. Wang, L. A. Perez, S. N. Patel, L. Ying, E. J. Kramer, T. Q. Nguyen, G. C. Bazan, *Adv. Mater.* **2014**, *26*, 2993.
- [18] C. Luo, A. K. K. Kyaw, L. A. Perez, S. Patel, M. Wang, B. Grimm, G. C. Bazan, E. J. Kramer, A. J. Heeger, *Nano Lett.* **2014**, *14*, 2764.
- [19] D. Venkateshvaran, M. Nikolka, A. Sadhanala, V. Lemaur, M. Zelazny, M. Kepa, M. Hurhangee, A. J. Kronemeijer, V. Pecunia, I. Nasrallah, *Nature* **2014**, *515*, 384.
- [20] R. Noriega, J. Rivnay, K. Vandewal, F. P. Koch, N. Stingelin, P. Smith, M. F. Toney, A. Salleo, *Nat. Mater.* **2013**, *12*, 1038.
- [21] S. G. Bucella, A. Luzio, E. Gann, L. Thomsen, C. R. McNeill, G. Pace, A. Perinot, Z. Chen, A. Facchetti, M. Caironi, *Nat. Commun.* **2015**, *6*, 8394.
- [22] S. Himmelberger, A. Salleo, *MRS Commun.* **2015**, *5*, 383.
- [23] S. Wang, S. Fabiano, S. Himmelberger, S. Puzinas, X. Crispin, A. Salleo, M. Berggren, *Proc. Natl. Acad. Sci. U.S.A.* **2015**, *112*, 10599.
- [24] S. Roth, D. Carroll, *One-dimensional Metals: Conjugated Polymers, Organic Crystals, Carbon Nanotubes and Graphene*, John Wiley & Sons, **2015**.
- [25] Y. Xu, H. Sun, E. Y. Shin, Y. F. Lin, W. Li, Y. Y. Noh, *Adv. Mater.* **2016**, *28*, 8531.
- [26] H. Klauk, D. J. Gundlach, T. N. Jackson, *IEEE Electron Device Lett.* **1999**, *20*, 289.
- [27] J. Zaumseil, H. Sirringhaus, *Chem. Rev.* **2007**, *107*, 1296.
- [28] L. Miozzo, A. Yassar, G. Horowitz, *J. Mater. Chem.* **2010**, *20*, 2513.
- [29] S. M. Sze, K. K. Ng, *Physics of Semiconductor Devices*, John Wiley & Sons, **2006**.
- [30] F. Maddalena, C. de Falco, M. Caironi, D. Natali, *Org. Electron.* **2015**, *17*, 304.
- [31] F. Zhang, C. a. Di, N. Berdunov, Y. Hu, Y. Hu, X. Gao, Q. Meng, H. Sirringhaus, D. Zhu, *Adv. Mater.* **2013**, *25*, 1401.
- [32] H. Abdalla, S. Fabiano, M. Kemerink, *Phys. Rev. B* **2017**, *95*, 085301.
- [33] V. D'Innocenzo, A. Luzio, H. Abdalla, S. Fabiano, M. Loi, D. Natali, A. Petrozza, M.

- Kemerink, M. Caironi, *J. Mater. Chem. C* **2016**, *4*, 11135.
- [34] H. Klauk, *Chem. Soc. Rev.* **2010**, *39*, 2643.
- [35] T. Uemura, C. Rolin, T. H. Ke, P. Fesenko, J. Genoe, P. Heremans, J. Takeya, *Adv. Mater.* **2016**, *28*, 151.
- [36] I. McCulloch, A. Salleo, M. Chabiny, *Science* **2016**, *352*, 1521.
- [37] H. Sirringhaus, *Adv. Mater.* **2014**, *26*, 1319.
- [38] C. Liu, G. Li, R. Di Pietro, J. Huang, Y.-Y. Noh, X. Liu, T. Minari, *Phys. Rev. Appl.* **2017**, *8*, 034020.
- [39] J. Li, Y. Zhao, H. S. Tan, Y. Guo, C.-A. Di, G. Yu, Y. Liu, M. Lin, S. H. Lim, Y. Zhou, H. Su, B. S. Ong, *Sci. Rep.* **2012**, *2*, 754.
- [40] H. Chen, Y. Guo, G. Yu, Y. Zhao, J. Zhang, D. Gao, H. Liu, Y. Liu, *Adv. Mater.* **2012**, *24*, 4618.
- [41] J. Lee, A.-R. Han, J. Kim, Y. Kim, J. H. Oh, C. Yang, *J. Am. Chem. Soc.* **2012**, *134*, 20713.
- [42] J. Lee, A.-R. Han, H. Yu, T. J. Shin, C. Yang, J. H. Oh, *J. Am. Chem. Soc.* **2013**, *135*, 9540.
- [43] H.-R. Tseng, L. Ying, B. B. Hsu, L. A. Perez, C. J. Takacs, G. C. Bazan, A. J. Heeger, *Nano Lett.* **2012**, *12*, 6353.
- [44] Y. Yuan, G. Giri, A. L. Ayzner, A. P. Zoombelt, S. C. Mannsfeld, J. Chen, D. Nordlund, M. F. Toney, J. Huang, Z. Bao, *Nat. Commun.* **2014**, *5*, 3005.
- [45] E. G. Bittle, J. I. Basham, T. N. Jackson, O. D. Jurchescu, D. J. Gundlach, *Nat. Commun.* **2016**, *7*, 10908.
- [46] G. O. Nikiforov, D. Venkateshvaran, S. Mooser, A. Meneau, T. Strobel, A. Kronemeijer, L. Jiang, M. J. Lee, H. Sirringhaus, *Adv. Electron. Mater.* **2016**, *2*, 1600163
- [47] A. Förster, F. Günther, S. Gemming, G. Seifert, *J. Phys. Chem. C* **2017**, *121*, 3714.
- [48] Y. Xu, H. Sun, W. Li, Y. F. Lin, F. Balestra, G. Ghibaudo, Y. Y. Noh, *Adv. Mater.* **2017**, *29*, 1702729
- [49] H. Sirringhaus, *Adv. Mater.* **2009**, *21*, 3859.
- [50] D. Natali, M. Caironi, *Adv. Mater.* **2012**, *24*, 1357.
- [51] M. Oehzelt, K. Akaike, N. Koch, G. Heimel, *Sci. Adv.* **2015**, *1*, e1501127.
- [52] H. Sirringhaus, *Adv. Mater.* **2005**, *17*, 2411.
- [53] N. Zhao, Y. Y. Noh, J. F. Chang, M. Heeney, I. McCulloch, H. Sirringhaus, *Adv. Mater.* **2009**, *21*, 3759.
- [54] H. Yan, T. Schuettfort, A. J. Kronemeijer, C. R. McNeill, H. W. Ade, *Appl. Phys. Lett.* **2012**, *101*, 093308.
- [55] D. Natali, M. Caironi, *Adv. Mater.* **2012**, *24*, 1357.
- [56] A. Köhler, H. Bässler, *Electronic Processes in Organic Semiconductors: An Introduction*, John Wiley & Sons, **2015**.
- [57] H. Sirringhaus, T. Sakanoue, J. F. Chang, *Phys. Status Solidi B* **2012**, *249*, 1655.
- [58] N. Tessler, Y. Preezant, N. Rappaport, Y. Roichman, *Adv. Mater.* **2009**, *21*, 2741.
- [59] A. Salleo, R. J. Kline, D. M. DeLongchamp, M. L. Chabiny, *Adv. Mater.* **2010**, *22*, 3812.
- [60] M. Mas-Torrent, C. Rovira, *Chem. Soc. Rev.* **2008**, *37*, 827.
- [61] J. E. Anthony, *Chem. Rev.* **2006**, *106*, 5028.
- [62] R. Hamilton, J. Smith, S. Ogier, M. Heeney, J. E. Anthony, I. McCulloch, J. Veres, D. D. Bradley, T. D. Anthopoulos, *Adv. Mater.* **2009**, *21*, 1166.
- [63] O. D. Jurchescu, M. Popinciuc, B. J. van Wees, T. T. Palstra, *Adv. Mater.* **2007**, *19*, 688.
- [64] H. Minemawari, T. Yamada, H. Matsui, J. y. Tsutsumi, S. Haas, R. Chiba, R. Kumai, T. Hasegawa, *Nature* **2011**, *475*, 364.
- [65] K. Rahimi, I. Botiz, N. Stingelin, N. Kayunkid, M. Sommer, F. P. V. Koch, H. Nguyen, O. Coulembier, P. Dubois, M. Brinkmann, *Angew. Chem. Int. Ed.* **2012**, *51*, 11131.

- [66] K. Rahimi, I. Botiz, J. O. Agumba, S. Motamen, N. Stingelin, G. Reiter, *RSC Adv.* **2014**, *4*, 11121.
- [67] S. Schott, E. Gann, L. Thomsen, S. H. Jung, J. K. Lee, C. R. McNeill, H. Sirringhaus, *Adv. Mater.* **2015**, *27*, 7356.
- [68] Y. Yamashita, J. Tsurumi, F. Hinkel, Y. Okada, J. Soeda, W. Zajączkowski, M. Baumgarten, W. Pisula, H. Matsui, K. Müllen, *Adv. Mater.* **2014**, *26*, 8169.
- [69] J. Lee, J. W. Chung, D. H. Kim, B.-L. Lee, J.-I. Park, S. Lee, R. Häusermann, B. Batlogg, S.-S. Lee, I. Choi, *J. Am. Chem. Soc.* **2015**, *137*, 7990.
- [70] S. P. Senanayak, A. Ashar, C. Kanimozhi, S. Patil, K. Narayan, *Phys. Rev. B* **2015**, *91*, 115302.
- [71] X. Gao, Z. Zhao, *Sci. China Chem.* **2015**, *58*, 947.
- [72] B. S. Ong, Y. Wu, P. Liu, S. Gardner, *J. Am. Chem. Soc.* **2004**, *126*, 3378.
- [73] I. McCulloch, M. Heeney, C. Bailey, K. Genevicius, I. MacDonald, M. Shkunov, D. Sparrowe, S. Tierney, R. Wagner, W. Zhang, M. L. Chabiny, R. J. Kline, M. D. McGehee, M. F. Toney, *Nat. Mater.* **2006**, *5*, 328.
- [74] M. L. Chabiny, L. H. Jimison, J. Rivnay, A. Salleo, *MRS Bull.* **2008**, *33*, 683.
- [75] G. Barbarella, M. Melucci, G. Sotgiu, *Adv. Mater.* **2005**, *17*, 1581.
- [76] J. Rivnay, R. Noriega, R. J. Kline, A. Salleo, M. F. Toney, *Phys. Rev. B* **2011**, *84*, 045203.
- [77] X. Zhang, H. Bronstein, A. J. Kronemeijer, J. Smith, Y. Kim, R. J. Kline, L. J. Richter, T. D. Anthopoulos, H. Sirringhaus, K. Song, *Nat. Commun.* **2013**, *4*, 2238.
- [78] V. Podzorov, *Nat. Mater.* **2013**, *12*, 947.
- [79] S. D. Kang, G. J. Snyder, *Nat. Mater.* **2017**, *16*, 252.
- [80] R. P. Fornari, A. Troisi, *Adv. Mater.* **2014**, *26*, 7627.
- [81] W. Zhang, J. Smith, S. E. Watkins, R. Gysel, M. McGehee, A. Salleo, J. Kirkpatrick, S. Ashraf, T. Anthopoulos, M. Heeney, *J. Am. Chem. Soc.* **2010**, *132*, 11437.
- [82] T. Liu, A. Troisi, *Adv. Funct. Mater.* **2014**, *24*, 925.
- [83] H. Bassler, A. Kohler, *Unimolecular and Supramolecular Electronics I: Chemistry and Physics Meet at Metal-Molecule Interfaces* **2012**, *312*, 1.
- [84] A. A. Bakulin, R. Lovrincic, X. Yu, O. Selig, H. J. Bakker, Y. L. A. Rezus, P. K. Nayak, A. Fonari, V. Coropceanu, J. L. Bredas, D. Cahen, *Nat. Commun.* **2015**, *6*.
- [85] J. L. Bredas, J. P. Calbert, D. A. da Silva, J. Cornil, *Proc. Natl. Acad. Sci. U.S.A.* **2002**, *99*, 5804.
- [86] C. B. Nielsen, M. Turbiez, I. McCulloch, *Adv. Mater.* **2013**, *25*, 1859.
- [87] D. Fazzi, M. Caironi, C. Castiglioni, *J. Am. Chem. Soc.* **2011**, *133*, 19056.
- [88] E. Giussani, D. Fazzi, L. Brambilla, M. Caironi, C. Castiglioni, *Macromolecules* **2013**, *46*, 2658.
- [89] G.-J. A. Wetzelaer, M. Kuik, Y. Olivier, V. Lemaire, J. Cornil, S. Fabiano, M. A. Loi, P. W. Blom, *Phys. Rev. B* **2012**, *86*, 165203.
- [90] E. Giussani, L. Brambilla, D. Fazzi, M. Sommer, N. Kayunkid, M. Brinkmann, C. Castiglioni, *J. Phys. Chem. B* **2015**, *119*, 2062.
- [91] C. Caddeo, D. Fazzi, M. Caironi, A. Mattoni, *J. Phys. Chem. B* **2014**, *118*, 12556.
- [92] A. Luzio, D. Fazzi, D. Natali, E. Giussani, K. J. Baeg, Z. Chen, Y. Y. Noh, A. Facchetti, M. Caironi, *Adv. Funct. Mater.* **2014**, *24*, 1151.
- [93] A. Zen, J. Pflaum, S. Hirschmann, W. Zhuang, F. Jaiser, U. Asawapirom, J. P. Rabe, U. Scherf, D. Neher, *Adv. Funct. Mater.* **2004**, *14*, 757.
- [94] R. J. Kline, M. D. McGehee, E. N. Kadnikova, J. Liu, J. M. Frechet, *Adv. Mater.* **2003**, *15*, 1519.
- [95] H. N. Tsao, D. M. Cho, I. Park, M. R. Hansen, A. Mavrinskiy, D. Y. Yoon, R. Graf, W. Pisula, H. W. Spiess, K. Mullen, *J. Am. Chem. Soc.* **2011**, *133*, 2605.
- [96] F. P. V. Koch, J. Rivnay, S. Foster, C. Müller, J. M. Downing, E. Buchaca-Domingo, P. Westacott, L. Yu, M. Yuan, M. Baklar, *Prog. Polym. Sci.* **2013**, *38*, 1978.

- [97] J. Rivnay, R. Noriega, J. E. Northrup, R. J. Kline, M. F. Toney, A. Salleo, *Phys. Rev. B* **2011**, *83*, 121306.
- [98] R. Street, J. Northrup, A. Salleo, *Phys. Rev. B* **2005**, *71*, 165202.
- [99] G. Horowitz, R. Hajlaoui, P. Delannoy, *J. Phys. III* **1995**, *5*, 355.
- [100] S. Mehraeen, V. Coropceanu, J.-L. Brédas, *Phys. Rev. B* **2013**, *87*, 195209.
- [101] H. Bassler, *Phys. Status Solidi B* **1993**, *175*, 15.
- [102] M. C. J. M. Vissenberg, M. Matters, *Phys. Rev. B* **1998**, *57*, 12964.
- [103] J.-F. Chang, T. Sakanoue, Y. Olivier, T. Uemura, M.-B. Dufourg-Madec, S. G. Yeates, J. Cornil, J. Takeya, A. Troisi, H. Sirringhaus, *Phys. Rev. Lett.* **2011**, *107*, 066601.
- [104] R. Noriega, A. Salleo, *Charge transport theories in organic semiconductors*, in *Organic Electronics II: More Materials and Applications*, Vol. 2, **2012**.
- [105] A. Troisi, G. Orlandi, *Phys. Rev. Lett.* **2006**, *96*, 086601.
- [106] A. S. Eggeman, S. Illig, A. Troisi, H. Sirringhaus, P. A. Midgley, *Nat. Mater.* **2013**, *12*, 1045.
- [107] E. J. Crossland, K. Tremel, F. Fischer, K. Rahimi, G. Reiter, U. Steiner, S. Ludwigs, *Adv. Mater.* **2012**, *24*, 839.
- [108] M. J. Lee, Z. Chen, R. d. Pietro, M. Heeney, H. Sirringhaus, *Chem. Mater.* **2013**, *25*, 2075.
- [109] R. Di Pietro, I. Nasrallah, J. Carpenter, E. Gann, L. S. Kölln, L. Thomsen, D. Venkateshvaran, K. O'Hara, A. Sadhanala, M. Chabinyc, C. R. McNeill, A. Facchetti, H. Ade, H. Sirringhaus, D. Neher, *Adv. Funct. Mater.* **2016**, *26*, 8011.
- [110] B. B. Y. Hsu, C. M. Cheng, C. Luo, S. N. Patel, C. Zhong, H. Sun, J. Sherman, B. H. Lee, L. Ying, M. Wang, *Adv. Mater.* **2015**, *27*, 7759.
- [111] V. Coropceanu, J. Cornil, D. A. da Silva Filho, Y. Olivier, R. Silbey, J.-L. Brédas, *Chem. Rev.* **2007**, *107*, 926.
- [112] B.-G. Kim, E. J. Jeong, J. W. Chung, S. Seo, B. Koo, J. Kim, *Nat. Mater.* **2013**, *12*, 659.
- [113] A. Luzio, L. Criante, V. D'Innocenzo, M. Caironi, *Sci. Rep.* **2013**, *3*, 3425
- [114] J.-F. Chang, B. Sun, D. W. Breiby, M. M. Nielsen, T. I. Sölling, M. Giles, I. McCulloch, H. Sirringhaus, *Chem. Mater.* **2004**, *16*, 4772.
- [115] H. Yang, T. J. Shin, L. Yang, K. Cho, C. Y. Ryu, Z. Bao, *Adv. Funct. Mater.* **2005**, *15*, 671.
- [116] D. H. Kim, Y. Jang, Y. D. Park, K. Cho, *J. Phys. Chem. B* **2006**, *110*, 15763.
- [117] D. H. Kim, Y. D. Park, Y. Jang, S. Kim, K. Cho, *Macromol. Rapid Commun.* **2005**, *26*, 834.
- [118] H. S. Lee, J. H. Cho, K. Cho, Y. D. Park, *J. Phys. Chem. C* **2013**, *117*, 11764.
- [119] T. K. An, I. Kang, H. j. Yun, H. Cha, J. Hwang, S. Park, J. Kim, Y. J. Kim, D. S. Chung, S. K. Kwon, *Adv. Mater.* **2013**, *25*, 7003.
- [120] E. J. Crossland, K. Rahimi, G. Reiter, U. Steiner, S. Ludwigs, *Adv. Funct. Mater.* **2011**, *21*, 518.
- [121] H. Sirringhaus, R. Wilson, R. Friend, M. Inbasekaran, W. Wu, E. Woo, M. Grell, D. Bradley, *Appl. Phys. Lett.* **2000**, *77*, 406.
- [122] A. M. van de Craats, N. Stutzmann, O. Bunk, M. M. Nielsen, M. Watson, K. Müllen, H. D. Chanzy, H. Sirringhaus, R. H. Friend, *Adv. Mater.* **2003**, *15*, 495.
- [123] L. H. Jimison, M. F. Toney, I. McCulloch, M. Heeney, A. Salleo, *Adv. Mater.* **2009**, *21*, 1568.
- [124] H. B. Bohidar, *Fundamentals of Polymer Physics and Molecular Biophysics*, Cambridge University Press, **2015**.
- [125] N. Kiriy, E. Jähne, H.-J. Adler, M. Schneider, A. Kiriy, G. Gorodyska, S. Minko, D. Jehnichen, P. Simon, A. A. Fokin, *Nano Lett.* **2003**, *3*, 707.
- [126] N. E. Jackson, K. L. Kohlstedt, B. M. Savoie, M. Olvera de la Cruz, G. C. Schatz, L. X. Chen, M. A. Ratner, *J. Am. Chem. Soc.* **2015**, *137*, 6254.

- [127] Y. D. Park, H. S. Lee, Y. J. Choi, D. Kwak, J. H. Cho, S. Lee, K. Cho, *Adv. Funct. Mater.* **2009**, *19*, 1200.
- [128] M. S. Chen, O. P. Lee, J. R. Niskala, A. T. Yiu, C. J. Tassone, K. Schmidt, P. M. Beaujuge, S. S. Onishi, M. F. Toney, A. Zettl, *J. Am. Chem. Soc.* **2013**, *135*, 19229.
- [129] U. Bielecka, P. Lutsyk, K. Janus, J. Sworakowski, W. Bartkowiak, *Org. Electron.* **2011**, *12*, 1768.
- [130] A. R. Aiyar, J. I. Hong, R. Nambiar, D. M. Collard, E. Reichmanis, *Adv. Funct. Mater.* **2011**, *21*, 2652.
- [131] M. Chang, J. Lee, N. Kleinhenz, B. Fu, E. Reichmanis, *Adv. Funct. Mater.* **2014**, *24*, 4457.
- [132] Y. D. Park, S. G. Lee, H. S. Lee, D. Kwak, D. H. Lee, K. Cho, *J. Mater. Chem.* **2011**, *21*, 2338.
- [133] Y. D. Park, J. K. Park, J. H. Seo, J. D. Yuen, W. H. Lee, K. Cho, G. C. Bazan, *Adv. Energy Mater.* **2011**, *1*, 63.
- [134] K. Zhao, H. U. Khan, R. Li, Y. Su, A. Amassian, *Adv. Funct. Mater.* **2013**, *23*, 6024.
- [135] H. Hu, K. Zhao, N. Fernandes, P. Boufflet, J. H. Bannock, L. Yu, J. C. de Mello, N. Stingelin, M. Heeney, E. P. Giannelis, *J. Mater. Chem. C* **2015**, *3*, 7394.
- [136] M. Lee, H. Jeon, M. Jang, H. Yang, *ACS Appl. Mater. Interfaces* **2016**, *8*, 4819.
- [137] J. Ruher, N. Colaneri, D. Bradley, R. Friend, G. Wegner, *J. Phys.: Condens. Matter* **1990**, *2*, 5465.
- [138] B. Xu, S. Holdcroft, *Macromolecules* **1993**, *26*, 4457.
- [139] Y. D. Park, J. K. Park, W. H. Lee, B. Kang, K. Cho, G. C. Bazan, *J. Mater. Chem.* **2012**, *22*, 11462.
- [140] S. Kim, B. Kang, M. Lee, S. G. Lee, K. Cho, H. Yang, Y. D. Park, *RSC Adv.* **2014**, *4*, 41159.
- [141] R. Steyrlleuthner, M. Schubert, I. Howard, B. Klaumünzer, K. Schilling, Z. Chen, P. Saalfrank, F. d. r. Laquai, A. Facchetti, D. Neher, *J. Am. Chem. Soc.* **2012**, *134*, 18303.
- [142] J. Rivnay, M. F. Toney, Y. Zheng, I. V. Kauvar, Z. Chen, V. Wagner, A. Facchetti, A. Salleo, *Adv. Mater.* **2010**, *22*, 4359.
- [143] J. Rivnay, R. Steyrlleuthner, L. H. Jimison, A. Casadei, Z. Chen, M. F. Toney, A. Facchetti, D. Neher, A. Salleo, *Macromolecules* **2011**, *44*, 5246.
- [144] T. Schuettfort, S. Huettner, S. Lilliu, J. E. Macdonald, L. Thomsen, C. R. McNeill, *Macromolecules* **2011**, *44*, 1530.
- [145] T. Schuettfort, L. Thomsen, C. R. McNeill, *J. Am. Chem. Soc.* **2013**, *135*, 1092.
- [146] P. J. Brown, H. Sirringhaus, M. Harrison, M. Shkunov, R. H. Friend, *Phys. Rev. B* **2001**, *63*, 125204.
- [147] Z. Chen, M. Bird, V. Lemaire, G. Radtke, J. Cornil, M. Heeney, I. McCulloch, H. Sirringhaus, *Phys. Rev. B* **2011**, *84*, 115211.
- [148] H. Xu, Y. Jiang, J. Li, B. S. Ong, Z. Shuai, J. Xu, N. Zhao, *J. Phys. Chem. C* **2013**, *117*, 6835.
- [149] C. Sciascia, N. Martino, T. Schuettfort, B. Watts, G. Grancini, M. R. Antognazza, M. Zavelani-Rossi, C. R. McNeill, M. Caironi, *Adv. Mater.* **2011**, *23*, 5086.
- [150] N. Martino, D. Fazzi, C. Sciascia, A. Luzio, M. R. Antognazza, M. Caironi, *ACS Nano* **2014**, *8*, 5968.
- [151] M. Majumder, C. S. Rendall, J. A. Eukel, J. Y. Wang, N. Behabtu, C. L. Pint, T.-Y. Liu, A. W. Orbaek, F. Mirri, J. Nam, *J. Phys. Chem. B* **2012**, *116*, 6536.
- [152] G. Pan, F. Chen, L. Hu, K. Zhang, J. Dai, F. Zhang, *Adv. Funct. Mater.* **2015**, *25*, 5126.
- [153] X. Xue, G. Chandler, X. Zhang, R. J. Kline, Z. Fei, M. Heeney, P. J. Diemer, O. D. Jurchescu, B. T. O'Connor, *ACS Appl. Mater. Interfaces* **2015**, *7*, 26726.
- [154] M. Grell, M. Redecker, K. Whitehead, D. Bradley, M. Inbasekaran, E. Woo, *Liq. Cryst.* **1999**, *26*, 1403.

- [155] J. C. Wittmann, P. Smith, *Nature* **1991**, 352, 414.
- [156] L. Kinder, J. Kanicki, J. Swensen, P. Petroff, "Structural ordering in F8T2 polyfluorene thin film transistors", presented at *Optical Science and Technology, SPIE's 48th Annual Meeting*, 2003.
- [157] J. Geary, J. Goodby, A. Kmetz, J. Patel, *J. Appl. Phys.* **1987**, 62, 4100.
- [158] M. Brinkmann, L. Hartmann, L. Biniek, K. Tremel, N. Kayunkid, *Macromol. Rapid Commun.* **2014**, 35, 9.
- [159] K. Sakamoto, T. Yasuda, K. Miki, M. Chikamatsu, R. Azumi, *J. Appl. Phys.* **2011**, 109, 013702.
- [160] G. Lu, J. Chen, W. Xu, S. Li, X. Yang, *Adv. Funct. Mater.* **2014**, 24, 4959.
- [161] N. Kleinhenz, C. Rosu, S. Chatterjee, M. Chang, K. Nayani, Z. Xue, E. Kim, J. Middlebrooks, P. S. Russo, J. O. Park, *Chem. Mater.* **2015**, 27, 2687.
- [162] G. Wang, N. Persson, P.-H. Chu, N. Kleinhenz, B. Fu, M. Chang, N. Deb, Y. Mao, H. Wang, M. A. Grover, *ACS Nano* **2015**, 9, 8220.
- [163] T. A. Skotheim, *Handbook of Conducting Polymers*, CRC press, **1997**.
- [164] M. Osagawara, K. Funahashi, T. Demura, T. Hagiwara, K. Iwata, *Synth. Met.* **1986**, 14, 61.
- [165] Y. Nogami, J.-P. Pouget, T. Ishiguro, *Synth. Met.* **1994**, 62, 257.
- [166] P. Dyreklev, G. Gustafsson, O. Inganäs, H. Stubb, *Solid State Commun.* **1992**, 82, 317.
- [167] P. Dyreklev, G. Gustafsson, O. Inganäs, H. Stubb, *Synth. Met.* **1993**, 57, 4093.
- [168] M. L. Chabiny, A. Salleo, Y. Wu, P. Liu, B. S. Ong, M. Heeney, I. McCulloch, *J. Am. Chem. Soc.* **2004**, 126, 13928.
- [169] B. O'Connor, R. J. Kline, B. R. Conrad, L. J. Richter, D. Gundlach, M. F. Toney, D. M. DeLongchamp, *Adv. Funct. Mater.* **2011**, 21, 3697.
- [170] W. C. Mara, *Liquid crystal flat panel displays: manufacturing science & technology*, Springer Science & Business Media, **2012**.
- [171] H. Heil, T. Finnberg, N. Von Malm, R. Schmechel, H. Von Seggern, *J. Appl. Phys.* **2003**, 93, 1636.
- [172] C. Yang, C. Soci, D. Moses, A. Heeger, *Synth. Met.* **2005**, 155, 639.
- [173] L. Biniek, N. Leclerc, T. Heiser, R. Bechara, M. Brinkmann, *Macromolecules* **2013**, 46, 4014.
- [174] K. Tremel, F. S. Fischer, N. Kayunkid, R. D. Pietro, R. Tkachov, A. Kiriya, D. Neher, S. Ludwigs, M. Brinkmann, *Adv. Energy Mater.* **2014**, 4, 1301659.
- [175] J. Wittmann, B. Lotz, *Prog. Polym. Sci.* **1990**, 15, 909.
- [176] A. Hamidi-Sakr, D. Schiefer, S. Covindarassou, L. Biniek, M. Sommer, M. Brinkmann, *Macromolecules* **2016**, 49, 3452.
- [177] M. Brinkmann, J. C. Wittmann, *Adv. Mater.* **2006**, 18, 860.
- [178] L. Scriven, *MRS Online Proc. Libr.* **1988**, 121, 717.
- [179] G. Wang, J. Swensen, D. Moses, A. J. Heeger, *J. Appl. Phys.* **2003**, 93, 6137.
- [180] S. Wang, A. Kiersnowski, W. Pisula, K. Müllen, *J. Am. Chem. Soc.* **2012**, 134, 4015.
- [181] L. Li, P. Gao, K. C. Schuermann, S. Ostendorp, W. Wang, C. Du, Y. Lei, H. Fuchs, L. D. Cola, K. Müllen, *J. Am. Chem. Soc.* **2010**, 132, 8807.
- [182] S. Wang, W. Pisula, K. Müllen, *J. Mater. Chem.* **2012**, 22, 24827.
- [183] J. Liu, Y. Sun, X. Gao, R. Xing, L. Zheng, S. Wu, Y. Geng, Y. Han, *Langmuir* **2011**, 27, 4212.
- [184] L. Yu, M. R. Niazi, G. O. N. Ndjawa, R. Li, A. R. Kirmani, R. Munir, A. H. Balawi, F. Laquai, A. Amassian, *Sci. Adv.* **2017**, 3, e1602462.
- [185] D. J. Gundlach, J. E. Royer, S. Park, S. Subramanian, O. Jurchescu, B. H. Hamadani, A. Moad, R. J. Kline, L. Teague, O. Kirillov, *Nat. Mater.* **2008**, 7, 216.
- [186] H. Wang, L. Chen, R. Xing, J. Liu, Y. Han, *Langmuir* **2014**, 31, 469.
- [187] N.-K. Kim, S.-Y. Jang, G. Pace, M. Caironi, W.-T. Park, D. Khim, J. Kim, D.-Y. Kim,

- Y.-Y. Noh, *Chem. Mater.* **2015**, *27*, 8345.
- [188] R. Matsidik, H. Komber, A. Luzio, M. Caironi, M. Sommer, *J. Am. Chem. Soc.* **2015**, *137*, 6705.
- [189] S.-Y. Jang, I.-B. Kim, J. Kim, D. Khim, E. Jung, B. Kang, B. Lim, Y.-A. Kim, Y. H. Jang, K. Cho, *Chem. Mater.* **2014**, *26*, 6907.
- [190] Y. Diao, L. Shaw, Z. Bao, S. C. Mannsfeld, *Energy Environ. Sci.* **2014**, *7*, 2145.
- [191] B. H. Lee, B. B. Hsu, S. N. Patel, J. Labram, C. Luo, G. C. Bazan, A. J. Heeger, *Nano Lett.* **2015**, *16*, 314.
- [192] J. Soeda, H. Matsui, T. Okamoto, I. Osaka, K. Takimiya, J. Takeya, *Adv. Mater.* **2014**, *26*, 6430.
- [193] H. A. Becerril, M. E. Roberts, Z. Liu, J. Locklin, Z. Bao, *Adv. Mater.* **2008**, *20*, 2588.
- [194] Y. Diao, B. C. Tee, G. Giri, J. Xu, D. H. Kim, H. A. Becerril, R. M. Stoltenberg, T. H. Lee, G. Xue, S. C. Mannsfeld, *Nat. Mater.* **2013**, *12*, 665.
- [195] M. Karakawa, M. Chikamatsu, Y. Yoshida, M. Oishi, R. Azumi, K. Yase, *Appl. Phys. Express* **2008**, *1*, 061802.
- [196] H. Yabu, M. Shimomura, *Adv. Funct. Mater.* **2005**, *15*, 575.
- [197] G. Giri, D. M. DeLongchamp, J. Reinspach, D. A. Fischer, L. J. Richter, J. Xu, S. Benight, A. Ayzner, M. He, L. Fang, *Chem. Mater.* **2015**, *27*, 2350.
- [198] W. Y. Lee, G. Giri, Y. Diao, C. J. Tassone, J. R. Matthews, M. L. Sorensen, S. C. Mannsfeld, W. C. Chen, H. H. Fong, J. B. H. Tok, *Adv. Funct. Mater.* **2014**, *24*, 3524.
- [199] J. Shin, T. R. Hong, T. W. Lee, A. Kim, Y. H. Kim, M. J. Cho, D. H. Choi, *Adv. Mater.* **2014**, *26*, 6031.
- [200] S.-R. Tseng, H.-F. Meng, K.-C. Lee, S.-F. Horng, *Appl. Phys. Lett.* **2008**, *93*, 382.
- [201] A. Pierre, M. Sadeghi, M. M. Payne, A. Facchetti, J. E. Anthony, A. C. Arias, *Adv. Mater.* **2014**, *26*, 5722.
- [202] Y.-H. Chang, S.-R. Tseng, C.-Y. Chen, H.-F. Meng, E.-C. Chen, S.-F. Horng, C.-S. Hsu, *Org. Electron.* **2009**, *10*, 741.
- [203] P.-H. Chu, N. Kleinhenz, N. Persson, M. McBride, J. L. Hernandez, B. Fu, G. Zhang, E. Reichmanis, *Chem. Mater.* **2016**, *28*, 9099.
- [204] F. C. Krebs, *Sol. Energy Mater. Sol. Cells* **2009**, *93*, 465.
- [205] A. Sandström, H. F. Dam, F. C. Krebs, L. Edman, *Nat. Commun.* **2012**, *3*, 1002.
- [206] J. Jensen, H. F. Dam, J. R. Reynolds, A. L. Dyer, F. C. Krebs, *J. Polym. Sci., Part B: Polym. Phys.* **2012**, *50*, 536.
- [207] J. Chang, C. Chi, J. Zhang, J. Wu, *Adv. Mater.* **2013**, *25*, 6442.
- [208] J. Chang, Z. Lin, J. Li, S. L. Lim, F. Wang, G. Li, J. Zhang, J. Wu, *Adv. Electron. Mater.* **2015**, *1*.
- [209] J. Chang, P. Sonar, Z. Lin, C. Zhang, J. Zhang, Y. Hao, J. Wu, *Org. Electron.* **2016**, *36*, 113.
- [210] A. K. K. Kyaw, L. S. Lay, G. W. Peng, J. Changyun, Z. Jie, *Chem. Commun.* **2016**, *52*, 358.
- [211] A. Tracz, T. Pakula, J. K. Jeszka, *Materials Science-Poland* **2004**, *22*, 415.
- [212] L. J. Richter, D. M. DeLongchamp, A. Amassian, *Chem. Rev.* **2017**, *117*, 6332.
- [213] L. Burda, A. Tracz, T. Pakula, J. Ulanski, M. Kryszewski, *J. Phys. D: Appl. Phys.* **1983**, *16*, 1737.
- [214] C. M. Duffy, J. W. Andreasen, D. W. Breiby, M. M. Nielsen, M. Ando, T. Minakata, H. Sirringhaus, *Chem. Mater.* **2008**, *20*, 7252.
- [215] Y. Su, X. Gao, J. Liu, R. Xing, Y. Han, *PCCP* **2013**, *15*, 14396.
- [216] P. Miskiewicz, M. Mas-Torrent, J. Jung, S. Kotarba, I. Glowacki, E. Gomar-Nadal, D. B. Amabilino, J. Veciana, B. Krause, D. Carbone, *Chem. Mater.* **2006**, *18*, 4724.
- [217] M. Mas-Torrent, S. Masirek, P. Hadley, N. Crivillers, N. Oxtoby, P. Reuter, J. Veciana, C. Rovira, A. Tracz, *Org. Electron.* **2008**, *9*, 143.

- [218] A. Tracz, J. K. Jeszka, M. D. Watson, W. Pisula, K. Müllen, T. Pakula, *J. Am. Chem. Soc.* **2003**, *125*, 1682.
- [219] W. Pisula, A. Menon, M. Stepputat, I. Lieberwirth, U. Kolb, A. Tracz, H. Sirringhaus, T. Pakula, K. Müllen, *Adv. Mater.* **2005**, *17*, 684.
- [220] D. V. Anokhin, M. Rosenthal, T. Makowski, A. Tracz, W. Bras, K. Kvashnina, D. A. Ivanov, *Thin Solid Films* **2008**, *517*, 982.
- [221] X. Gao, J.-G. Liu, Y. Sun, R.-B. Xing, Y.-C. Han, *Chin. Chem. Lett.* **2013**, *24*, 23.
- [222] M. J. Lee, D. Gupta, N. Zhao, M. Heeney, I. McCulloch, H. Sirringhaus, *Adv. Funct. Mater.* **2011**, *21*, 932.
- [223] T. Schuettfort, B. Watts, L. Thomsen, M. Lee, H. Sirringhaus, C. R. McNeill, *ACS Nano* **2012**, *6*, 1849.
- [224] C. Tang, A. Tracz, M. Kruk, R. Zhang, D.-M. Smilgies, K. Matyjaszewski, T. Kowalewski, *J. Am. Chem. Soc.* **2005**, *127*, 6918.
- [225] D. M. DeLongchamp, R. J. Kline, Y. Jung, D. S. Germack, E. K. Lin, A. J. Moad, L. J. Richter, M. F. Toney, M. Heeney, I. McCulloch, *Acs Nano* **2009**, *3*, 780.
- [226] S. Lee, G. D. Moon, U. Jeong, *J. Mater. Chem.* **2009**, *19*, 743.
- [227] R. Steyrlleuthner, M. Schubert, F. Jaiser, J. C. Blakesley, Z. Chen, A. Facchetti, D. Neher, *Adv. Mater.* **2010**, *22*, 2799.
- [228] H. Yan, Z. Chen, Y. Zheng, C. Newman, J. R. Quinn, F. Dötz, M. Kastler, A. Facchetti, *Nature* **2009**, *457*, 679.
- [229] D. Khim, H. Han, K. J. Baeg, J. Kim, S. W. Kwak, D. Y. Kim, Y. Y. Noh, *Adv. Mater.* **2013**, *25*, 4302.
- [230] E. D. Cohen, E. B. Guttoff, *Modern coating and drying technology*, Jacaranda, **1992**.
- [231] B. Dan, G. C. Irvin, M. Pasquali, *ACS Nano* **2009**, *3*, 835.
- [232] A. A. Tracton, *Coatings technology handbook*, CRC press, **2005**.
- [233] J. Wang, M. Liang, Y. Fang, T. Qiu, J. Zhang, L. Zhi, *Adv. Mater.* **2012**, *24*, 2874.
- [234] F. Guo, A. Mukhopadhyay, B. W. Sheldon, R. H. Hurt, *Adv. Mater.* **2011**, *23*, 508.
- [235] K. I. Park, C. K. Jeong, J. Ryu, G. T. Hwang, K. J. Lee, *Adv. Energy Mater.* **2013**, *3*, 1539.
- [236] C. T. Hong, Y. Yoo, Y. H. Kang, J. Ryu, S. Y. Cho, K.-S. Jang, *RSC Adv.* **2015**, *5*, 11385.
- [237] W. Lee, C. T. Hong, O. H. Kwon, Y. Yoo, Y. H. Kang, J. Y. Lee, S. Y. Cho, K.-S. Jang, *ACS Appl. Mater. Interfaces* **2015**, *7*, 6550.
- [238] W. J. Lee, W. T. Park, S. Park, S. Sung, Y. Y. Noh, M. H. Yoon, *Adv. Mater.* **2015**, *27*, 5043.
- [239] J. Ouyang, T.-F. Guo, Y. Yang, H. Higuchi, M. Yoshioka, T. Nagatsuka, *Adv. Mater.* **2002**, *14*, 915.
- [240] C. E. Murphy, L. Yang, S. Ray, L. Yu, S. Knox, N. Stingelin, *J. Appl. Phys.* **2011**, *110*, 093523.
- [241] D. Khim, G. S. Ryu, W. T. Park, H. Kim, M. Lee, Y. Y. Noh, *Adv. Mater.* **2016**, *28*, 2752.
- [242] L. Biniek, S. p. Pouget, D. Djurado, E. Gonthier, K. Tremel, N. Kayunkid, E. Zaborova, N. Crespo-Monteiro, O. Boyron, N. Leclerc, *Macromolecules* **2014**, *47*, 3871.
- [243] X. Liu, M. Kanehara, C. Liu, K. Sakamoto, T. Yasuda, J. Takeya, T. Minari, *Adv. Mater.* **2016**, *28*, 6568.
- [244] G. Giri, E. Verploegen, S. C. Mannsfeld, S. Atahan-Evrenk, D. H. Kim, S. Y. Lee, H. A. Becerril, A. Aspuru-Guzik, M. F. Toney, Z. Bao, *Nature* **2011**, *480*, 504.